AED R-4013F
May 31, 1974

NASA CR-
147409

Solid State Electro-Optic Color Filter and Iris

Interim Report

July 1973 through March 1974

Prepared for
National Aeronautics and Space Administration
Johnson Space Center
Houston, Texas
Under Contract No. NAS9-13549

RCA

ORIGINAL CONTAINS
COLOR ILLUSTRATIONS

RCA Government and Commercial Systems
Astro Electronics Division Princeton, New Jersey

ERRATA FOR INTERIM REPORT (JULY 1973 - MARCH 1974)
SOLID STATE ELECTRO-OPTIC COLOR FILTER AND IRIS
Contract No. NAS9-13549 (AED R-4013F)

Page	
v	The titles for Figures 5 and 6 are transposed. The correct title for Figure 7 is "Wafer No. 6, Showing Electrode Discontinuities."
ix	The correct title for Table 4 is "PLZT Plate Readings Corrected for Shading."
10	In Figure 2, the bottom electrode should be connected only to the left "bus."
16	The title for Figure 7 should be: "Wafer No. 6, Showing Electrode Discontinuities."
22	In Figure 9, the upper right callout should be "Spectra UB 1/2 Photometer."
45	The title of Figure 14 should be: "Transmission Measurements on Type HN-32 Polarizers With Axes Parallel."
67	Note 5 of Figure 29 should be: "PLZT Rotated Clockwise About Its Vertical Axis." The plot shown here is of absolute values, and the curves should be shown as Figure 30.
69	The plot shown here is of normalized values, and the curves should be shown as Figure 29.
70	The transistor type for Q4 in Figure 47 should be 2N4124.

AED R-4013F
May 31, 1974

Solid State Electro-Optic Color Filter and Iris

Interim Report

July 1973 through March 1974

Prepared for
National Aeronautics and Space Administration
Johnson Space Center
Houston, Texas
Under Contract No. NAS9-13549

RCA Government and Commercial Systems
Astro Electronics Division Princeton, New Jersey

PREFACE

This is an interim report of the progress on the project "Solid State Electro-Optic Color Filter and Iris," being performed by the Astro-Electronics Division of RCA for the Johnson Space Center of the National Aeronautics and Space Administration under Contract NAS 9-13549. It covers work performed from July 1973 through March 1974, and responds to the documentation requirements set forth in Article I-34, Items 4 and 5 of the contract.

TABLE OF CONTENTS

Section		Page
I	INTRODUCTION AND SUMMARY	1
II	TECHNICAL DISCUSSION	3
	A. Theory of Operation	3
	B. Sample Material Preparation	8
	1. Blank Material	8
	2. Electrode Pattern	9
	3. Applied Coatings	15
	a. Reflection Losses	17
	b. High Voltage Breakdown	20
	C. Optical Test Setup	23
	1. Optical Bench Equipment	23
	2. Petrographic Microscope Measurements	26
	D. Test Type Descriptions	31
	1. Neutral Density Transfer Curve . . .	31
	2. Temperature Effects	32
	3. Resolution	32
	4. Angle of Incidence	33
	5. Time Constant	33
	6. Anti-Reflection Coatings	34
	7. Retardation Versus Voltage	34
	8. Shading	35
	9. Spectral Response	35
	E. Discussion of Electrode Contact Problems	37
	F. Test Results (Optical Bench)	44
	1. General	44
	2. Neutral Density Transfer Curve . . .	47

TABLE OF CONTENTS (Continued)

Section			Page
		3. Temperature Effects	52
		4. Resolution	66
		5. Angle of Incidence	66
		6. Time Constant	70
		7. Retardation Variations	74
		a. Variation With Applied Voltage	74
		b. Variation of Retardation Across a Single Electrode Pair	74
		c. Variation With Overall Position	78
		8. Shading	81
		a. Photometric Measurement	81
		b. Photographic Method	81
		9. Spectral Response	85
		10. Anti-Reflection Coatings	95
	G.	Interface With Camera	98
		1. Mechanical	98
		2. Electrical	100
	H.	Test Results With Camera	111
		1. ALC Operation	111
		2. Resolution	113
		3. Response Time	115
		4. Spectral Filter Observation	117
III		THEORETICAL ANALYSIS	123
	A.	General	123
	B.	Angular Aperture of Solid-State Electro-Optical Filter Devices	123
	C.	Spectral Response of Solid-State Electro-Optical Filters - Optical Network Synthesis	135

TABLE OF CONTENTS (Continued)

Section		Page
IV	SYSTEM PERFORMANCE AND FUTURE RECOMMENDATIONS	143
	A. Anticipated System Effectiveness	143
	1. Neutral Density Filter Operation . . .	143
	2. Spectral Filter Operation	148
	B. Recommendations for Future Effort	153
	1. Phase 2	153
	2. Succeeding Phases	156
Appendix		
A	Bibliography.	A-1

LIST OF ILLUSTRATIONS

Figure		Page
1	Solid State Electro-Optical Filter Configuration	6
2	Electrode Configuration	10
3	Single Electrode, Showing Breaks	11
4	Single Electrode, Showing Epoxy Repair	12
5	Single Electrode, Showing Desired (Unrepaired) Configuration	13
6	Wafer No. 6, Showing Epoxy Repairs	14
7	Wafer No. 20, Showing Electrode Discontinuities	16
8	Spectral Measurements for Reflection From PLZT Coated Disc #1	18
9	Optical Bench Used for Tests of PLZT Device Characteristics	22
10	SSEF Holding Fixture	24
11	Optical Planes in Conventional and Conoscopic Microscopy	29
12	Birefringence Effect With Operation in the Variable Neutral Density Mode	38
13	Birefringence Effect With Operation in the Spectral Filter Mode	40
14	Transmission Measurements on Type HN-32 Polarizers With Axes Parallel	45
15	Transfer Curve of PLZT Sample, Going to Full Voltage	48
16	Transfer Curve of PLZT Sample, With Reversed Polarity	50
17	Transfer Curve of PLZT Sample With Parallel (Rather Than Orthogonal) Polarizer Axes	51

LIST OF ILLUSTRATIONS (Continued)

Figure		Page
18	Density Transfer Characteristic as a Function of Temperature of PLZT Sample, T = 21°C	54
19	Density Transfer Characteristic as a Function of Temperature of PLZT Sample, T = 30°C	55
20	Density Transfer Characteristic as a Function of Temperature of PLZT Sample, T = 50°C	56
21	Density Transfer Characteristic as a Function of Temperature of PLZT Sample, T = 60°C	57
22	Density Transfer Characteristic as a Function of Temperature of PLZT Sample, T = 22°C	58
23	Density Transfer Characteristic as a Function of Temperature of PLZT Sample, T = 11°C	59
24	Density Transfer Characteristic as a Function of Temperature of PLZT Sample, T = 0°C	60
25	Density Transfer Characteristic as a Function of Temperature of PLZT Sample, T Returned to 22°C	61
26	Delayed Measurement of Density Transfer Characteristic of PLZT Sample at Reference (T = 22°C) Temperature	62
27	Density Variation With Temperature of PLZT Sample for Several Control-Voltage Levels . . .	63
28	Defect Occurring at 60°C in Full Field Transmission	64
29	Effect of Off-Axis Incident Light (Normalized Deviations)	67

LIST OF ILLUSTRATIONS (Continued)

Figure		Page
30	Effect of Off-Axis Incident Light (Absolute Values)	69
31	Effect of Increasing DC Voltage on Birefringent Retardation	75
32	Effect of Position Between Electrode Fingers on Birefringent Retardation	76
33	Variation in Birefringent Retardation Over Central Region of Disc (at 500V)	79
34	Single-Stage PLZT Filter Assembly Performance, Test No. 3	86
35	Single-Stage PLZT Filter Assembly Performance, Test No. 9	87
36	Single-Stage PLZT Filter Assembly Performance, Test No. 11	88
37(a)	Spectral Response Curves Obtained Using the Scanning Spectrophotometer, Tests 1 Through 4	90
37(b)	Spectral Response Curves Obtained Using the Scanning Spectrophotometer, Tests 5 Through 8	91
37(c)	Spectral Response Curves Obtained Using the Scanning Spectrophotometer, Tests 10 Through 15	92
38	Transmission Loss PLZT Wafer Across Spectrum for 7/4 λ Coating on Electrode Surface (λ = 520 nm)	96
39	Transmission Loss of PLZT Wafer for 7/4 λ Coating on Electrode Surface and 1/4 λ Coating on Opposite Surface (λ = 520 nm)	97
40	SSEF Housing and Zoom Lens Installed on Camera	99
41	SSEF Holder, Front View	101

LIST OF ILLUSTRATIONS (Continued)

Figure		Page
42	SSEF Holder, Rear View	102
43	SSEF Holder Assembled to Camera, Cross Section	103
44	Automatic Light Control System, Block Diagram	104
45	Control Panel for ALC Operation	105
46	Automatic Light Control Circuitry, Schematic Diagram	107
47	High-Voltage Switching Driver, Schematic Diagram	109
48	Overall SSEF/CTV Test Set-Up	112
49	Dynamic Range of SSEF With CTV	114
50	Video Output, SSEF Switched On	116
51	Video Output, SSEF Switched Off	116
52	Photodiode Output, SSEF Switched On	118
53	Photodiode Output, SSEF Switched Off	118
54	SSEF Applied Switching Voltage Step	119
55	Normalized Response to Color Sample Chips . . .	122
56	Special Cases for Directions of Incident Light Rays	126
57	Transmission of Light Through PLZT Plate	128
58	Fresnel Ellipsoid-of-Wave Normals Construction for Determining n_i	131
59	Compensation Scheme for Decreasing the Variation of Retardation With Angle of Incidence (Exploded Drawing)	134
60	Disassembled Representation of Optical Network	140

LIST OF TABLES

Table		Page
1	Optical Response Times	72
2	Photometric Shading Data	82
3	Film Densities for the PLZT Plate	83
4	PLZT Plate Readings Collected for Shading . . .	84
5	Retardation Plate Colors and Applied Voltages	89
6	Normalized Color Chip Measurements	120

SECTION I

INTRODUCTION AND SUMMARY

The Astro-Electronics Division (AED) of RCA submits to NASA this engineering study report covering the engineering design, development and test of a prototype Solid State Electro-Optic Filter (SSEF) under Contract No. NAS 9-13549.

The primary purpose of this contract was to evaluate the electro-optic properties of PLZT ceramic material when utilized as a variable density and/or spectral filter in conjunction with a television scanning system.

Existing designs for spacecraft television cameras utilize rotating color filter wheels for spectral separation, and mechanical irises for exposure control. Reliability of a camera system is compromised by these electromechanical elements and lifetime is limited. Recently developed ferroelectric polycrystalline ceramics offer the potential of solid state replacement of both the spectral filter and iris functions. In particular, the use of lanthanum-modified lead zirconate titanate (PLZT) ceramic compounds provides significantly increased optical transparency when compared to previously available materials. The work reported here has been devoted to evaluating the existing and potential properties of PLZT filters applied to spacecraft television systems.

Test results obtained have confirmed the practicality of the SSEF as an optical control element in a television system. Neutral-density control range in excess of 1000:1 has been obtained on sample filters.

Observed spectral filter performance for single stage devices was not as dramatic; cascaded networks and/or improved devices hold forth promise of improved performance.

Included in this report are the test results, measurements in a complete camera system, discussions of problem areas, analytical comparions, and recommendations for future investigations. Also included as Appendix A is a complete bibliography of related literature which was prepared during the performance of the contract effort.

SECTION II

TECHNICAL DISCUSSION

A. THEORY OF OPERATION

Electro-optic operation of the PLZT ceramic plate is achieved by virtue of its electrically controlled birefringence characteristic, combined with its inherent high optical transparency. When compared to other single crystal materials, it offers the advantages of relatively unlimited size, optical uniformity, and large electro-optic effect.

Birefringent materials are classed as optically anisotropic; that is, their optical properties are different in different directions. In particular, the refractive index for light waves polarized parallel to the materials polarization axis is different than for light waves polarized perpendicular to this axis.

When light rays travel through such a birefringent material, the two refractive indices cause two paths to be traveled at slightly different velocities. When the rays are recombined after exiting the plate, the phase relation between them will have changed. Since the plate causes one wave to lag the other, it is frequently referred to as a retardation plate. The amount of retardation achieved by a given plate is proportional to the difference in

the two refractive indices, times the path length (or plate) thickness. That is:

$$\Gamma = t\,(n_2 - n_1)$$

where,

Γ is the retardation

t is the plate thickness

$(n_2 - n_1)$ is the difference between refractive indices

The units of retardation are the same as the units for the thickness.

If for example we pass a beam of linear light through a plate whose retardation is one-half wavelength, it will exit with its azimuth rotated by 90°, provided the light is incident on the plate with its electric vector making an angle of 45° with the optic axis. The result from plates other than half wave is to produce elliptic polarized light where the degree of ellipticity depends on the retardation.

Since the PLZT material permits electrical control of the magnitude of its birefringence (and thus retardation), it can be used as an optical control element in conjunction with two polarizers (an input polarizer and output analyzer).

The basic configuration for a practical device consists of a polished plate of PLZT ceramic mounted between a pair of crossed polarizers. The PLZT surfaces contain a deposited electrode pattern for application of control voltages. The filter configuration is shown diagramatically in Figure 1. Unpolarized light at the system input is selectively filtered by polarizer 1 to provide linearly polarized light at an angle of 45° to the x - x reference axis. This light then passes through the ceramic plate and impinges on polarizer 2, whose polarization axis is at an angle of 135° to the reference. In the absence of any electric field, the PLZT plate is isotropic and the crossed polarizers effectively block transmission of light (OFF state). Application of an electric field to the ceramic plate by voltage on the interdigitated electrodes causes the plate to become birefringent. The refractive index, n_e, along the polar axis (y-y) changes from the index, n_o, along the x-x axis. For this case, a component will pass through the analyzer. When the potential is adjusted to provide half-wave retardation through the plate, the resultant output from the PLZT plate is linear polarized at 90 degrees to the polarizer axis and maximum transmission is achieved (ON state). The operating potential can be controlled between the ON and OFF states thus permitting use of the PLZT plate as a voltage-dependent variable-density filter.

The same basic configuration can be used to provide spectral filtering by increasing the retardation in the plate beyond one-half wavelength. In this case destructive interference is

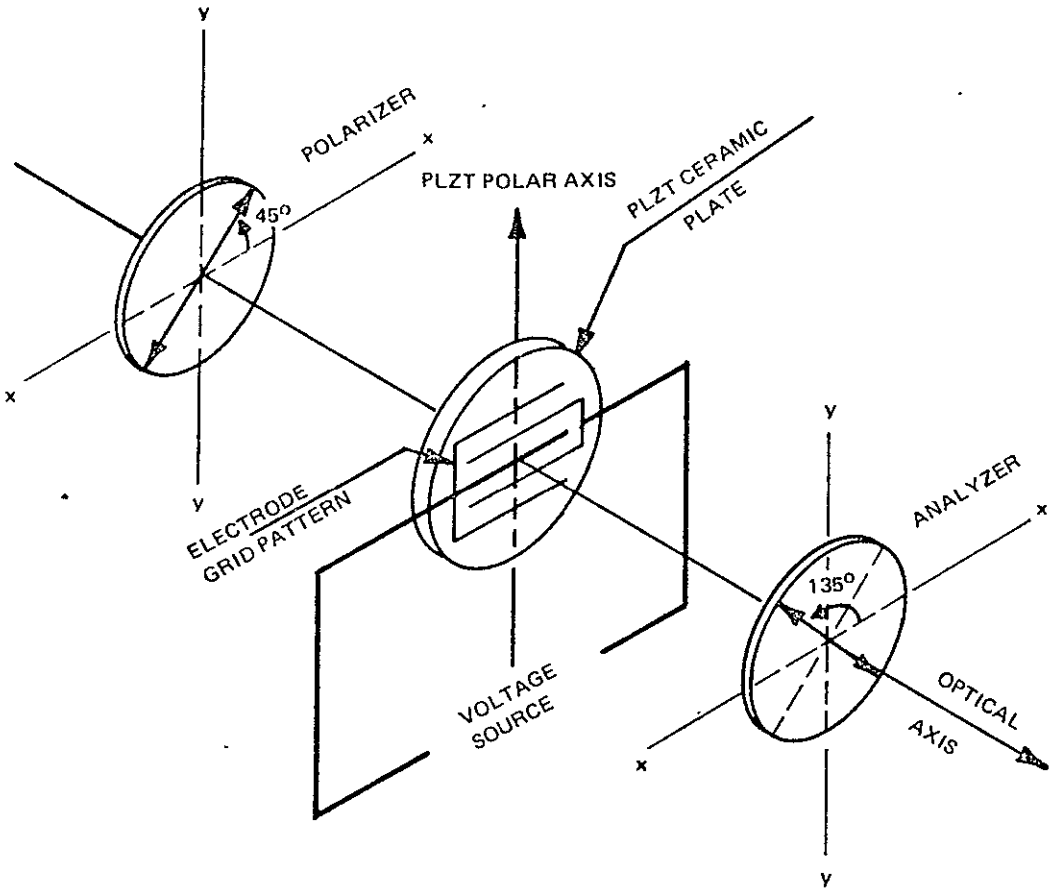

Figure 1. Solid State Electro-Optical Filter Configuration

obtained for certain wavelengths of light, depending on the amount of retardation. The remaining wavelengths combine to give the characteristic interference colors identified by Newton's series. This series consists of a succession of "orders", where each order represents one full wavelength of retardation. The colors within each order are not spectrally pure, nor do they follow the same spectrum sequence. By superimposing selected colors from one order over those of another, narrow spectral filtering can be achieved. The spectral bandwidth which can be achieved is limited only by the number of such orders (filter assemblies) one is willing to asemble. The Lyot filter[98] represents a practical application of this technique. A chart showing color reproductions of the Newton series colors for the first three orders can be found in reference 14, page 47.

---

98. This and succeeding references in this report are identified in the Bibliography, attached as Appendix A.

B. SAMPLE MATERIAL PREPARATION

1. Blank Material

The ferroelectric ceramic samples used for evaluation in this program were composed of a homogeneous solid solution of lead zirconate and lead titanate, modified with lanthanum oxide (commonly referred to as PLZT). A ferroelectric ceramic is an aggregate of many small (2 to 8 micron) single-crystal grains, each randomly oriented with respect to all the others. The PLZT composition, fabricated by hot-pressing at temperatures in excess of 1000°C, provides significantly improved optical transparency when compared to earlier ceramics. It also overcomes the traditional limitations of single crystal ferroelectric materials, i.e., limited size, optical non-uniformity, and small electro-optic effect.

Twenty samples of composition 9065 (9/65/35, La/Zr/Ti ratio) were procured from Sandia Research Laboratories where this composition was first developed. This particular composition exhibits a quadratic electro-optic effect. The samples were supplied as slices, 1-1/2" in diameter and 0.020" thick. These slices were ground and polished to a finished thickness of 0.010" by Statek Corporation.

2. Electrode Pattern

To permit operating the devices in the transverse mode (optic axis transverse to the direction of light propagation), an interdigitated array of narrow electrodes was deposited on both sides of the polished ceramic wafer. The electrode pattern and associated dimensions used are shown in Figure 2. Vacuum-deposition and photo etching techniques were employed by Statek to affix the electrode pattern to the ceramic. The quality of the electrodes was not good, although it was expected to be satisfactory for the planned measurements.

In the process of evaporation and etching, numerous discontinuities developed which necessitated patching with conductive epoxy applied with a brush by hand. Microscopic photographs have been taken, copies of which accompany this report. The photomicrograph of sample No. 20 (Figure 3) shows the nature of the breaks in the electrode; and photomicrographs for the No. 6 (Figures 4 and 5) show the repairs which were made to this type of break. Photomicrograph (Figure 6) of another portion of No. 6 show the type of quality desired. A full view photograph of No. 6 (Figure 7) indicates the number of lesions involved.

It should also be noted from the dimensions in Figure 2 that the optical masking by the electrode fingers results in a transmission insertion loss of 6.25 percent exclusive of any loss created by the PLZT sample and associated polarizers.

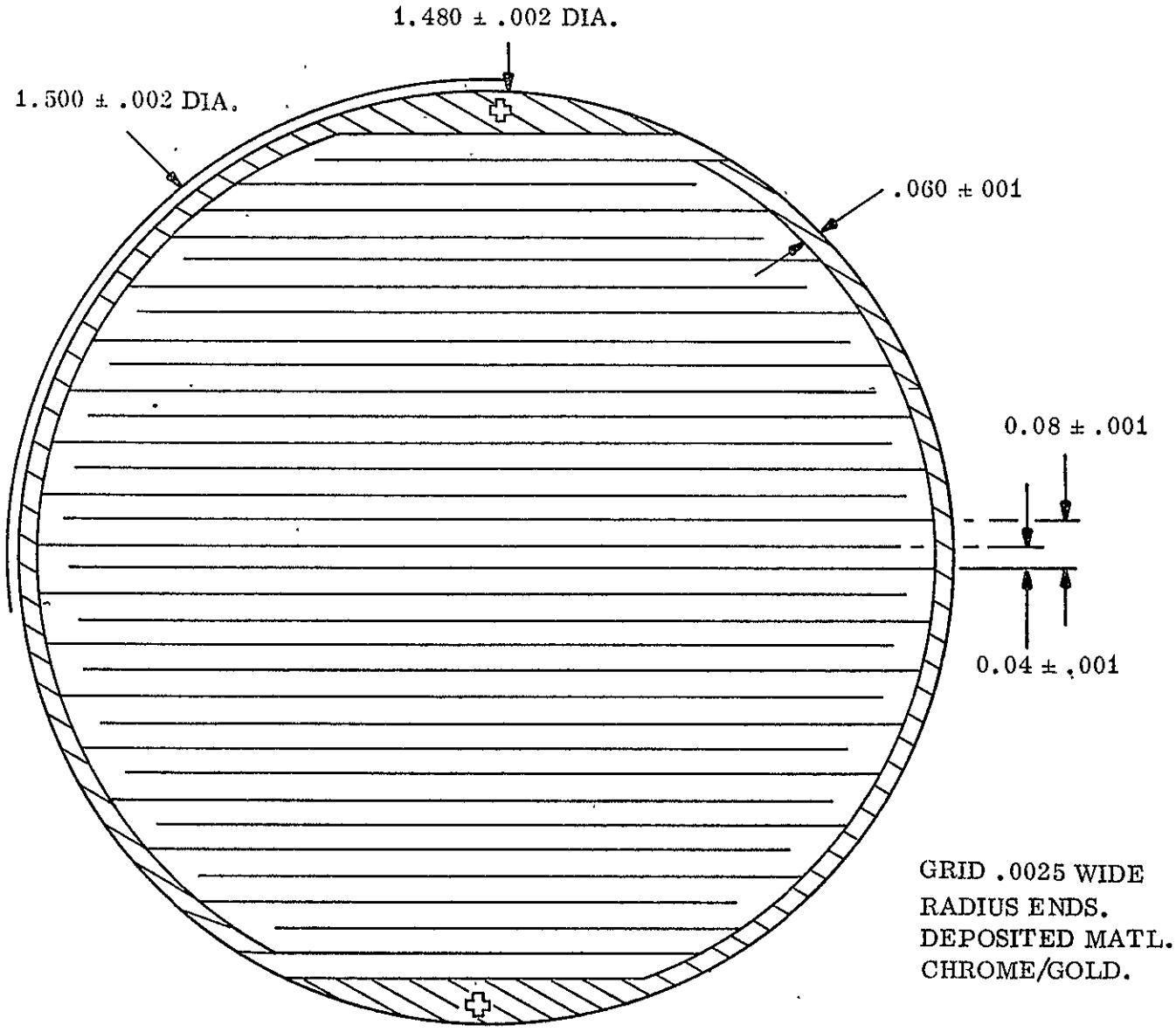

Figure 2. Electrode Configuration

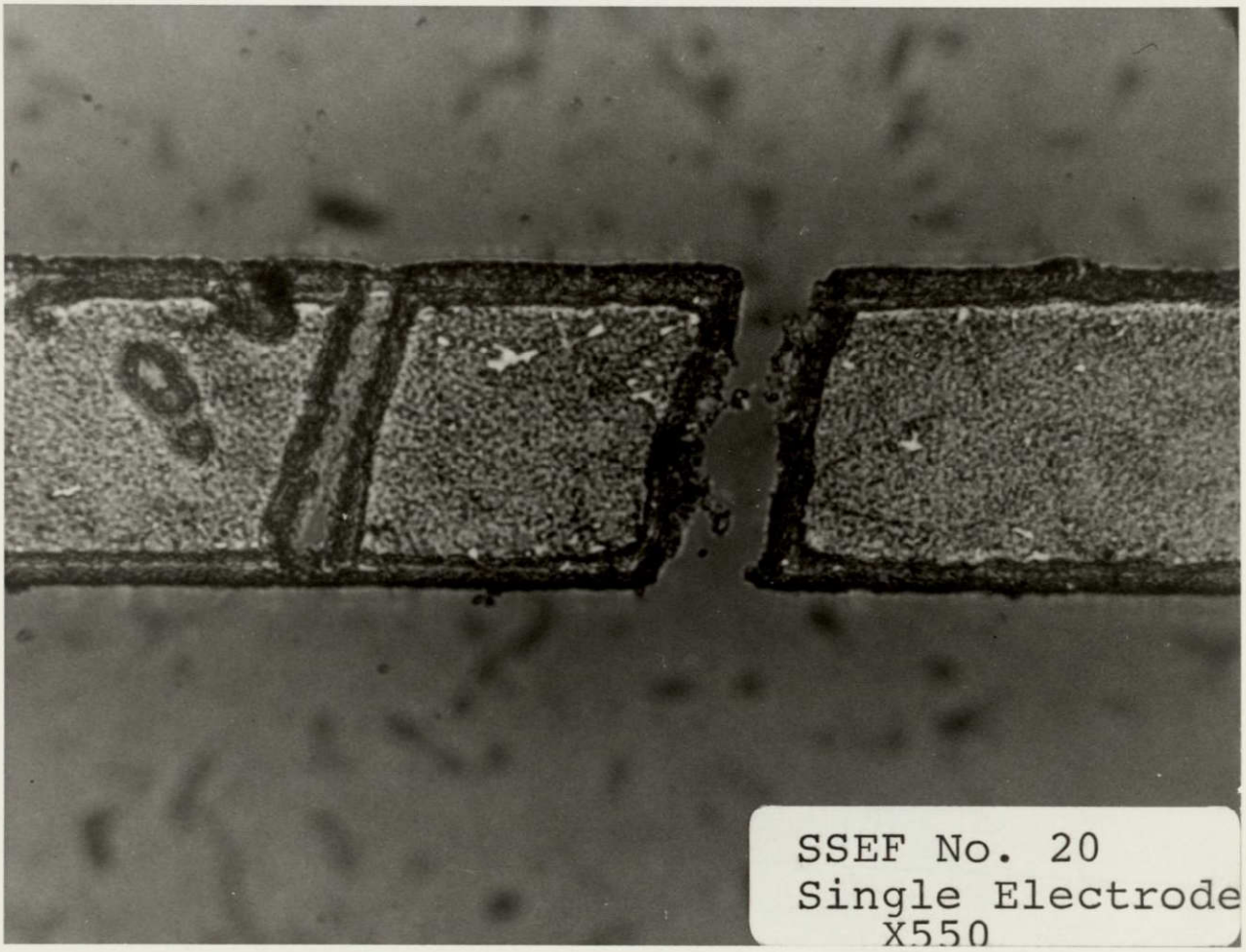

Figure 3. Single Electrode, Showing Breaks

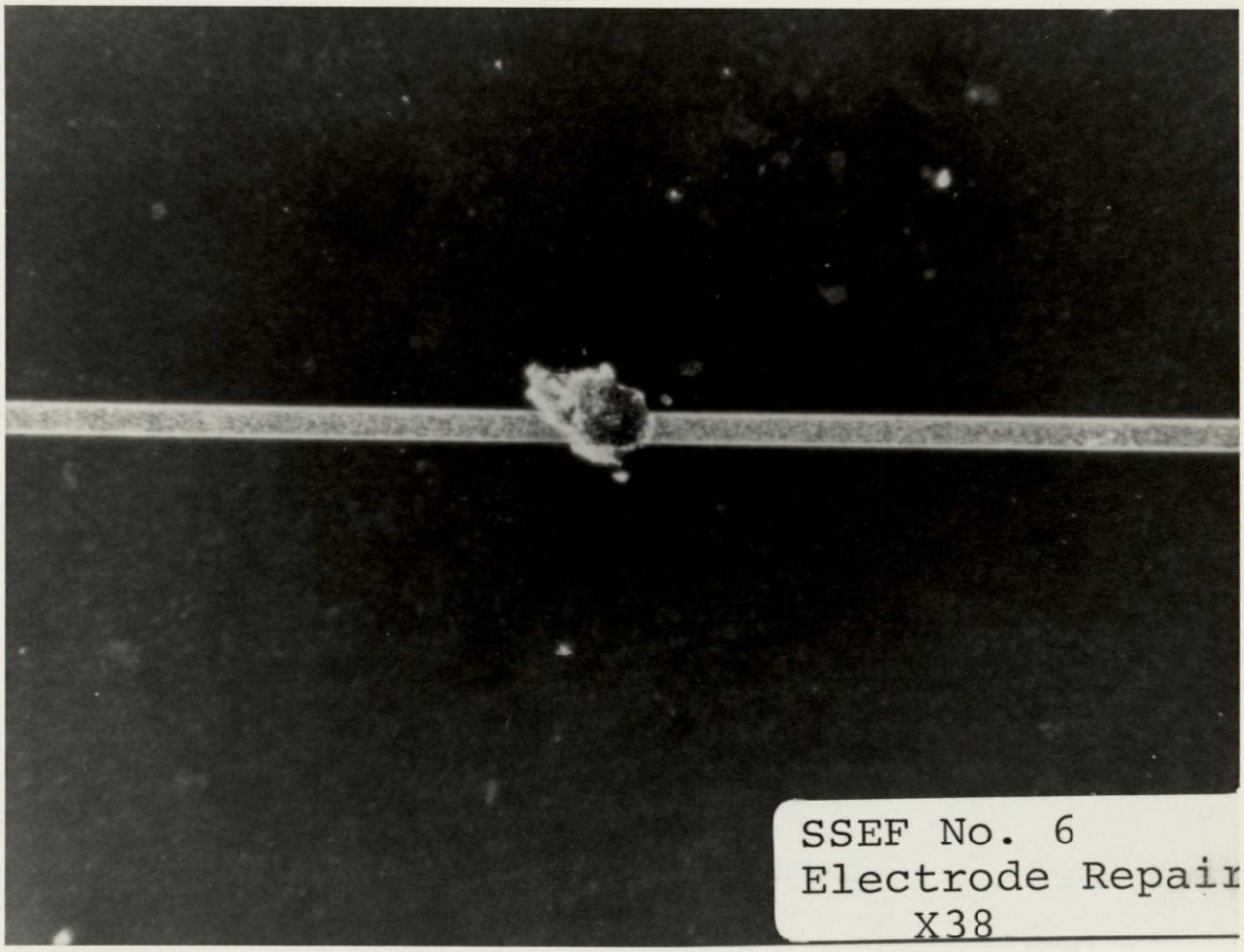

Figure 4. Single Electrode, Showing Epoxy Repair

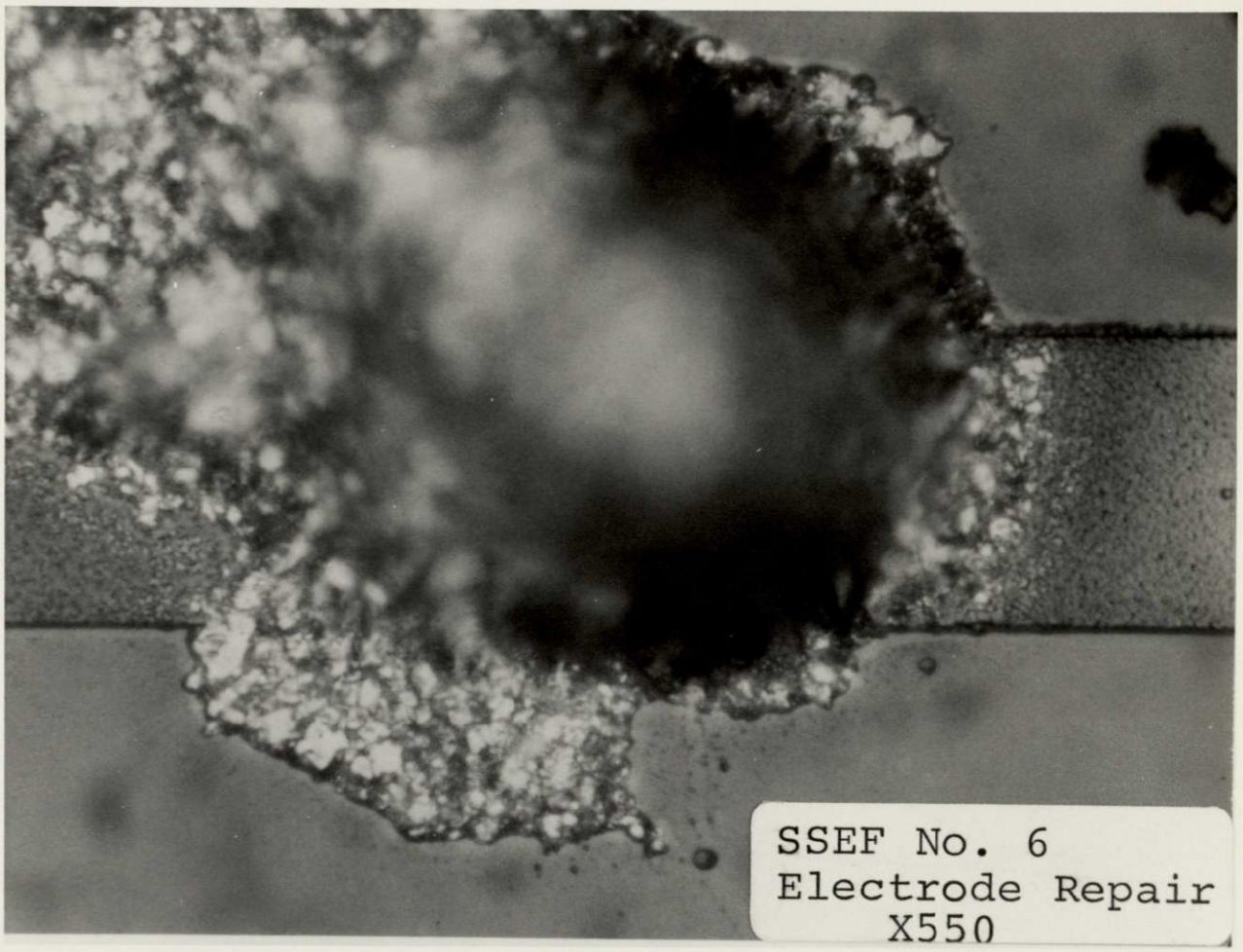

Figure 5. Wafer No. 6 Showing Epoxy Repairs

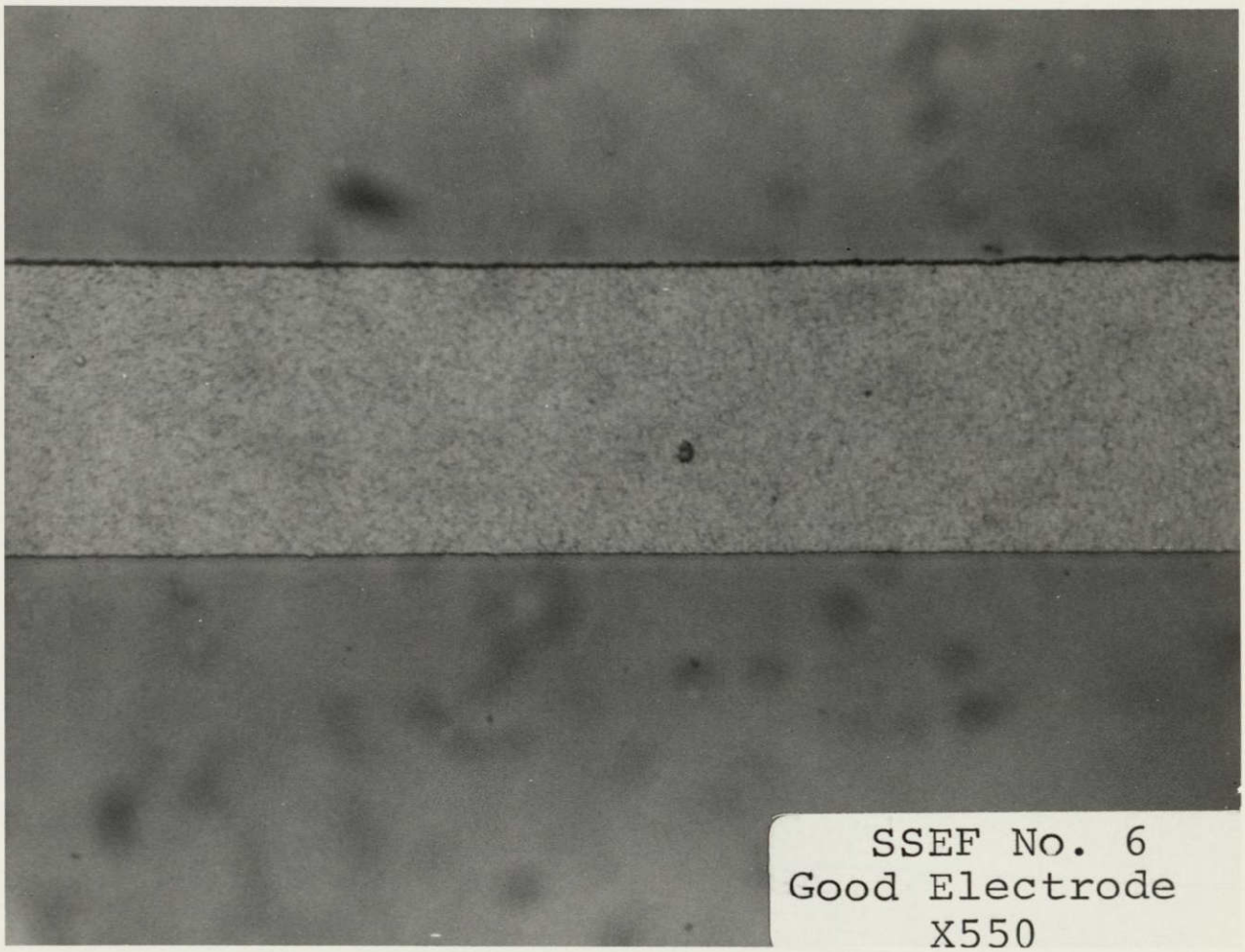

Figure 6. Single Electrode, Showing Desired (Unrepaired) Configuration

Later operational measurements indicate that the efficacy of the contact interface between the electrodes and the ceramic plate was a more serious deficiency in obtaining desired performance. The effects attributed to this problem are discussed in detail in Section II-E.

During the progress of the study, several samples developed transverse cracks. While investigating these cracks, the other samples processed by Statek were examined. Most of the units which had electrodes applied were found to have small chips or cracks near the periphery, while units which were only polished showed no evidence of cracks. Based on telephone conversations with Statek, it appears that the edge cracks are introduced by the handling and fixtures involved in their present deposition process. In any future development directed to improving the electrode interface caution should be observed to minimize or eliminate the possibility of introducing these edge defects.

3. Applied Coatings

Two problems are encountered when using uncoated PLZT wafers. First, the high index of refraction of PLZT ($\simeq$ 2.5) results in significant reflection losses at the air/PLZT interface. Second, the voltage gradient (volts/mil) required to produce the desired degree of birefringence exceeds the normal air dielectric breakdown.

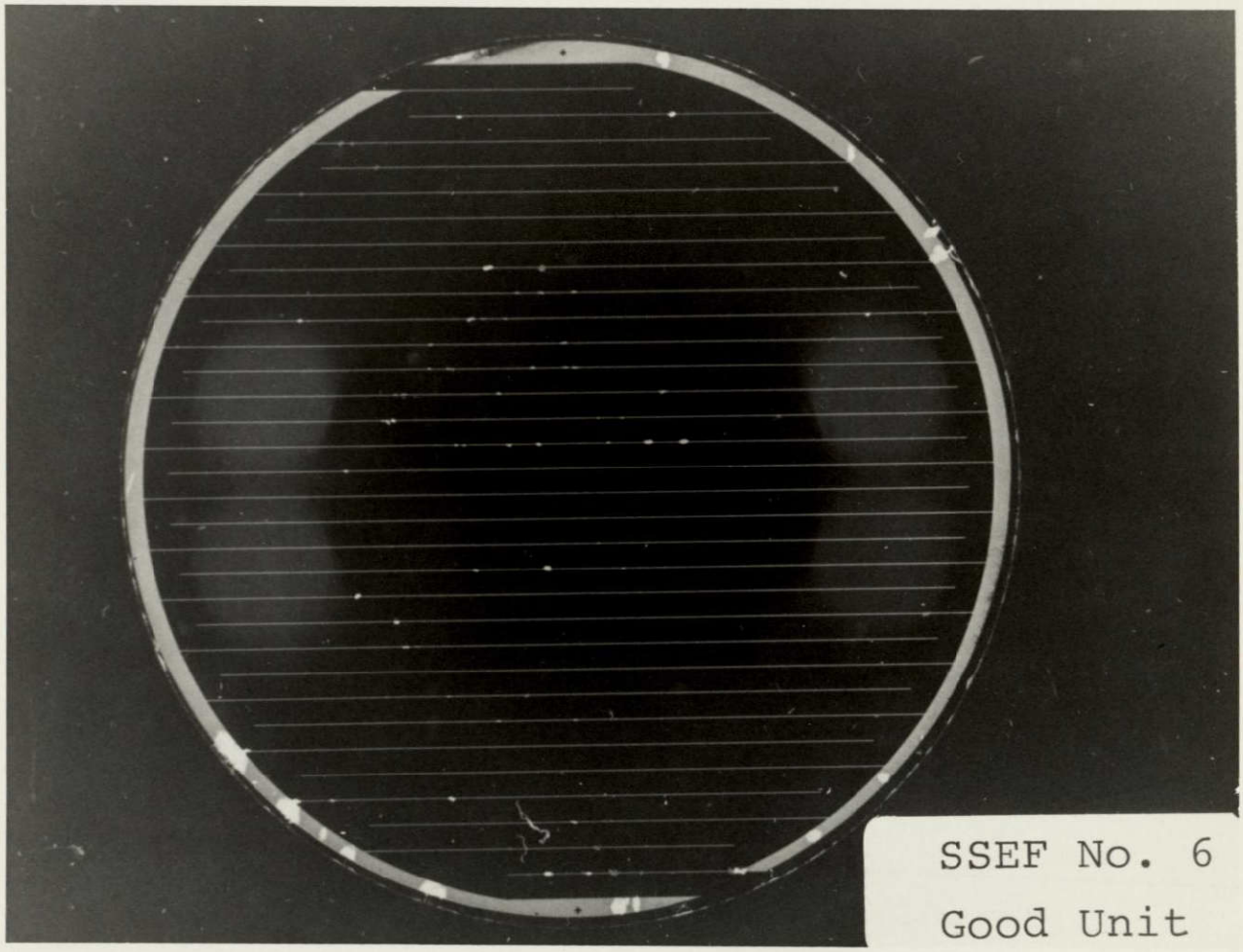

Figure 7. Wafer No. 20, Showing Electrode Discontinuities

a. Reflection Losses

The reflection (R) at each surface for normal incident light passing from medium 1 to medium 2 is given by:

$$R_{12} = \left(\frac{\frac{n_2}{n_1} - 1}{\frac{n_2}{n_1} + 1} \right)^2$$

where n is the index of refraction of the medium.

For the case of an air to PLZT interface, neglecting second order re-reflections,

$$R_{TOTAL} = R_{12} + R_{21} (1 - R_{12})$$

$$= \left(\frac{2.5 - 1}{2.5 + 1} \right)^2 + \left(\frac{\frac{1}{2.5} - 1}{\frac{1}{2.5} + 1} \right)^2 \left(1 - R_{12} \right)$$

$$= .184 + .184 (1 - .184)$$

$$= .184 + .150$$

$$= .334, \text{ or about } 33\%$$

This calculated value is in close agreement with published data[31], and measurements taken on a PLZT sample as shown in Figure 8.

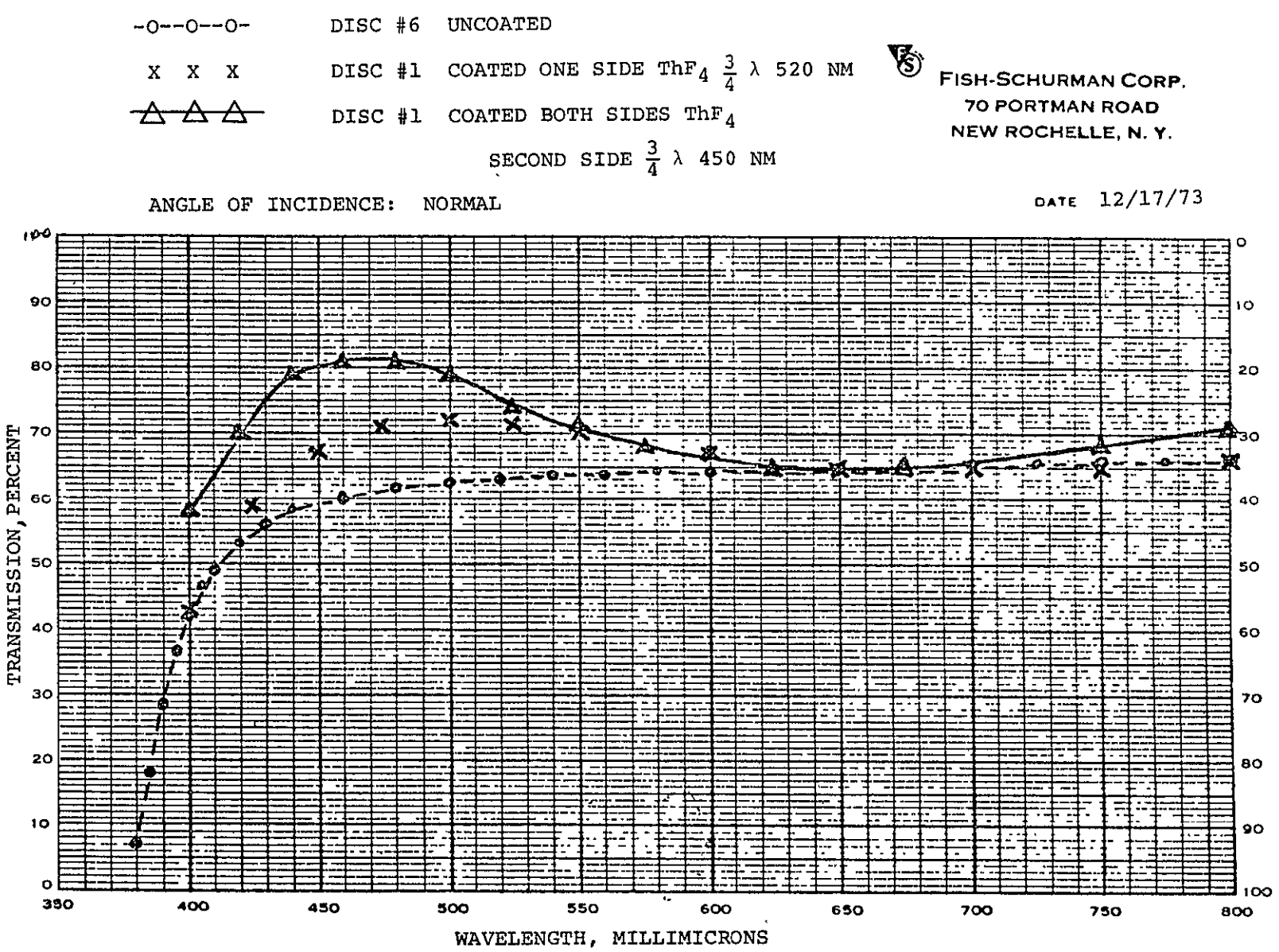

Figure 8. Spectral Measurements for Reflection From PLZT Coated Disc #1

If a dielectric film, whose optical thickness is an odd multiple of 1/4 wavelength, is placed between two homogenous media, then the reflection (R) is given by:

$$R = \left(\frac{n_1 n_3 - n_2^2}{n_1 n_3 + n_2^2} \right)^2$$

From this we see that the reflection loss can be reduced to zero if one chooses $n_2 = \sqrt{n_1 n_3}$.

Thus for air/PLZT interfaces where

$n_1 = 1$

$n_3 = 2.5$

the optimum value of n_2 should be 1.58.

A readily available material, Thorium Fluoride (Th F_4) has an index of refraction of 1.5 which closely approximates the optimum value. Several samples of the PLZT wafers were coated with this material; however, the coating thickness was adjusted to 3/4 λ rather than 1/4 λ. This thickness was chosen to improve the voltage breakdown protection provided by the coatings. Also the selected wavelength for each side of the sample was chosed at a different point in an attempt to "stagger tune" the reflection loss. The results as shown in Figure 8 are not optimum in terms of minimized and uniform

reflection loss; however, they do indicate that the basic technique can be applied to optimize the transmission. (When examining the data, recall the theoretical maximum throughput is 94%, as discussed previously).

b. High Voltage Breakdown

The electric field required to achieve $\lambda/2$ retardation, with the PLZT composition being evaluated, is on the order of 8,000 volts/cm (20 volts/mil). The normal breakdown voltage for air dielectric (as exists on the plain PLZT surface) at ambient pressure is on the order of 25 volts/mil. Since operating the filter in the spectral separation mode may well require greater than $\lambda/2$ retardation, increased voltage breakdown protection is required. Two types of coatings to provide the protection were evaluated during this program. On filter sample No. 19, a brush coat of RTV-602 was applied to both sides. RTV-602 is a silicone plastic which is highly transparent. Experiments showed that an electric field of up to 61 volts/mil could be applied to this sample before breakdown occurred. Since the RTV was applied by brush coat, rather than using a fixture, the surface was of poor optical quality. This in turn degraded the image quality through the filter. The experiments showed, however, that this approach may be useful when accomplished with adequate fixturing and molding techniques.

Filter samples Nos. 1, 6 and 20 were coated with ThF_4, primarily to investigate the anti-reflection properties; however, an expected secondary result was an increase in the breakdown characteristics. No. 20 was coated on one side with a 1/4 λ thickness, and on the other side with a 7/4 λ thickness. Voltage tests on each side of this unit showed breakdown at 43 and 61 volts/mil respectively.

Filters Nos. 1 and 6 were not initially subjected to breakdown measurements. These units had 3/4 λ coatings applied to both sides. Sample No. 1 was cracked during evaluation, rendering it unfit for optical data; therefore, it was then tested to breakdown after sealing the crack with RTV-602. Again breakdown was observed at about 60 volts/mil.

Thus, both of these methods afford significant voltage breakdown protection and should be considered when the final packaged filter configuration is designed.

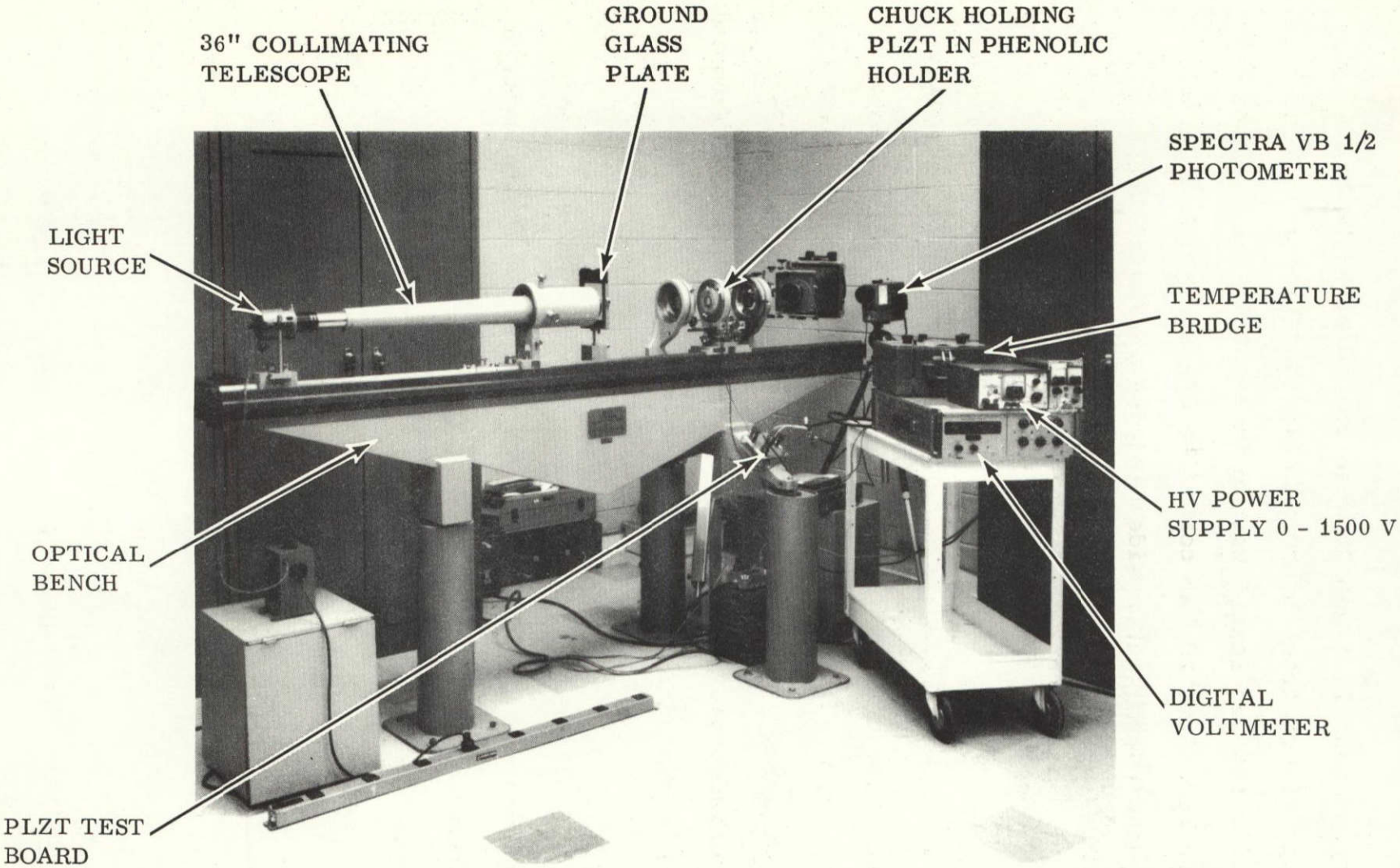

Figure 9. Optical Bench Used for Tests of PLZT Device Characteristics

C. OPTICAL TEST SETUP

1. Optical Bench Equipment

Basic electro-optical characteristics of the PLZT devices were evaluated using the test setup shown in Figure 9. A Beck research optical bench was used to mount and hold in alignment each of the optical components. A tungsten lamp was used as the source of illumination. The light from this lamp was imaged at infinity by using a 36" collimating telescope. A ground glass plate at the exit port of the telescope was used to provide a diffuse viewing object. Type HN-32 glass enclosed polarizers are installed in front and in back of the PLZT sample to serve as polarizer and analyzer. These are mounted in rotating chucks to permit rotation of their respective optic axes.

The PLZT sample itself is mounted in a supporting phenolic block, fabricated as shown in Figure 10. This block in turn was secured in a rotating chuck which could be tilted in the horizontal plane to evaluate angle-of-incidence effects.

The mounting block provided for the SSEF Study nestled the filter in a cavity in a phenolic disc. The filter was constrained in the disc by two pairs of spring fingers which also provided electrical contact to the electrodes. The fingers applied less than two grams of clamping force to the disc

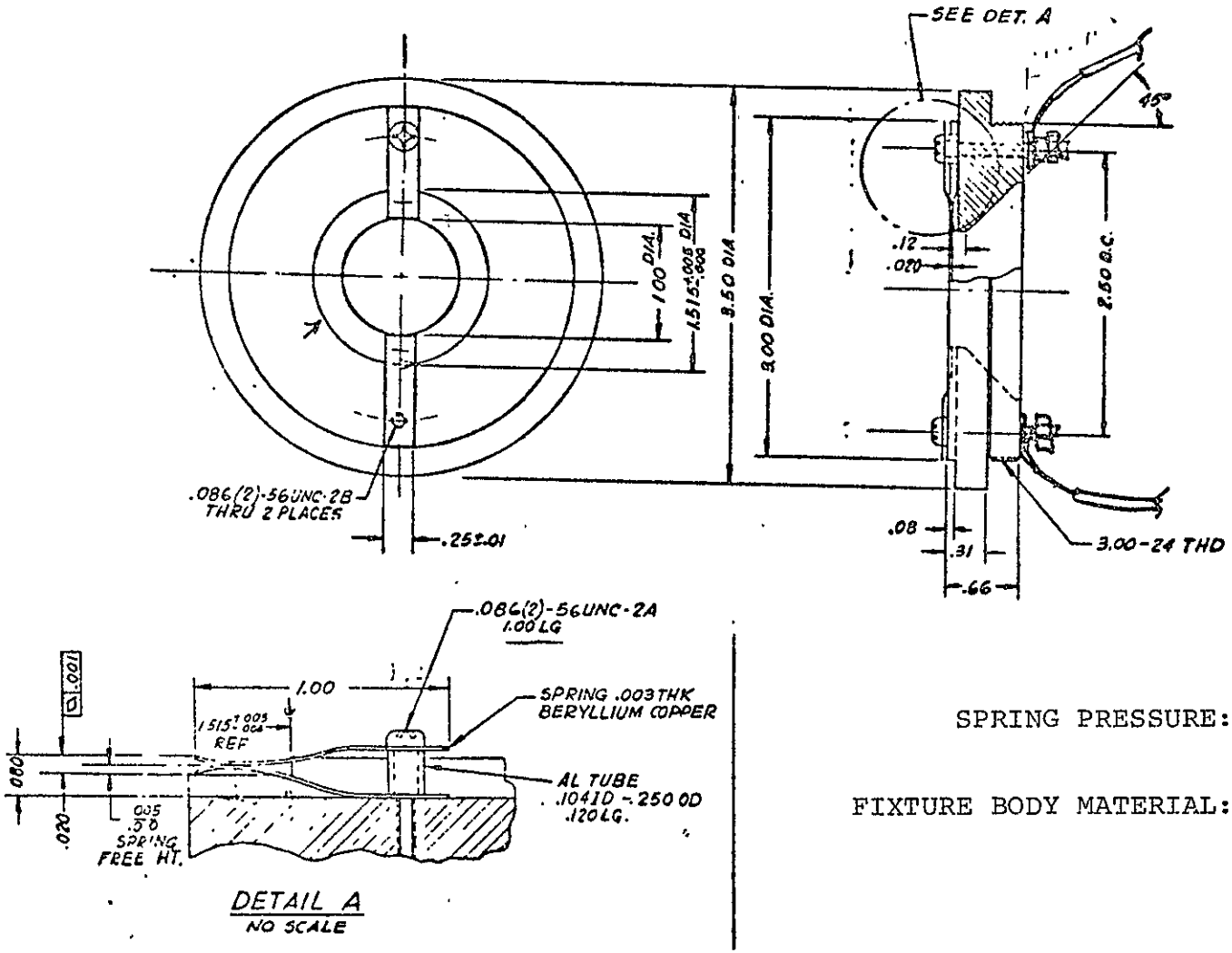

SPRING PRESSURE: UPPER 3 GRAM
LOWER 1 GRAM

FIXTURE BODY MATERIAL: PHENOLIC

Figure 10. SSEF Holding Fixture

through the curved surfaces of the springs. This applied force was $< \frac{1}{200}$ of that necessary to strain the disc for 1/2 λ of retardation.

Our experience showed, however, that the springs, although soft, caused high local stress due to misalignment or lack of uniformity of the springs. In addition, the springs can cause bending forces across the disc which, if the disc had initial edge cracks from the polishing or electroding process, can cause breakage. This method of attachment was discarded.

A modified approach located the disc loosely on its diameter in the phenolic plate. Lead wires were attached to the electrode pads using conductive cement and the leads were used to secure the substrate to the fixture disc using an adhesive tape. This method proved adequate for the purpose of the study.

An additional chuck was used to insert a fixed (multiples of 1/4 λ) retardation plate between the polarizer and PLZT element for certain of the spectral measurements.

A Spectra UB-1/2 Photometer was employed to measure the image brightness transmitted through the PLZT filter assembly. In addition, a photographic camera (film and Polaroid) was used to provide records of significant data points.

A variable power supply provided the operating voltage for the PLZT filter, and was applied through a large (10 megohms) series resistor to limit the current in the event of any arcing at the electrode contacts.

To evaluate performance as a function of temperature, a separate insulated box was used to enclose the PLZT filter. A controlled temperature air flow, supplied by a Tenney chamber, was directed through the box to set the operating temperature of the filter.

Additionally, a Perkin-Elmer scanning spectro-photometer was used to provide calibrated curves of transmission between 350 and 750 millimicrons. For these measurements the PLZT element and associated polarizer and analyzer were removed from the optical bench and installed in the spectro photometer.

The absolute value of the retardation available from a PLZT sample was measured at the RCA Laboratories by using a Leitz petrographic microscope equipped with a Berek compensator. The calibrated accuracy of this instrumentation is 5 millimicrons for measured retardation of about 100 millimicrons.

2. Petrographic Microscope Measurements

The petrographic microscope provides convenient and powerful means for measuring certain characteristics of Solid-State

Electro-Optical Filters. Variation of the birefringent retardation with applied voltage and position on the plate can be measured fairly accurately. A semi-quantitative estimate of the variation of retardation with angle of incidence of the light can be obtained very easily. On the other hand, measurements of the optical transmission of a filter device as a function of the applied voltage, angle of incidence, or other parameters are not readily made with the petrographic microscope, and are best made by the methods described previously in this report.

The petrographic microscope differs from the conventional microscope in that means are provided for accurately orienting the specimen not only azimuthally, but along other angular degrees of freedom. Provisions are also made for the introduction into the optical path of certain accessories and an auxiliary lens, as described below.

One of the most useful accessories is the Berek compensator, which can be inserted in the microscope barrel between the two crossed polars. This device adds a variable, calibrated birefringent retardation to whatever retardation (due to the specimen) already exists in the optical path. The device consists of an optically uniaxial plate of a material such as rutile (TiO_2) cut with the optic axis normal to the plate. When the optic axis of the compensator plate coincides with

the direction of the light path through the microscope, there is no additional birefringence. As the plate is tilted so that the light is transmitted at an angle to the optic axis, birefringence is introduced. The angle of tilt is measured on a scale external to the barrel of the microscope, and from calibration data, the corresponding birefringent retardation can be obtained.

Measurements are made by adjusting the azimuthal orientation of the specimen so that its birefringent retardation is in the opposite direction to that introduced by the Berek compensator. The compensator is then adjusted so that its retardation exactly cancels that of the specimen, and the light is extinguished by the crossed polars. The calibrated retardation provided by the compensator at this point is equal and opposite to that of the specimen. Using this technique we are able to estimate retardations to an accuracy of about 5×10^{-7} cm, even on specimen areas no more than several microns on a side.

The variation of retardation with the direction of the incident light can be estimated very conveniently by observation of the conoscopic figure through the petrographic microscope. The principle of conoscopic observations can be explained by reference to Figure 11. Each point on the specimen is imaged by the objective lens onto a point in the image plane, as shown by the dashed lines in the figure. In conventional microscopy the occular lens system is focused on this magnified

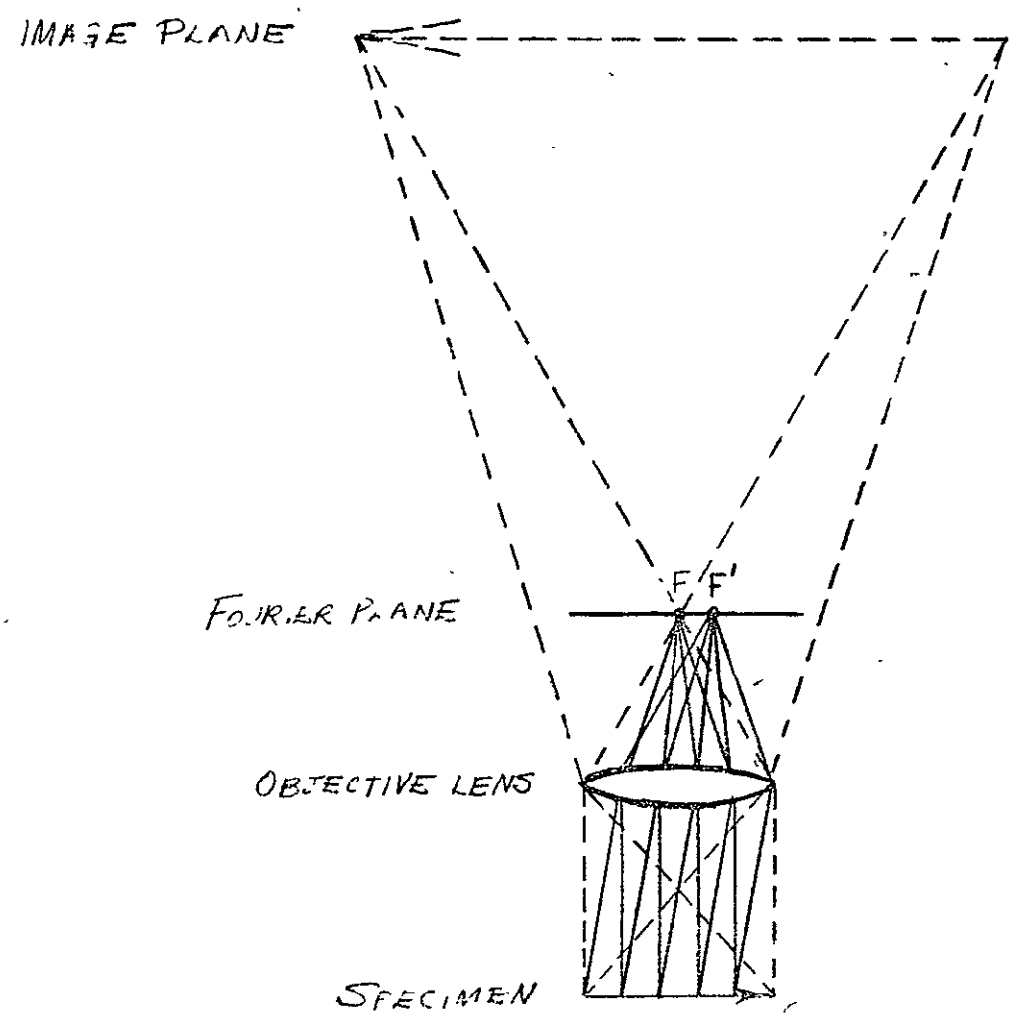

Figure 11. Optical Planes in Conventional and Conoscopic Microscopy

real image of the specimen. Another plane of special significance is the Fourier plane of the objective, which is located one focal length from the lens on the side away from the specimen. Note that all rays passing through the specimen in a direction parallel to the axis of the microscope are brought to a focus in the Fourier plane at point F. Any other parallel set of rays will also be brought to focus in this plane, but at a different point such as F'. This focusing behavior is shown by the solid lines on the figure. (The Fourier plane owes its name to the fact that when collimated monochromatic light is used to illuminate the specimen, what is formed in this plane is essentially the diffraction pattern, or Fourier transform of the speciment.)

The petrographic microscope is equipped with an auxilliary lens (called the conoscopic or Bertrand lens) that may be inserted below the ocular lens system to permit the latter to focus on the Fourier plane rather than on the image plane. The specimen as such is no longer in focus. Each point in the image seen in this case corresponds to a particular direction of light passing through the specimen, rather than to a point on the specimen. The conoscopic system can be used to observe the dependence of birefringent retardation on the direction of incident light by viewing the specimen between crossed polars, and ensuring that the illumination is sufficiently uncollimated that the desired range of incidence directions is present.

D. TEST TYPE DESCRIPTIONS

Described in this section are the types of tests (and test methods) performed on the PLZT samples using the equipment described in Section II-C. The test types and test program were selected to provide qualitative and quantitative data on the parameters of importance in the planned application. A number of the tests were performed on several samples to verify the repeatability of characteristics in different units.

1. Neutral Density Transfer Curve

The optical bench setup was used to obtain the average transmission of a crossed polar/PLZT filter system as a function of applied dc voltage. The Spectra brightness meter was positioned so as to view an area whose diameter was approximately four times the separation between adjacent electrodes. Thus, the measurement integrated the transmitted light over this area (including any undesired effects at the electrode boundaries)

The transmission was measured from zero volts to the point of maximum transmission which should correspond to $\lambda/2$ retardation (about 20 volts/mil or 750 volts total). Data was obtained for both polarities of applied voltage, in the conventional or "normal" polar mode, i.e., polarizer and analyzer axes crossed at 90°, and both at 45° to the transverse field on the PLZT sample. One run of data was purposely taken with the polarizer and analyzer axes aligned at 0°, and both at 45° to the PLZT

axis. This data was then plotted as optical density $\left(OD = \log \frac{1}{T}\right)$ versus applied voltage. Additionally, photographs of the full filter plate at different potentials were taken to record the qualitative optical quality.

To confirm the theoretical ultimate performance for the two polar/PLZT system, similar data was obtained for the polarizers with zero potential on the PLZT filter, with the polarizer axes crossed and parallel. The values obtained were OD = 4.08 and OD = 0.789. This represents a theoretical maximum range of 1900:1, and a minimum insertion loss of 6:1.

2. Temperature Effects

To evaluate the effect of temperature variations on the PLZT sample, the special test chamber described in Section II-C-1 was used. The transfer curve of density versus voltage was used as the measurement criteria, since it provides a direct indication of the field induced birefringence. Data was taken over the range of 0°C to +60°C, at 10°C increments. Transfer curve and photographs were obtained at each temperature plateau. For these tests, the polarizers and filter were again configured in the "normal" mode.

3. Resolution

An Air Force, 3 Bar-1951, Resolution Test Chart was used to evaluate the effect of the polar/PLZT assembly on the system resolution. This chart was mounted at the entrance port to the

collimator. A Taylor-Hobson 30 mm lens was used in conjunction with a microscope to view the image through the filter assembly. Data was obtained on the visual limiting resolution as a function of applied voltage, over the range of zero to $\lambda/2$ retardation.

4. Angle of Incidence

The effect, on transmission, of varying the angle of incident light was observed by rotating the PLZT plate about a vertical axis while maintaining the other elements of the system in their original configuration. Data was taken at 5° increments for four values of applied voltage.

The conoscopic system of the petrographic microscope was also used to view the effects of angle of incidence on the retardation through the sample. The aperture size chosen for the measurement permits observation over a cone of illumination with 14.5° half-angle, which corresponds to approximately f/2 optics.

5. Time Constant

Response time of the PLZT samples was evaluated by applying step changes in applied voltage, through a series protective resistor. The effective time constant was measured by observing the time required for the transmission density through the filter to stabilize after each voltage step. The protective resistor was used to limit the current in the event that voltage breakdown would occur at the surface of the PLZT sample.

6. Anti-Reflection Coatings

The transmission of PLZT samples, with anti-reflection coatings applied to the surfaces, was measured as a function of the wavelength of the incident light. This data was compared to similar information obtained for uncoated PLZT samples.

In addition, the increase in voltage breakdown provided by the presence of the coatings was measured by applying voltage through a series protective resistor (1 megohm) and observing the point at which arcing occurred. This data was again compared to the results obtained for uncoated samples.

7. Retardation Versus Voltage

The petrographic microscope was used to measure the transfer curve of retardation (in millimicrons) versus voltage, from 0 to 900 volts. For a fixed voltage of 500 volts, retardation measurements were made as a function of position between two adjacent electrode fingers. The orientation of the PLZT sample with respect to the transit direction of the microscope stage micrometer was such that a line was traversed at an angle of 45 degrees to the electrode strips. Measurements were taken at 100 micron intervals over most of the region, and at 25 or 50 micron intervals near the electrode.

Again with 500 volts applied, the retardation was measured at various widely separated parts of the sample, to evaluate the

uniformity of retardation. These measurements were taken at points that were nearly midway between electrode pairs.

8. Shading

To evaluate the shading across the PLZT surface, the optical bench setup was used. A film negative was taken through the polar/PLZT sample, and also with the filter removed for reference. The film density was then measured at various points within the image area using a microdensitometer to permit plotting absolute transmission versus position.

In addition, the Spectra brightness meter was used to measure brightness at nine points within the useful area of the filter. These measurements allow comparison of the average transmission at each point. Again reference measurements of the light source shading were taken at the same points with the filter replaced by a fixed retardation plate adjusted to give the same relative brightness.

9. Spectral Response

The spectral transmission of a PLZT sample between crossed polars was observed by photographing the transmission for various combinations of applied voltage and fixed retardation plates. The retardation plates were used to provide greater than $\lambda/2$ total retardation while maintaining the applied voltage within known safe limits.

Additionally, a Perkin-Elmer scanning spectro-photometer was used to plot the relative spectral transmission between 350 and 750 millimicrons for selected combinations of filter voltage and retardation plates, thus allowing comparison with the data described above.

E. DISCUSSION OF ELECTRODE CONTACT PROBLEMS

In the course of evaluating the electro-optical properties of the filters fabricated during this project, a number of effects were observed that all appear to be related to the interface between the metallic electrode fingers and the PLZT electro-optical ceramic. The effects are generally deleterious to device performance. Some experimentation, to determine the probability of a solution to the observed problems, was performed during the course of this project.

The first effect to be observed was an inhomogeneity of the birefringent retardation in the vicinity of the electrode fingers when dc was applied to the electrodes. This phenomena was most evidenced at every other finger, i.e., those having a common polarity.

Another effect is that when the dc is turned off, birefringence persists in the immediate regions about alternate electrodes. This so-called "white-line effect" vanishes only gradually, and is responsible for a limited dynamic range once the filters have been cycled electrically. Figures 12 and 13 shows the nature of the observed problem when operating the device in the variable neutral density mode and spectral filter mode, respectively. A third effect that is probably related to the interface between the metallic electrodes and the ceramic is the long times required (greatly in excess of the RC time-

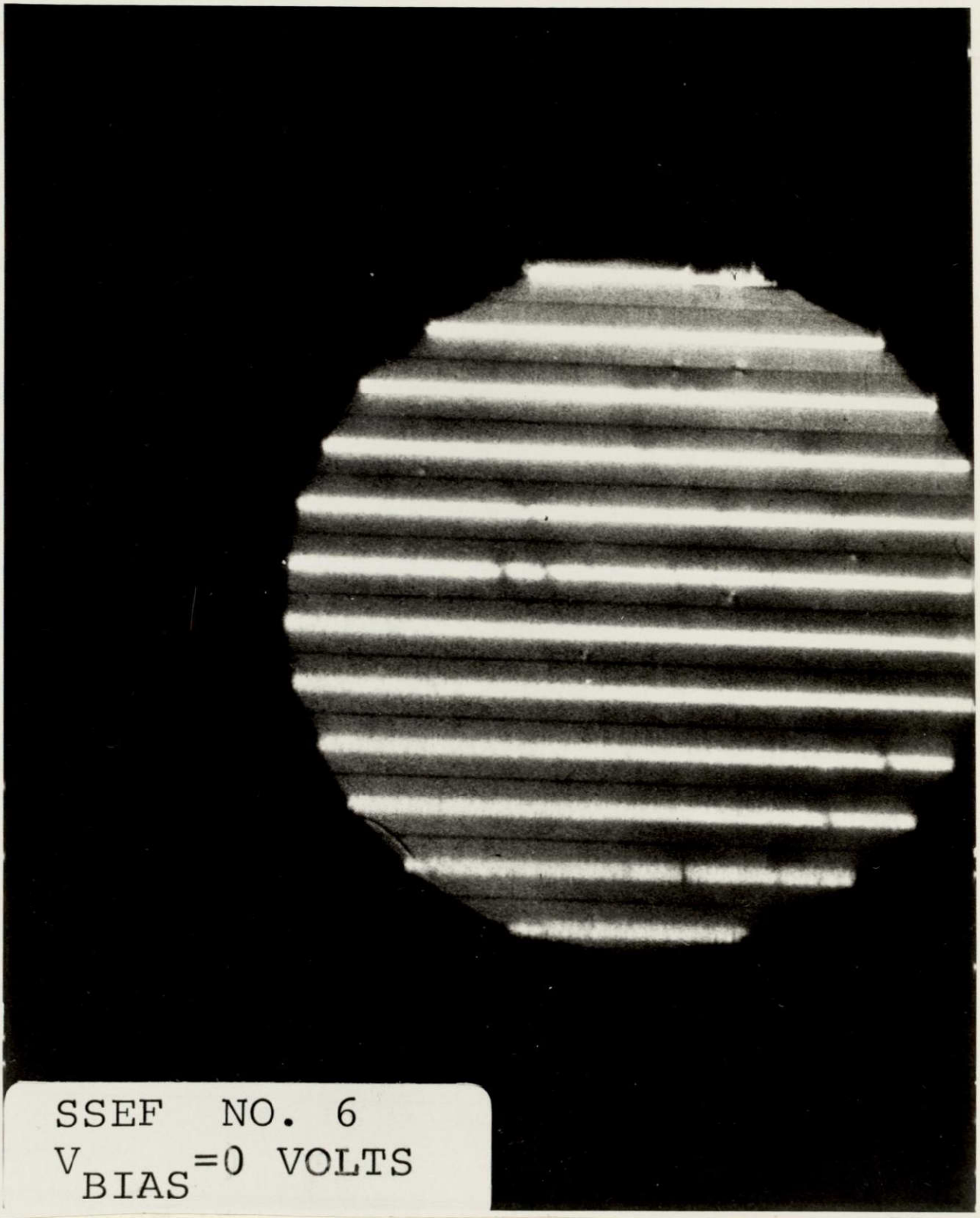

Figure 12. Birefringence Effect With Operation in the Variable Neutral Density Mode

constant) for stabilization of the transmission through the filter after the applied voltage is abruptly changed. The long-range variation of birefringent retardation with position on the filter may also be related to the metal-ceramic interface. These phenomena are described in more detail later in this report, and in Monthly Reports No. 5 and 7. It is important to note that these effects do not seem to have occurred in many of the filter devices investigated at Sandia Laboratories. The ceramic, fabrication, and electrode processing employed in the Sandia devices are nominally identical to those employed for the devices reported here.

The observed behavior, especially the fact that these phenomena occur at every other finger, suggests strongly that the problems are due to contacts between the metallic fingers and the ceramic substrate that block the electrical carrier that is responsible for the (small) conductivity of the ceramic. If such is indeed the nature of the contacts, then the following sequence of events is expected to occur.

Application of a voltage across the electrodes drives the carriers in the ceramic away from one electrode. (Replenishment of these carriers in the depleted region of the ceramic is prevented by the blocking contact.) The depleted region has a higher resistivity than the bulk of the ceramic. Consequently a larger electric field, and a greater field-induced birefringence occurs in the depleted region than elsewhere. After the external

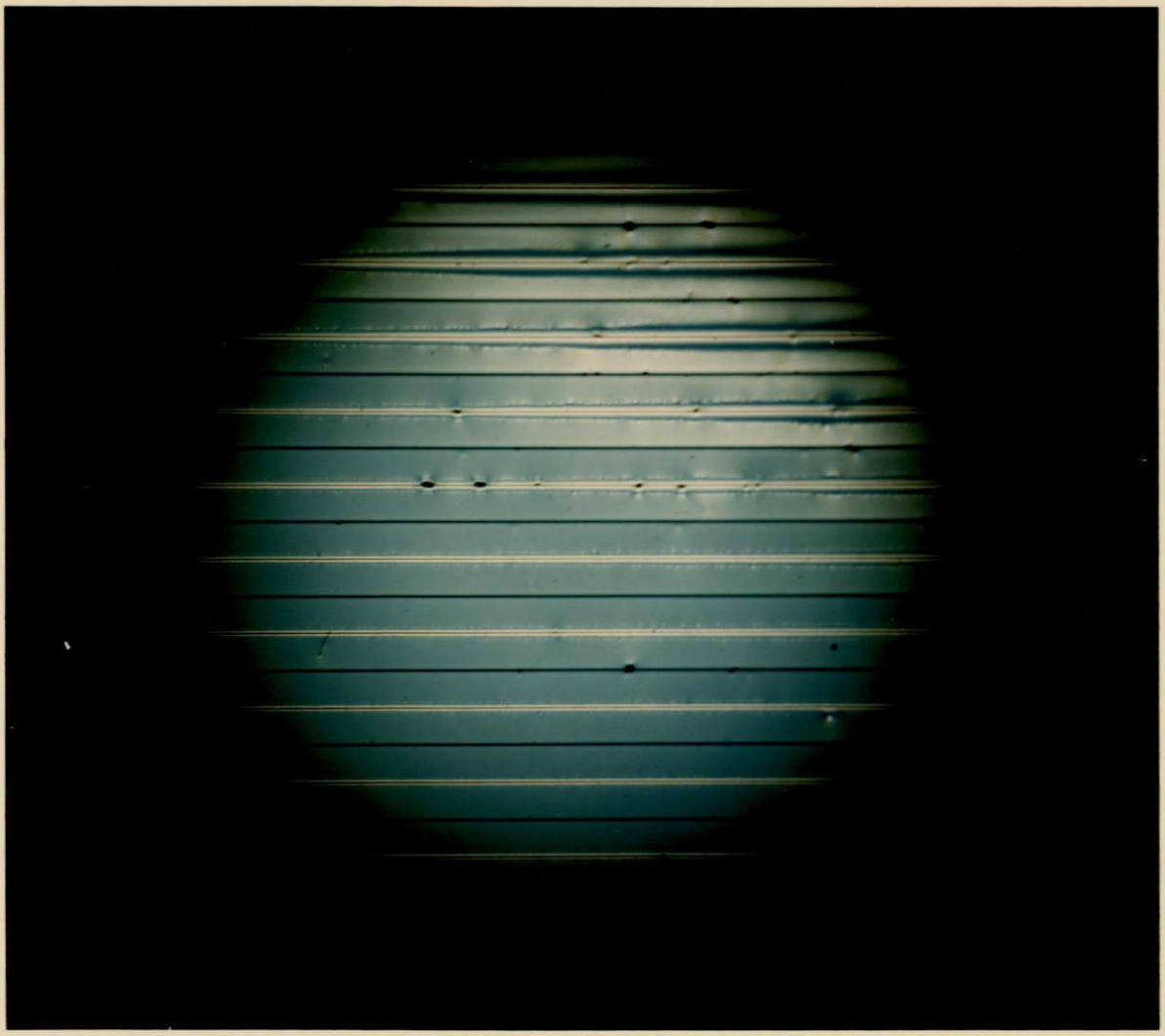

Figure 13. Birefringence Effect With Operation in the Spectral Filter Mode

electrical potential is removed it takes appreciable time for the carriers to relax back into the high-resistivity depleted region and restore electrical neutrality there. Thermal excitation of the carriers out of traps in the non-depleted region may be necessary before re-equilibration can take place. Until this happens, space-charge effects create an electric field that causes the region near the electrodes to exhibit birefringence. The slowness of these effects is probably responsible for the long stabilization times required after an abrupt change in the applied voltage.

The characteristics of the interface between the electrodes and the ceramic substrate can change somewhat in different parts of the filter plate. For constant applied voltage the electric fields in the immediate vicinity of the electrodes may therefore be greater in one part of the plate than in another. If the field is greater near an electrode it is necessarily smaller in the adjacent region more or less remote from the electrode. (This is because the average electric field is the same for all interelectrode gaps of equal spacing.) The electric fields in the "bulk" of the ceramic may therefore be different in various parts of the plate. This may account for the observed long-ranged variation in birefringent retardation.

Problems due to blocking contacts can sometimes be solved by proper treatment of the substrate surface, choice of electrode materials, and/or electrode deposition processes. The following

experiements which were performed indicate that the solution to these problems may lie in obtaining a clean, sufficiently intimate contact between the metallic electrodes and the PLZT ceramic. A thin strip of plastic-backed adhesive tape was placed on the clean, un-electroded surface of a PLZT wafer. The region on both sides of the strip was rubbed with gallium-indium eutectic alloy. This metal, which is liquid at room temperature, differs remarkably from mercury in that it wets nearly any surface with which it comes in contact. The plastic tape was removed, leaving what was effectively a pair of electrodes separated by a gap whose width was approximately the same as those in the filter devices. The birefringence was observed in the petrographic microscope while a dc voltage was applied to the electrode pair. Neither inhomogeneity of the birefringent retardation in the vicinity of the electrodes nor persistence of birefringence after removal of the voltage could be observed.

In a separate experiment, an array of chrome-gold electrodes was deposited on a PLZT ceramic plate using an evaporation-mask rather than a photoresist technique. The interelectrode spacing was considerably greater than that used for the filter plates. There was a mask-alignment problem that resulted in the actual edge of the electrode consisting of a thin, optically transparent layer of chromium. A bright line at this edge could be observed both during and after the application of voltage when the plate was viewed between crossed polars, but the effects were much less prominent than what is observed on the

photoresist-fabricated plates. The bright line disappeared fairly rapidly after the removal of the voltage. Measurements of the retardation using a Berek compensator indicated no variation across the gap. The inhomogeneities appear to be confined to a region no more than a few microns wide near the electrode.

Thus one concludes that the observed problem represents a serious shortcoming of the devices examined to date; however, it appears amenable to solution. The solution of this problem should clearly be a high priority item in the future studies.

F. TEST RESULTS (OPTICAL BENCH)

1. General

This section contains the test results obtained on various PLZT samples using the optical bench and other associated optical test equipment described in Section II-C. Test methods are described in greater detail in Section II-D. Performance measurements with the filter assembly integrated with a television camera are discussed in Section II-H.

During the process of the evaluation program a number of the test samples developed cracks across their total geometry. These were due in some cases to operating at a potential high enough to cause arcing. The mechanical strain induced in the ceramic by the arcing appears to be sufficient to result in breakage. The initial presence of small edge cracks or chips in the samples is thought to emphasize the possibility of cracking either as a result of arcing or as a result of the mechanical strain induced by the normal voltage field. Several samples also developed cracks without being subjected to arcing although this may have been due to pressure of the contact fingers initially used for mounting, or to mechanical shock induced by handling. Filter sample No. 6 survived the entire gamut of tests without developing any cracks; thus the majority of data presented was obtained with this unit.

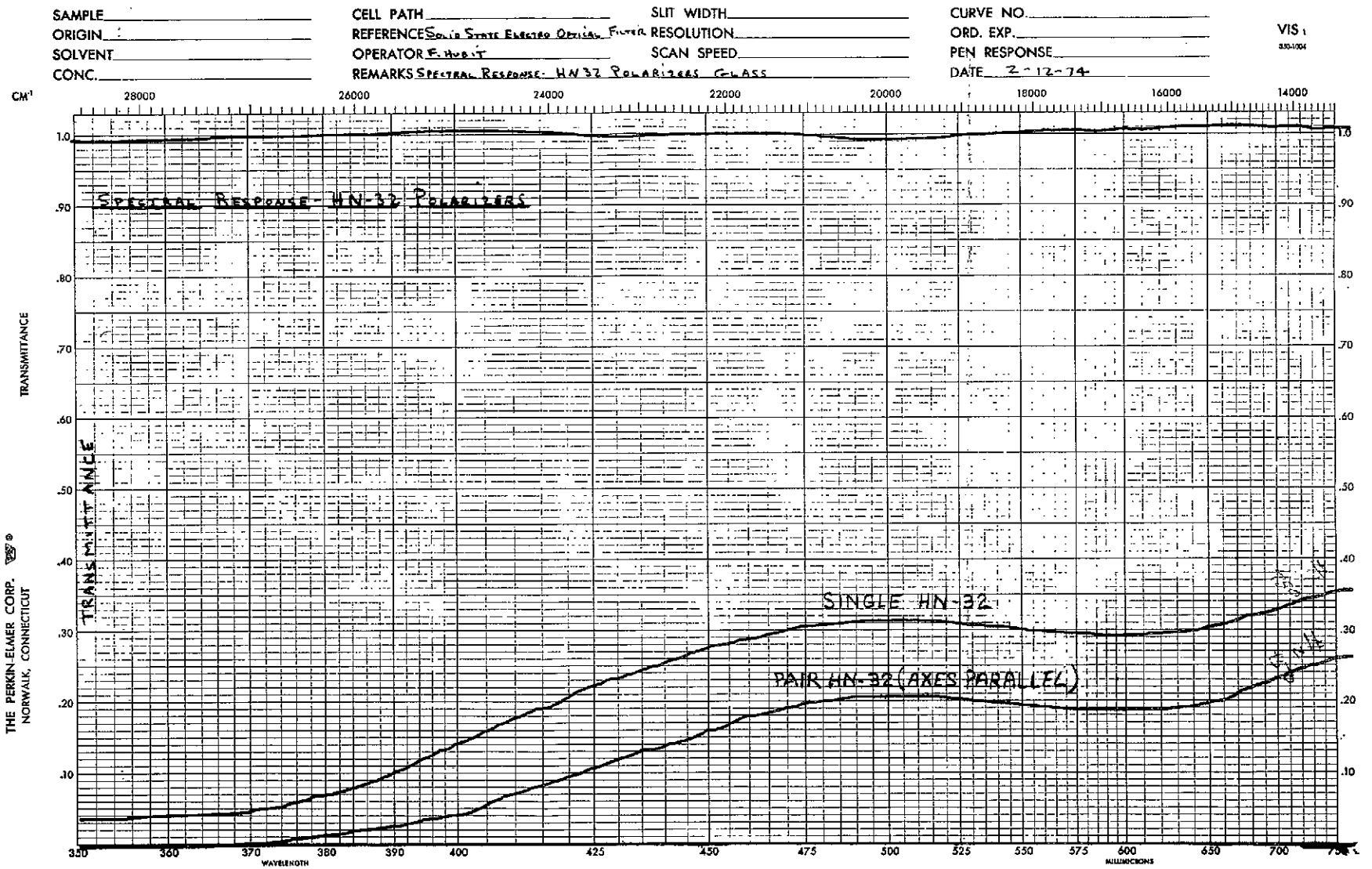

Figure 14. Transmission Measurements on Type AN-32 Polarizers With Axes Parallel

FOLDOUT FRAME 1

FOLDOUT FRAME 2

2. Neutral Density Transfer Curve

The stated goal of the program (Work Statement, Paragraph 3.2.3) is a relative continuous attenuation of 140 to 1, and a minimum attenuation equivalent to an f/4 lens stop or less. If we assume the f/4 is referenced to the normal Apollo GCTA lens (f/2.2), the maximum transmission should be 30% (N.D. = 0.52). The 140 to 1 relative attenuation corresponds to an N.D. range of 2.15.

The maximum transmission is established by the performance of the polarizers in their parallel state, coupled with the unbiased insertion loss of the PLZT sample. Catalog data[9 1] shows the expected transmission of type HN-32 polarizers with axes parallel as 25%. Measurements as shown in Figure 14 indicate the actual value for the pair used in the test to be about 20%. The PLZT transmission will be between 64% (uncoated case) and 80% (present A.R. coatings). Thus the anticipated maximum transmission for the crossed polar case with $\lambda/2$ retardation in the PLZT is about 16% (N.D. = .795).

In evaluating the range available with the existing PLZT samples, the "white line" effects are typically observed after the first application of full voltage, starting from an unpoled state.

Figure 15 shows the transfer curve obtained by starting from such an unpoled state (point A), moving through 850 volts (point B), and returning to 0 volts (point C).

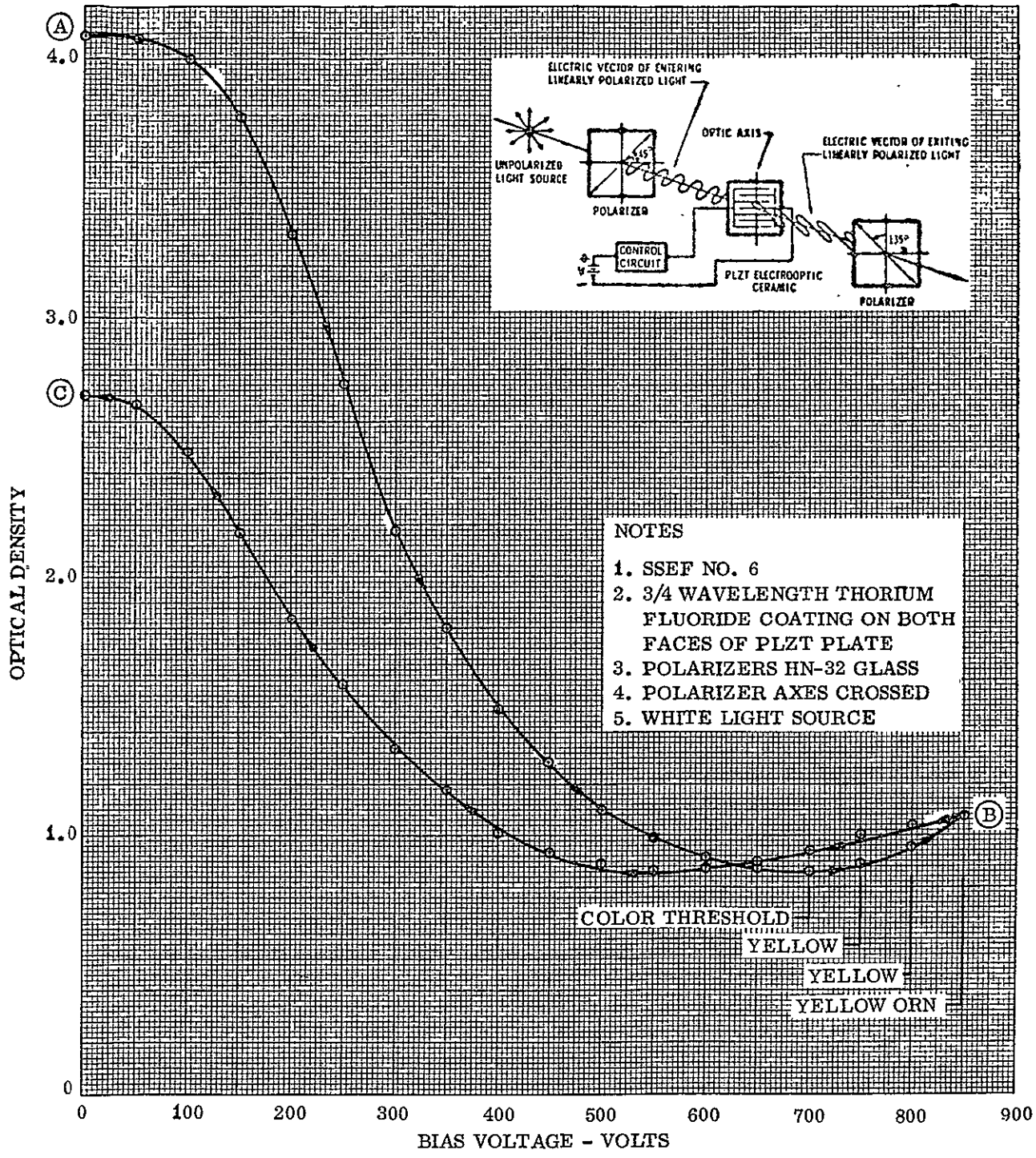

Figure 15. Transfer Curve of PLZT Sample, Going to Full Voltage

The curve from A to B agrees closely with previously published data[13], and provides a density range from OD. = 4.08, to OD = 0.87 (delta of 3.21) which is a dynamic range of 1600 to 1.

On the return curve from B to C the dynamic range appears to be severely compressed; however the data is misleading. Due to the presence of the white lines (residual polarization) within the photometer field-of-view, a bias is introduced into the measurements. The photometer measures the average brightness of an area which includes four electrode pairs. Thus to obtain an indication of the maximum device capability it is required that one start with a normalized PLZT plate.

The test was repeated with the polarities reversed, yielding the curves in Figure 16. Again the reduced range is observed due to the white line effect. The hysteresis shown in Figure 16 is believed to be in part attributable to the same effect. Until samples can be obtained which solve this problem, an exact measure of included hysteresis cannot be obtained.

All of the previous data was taken in the normal mode of operation, wherein the polarizer axes were orthogonal, and the PLZT optic axis was at 45° to the polarized light vector. A set of data was obtained for the case of parallel polarizers, yielding the curve of Figure 17. Here again a hysteresis

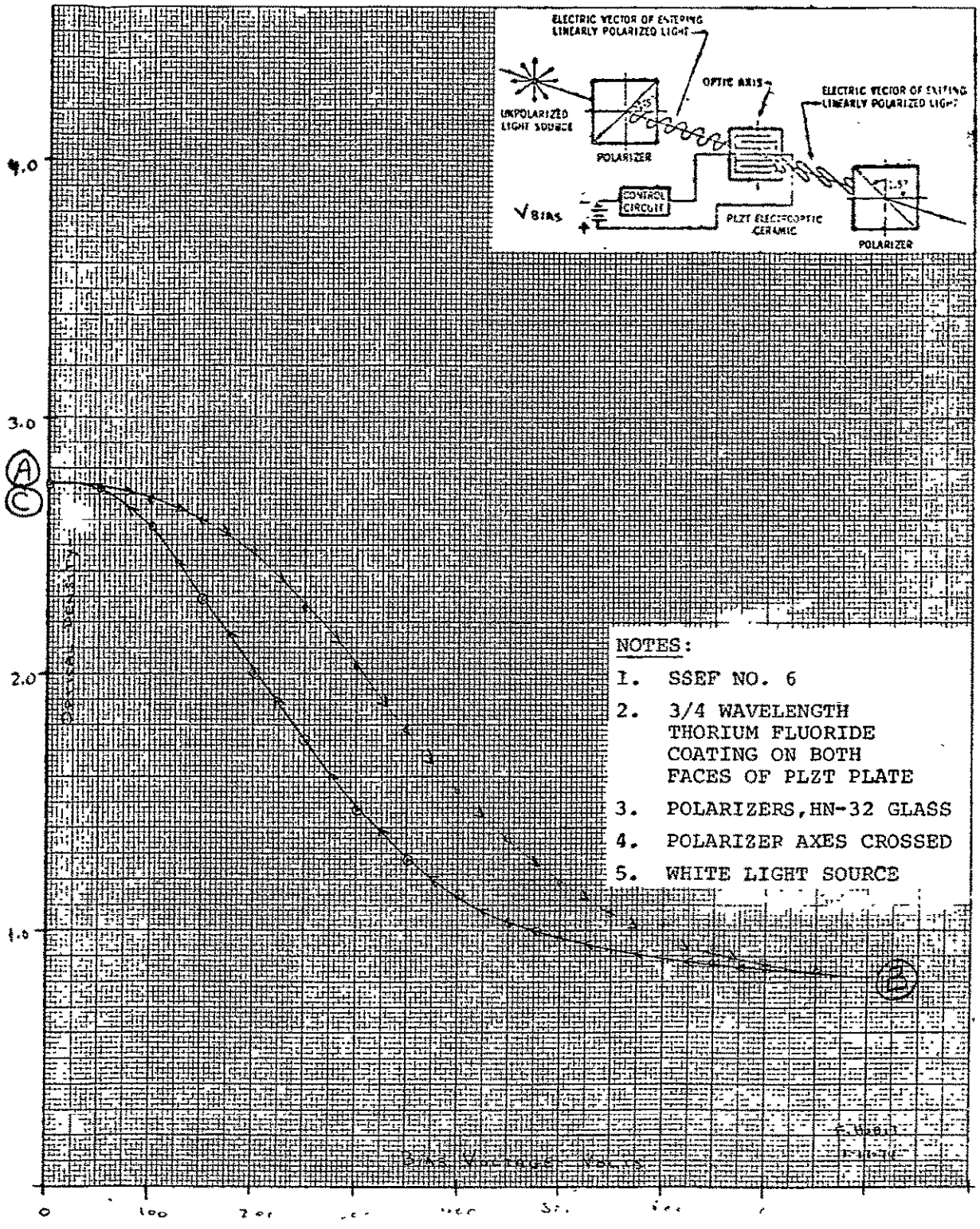

Figure 16. Transfer Curve of PLZT Sample, With Reversed Polarity

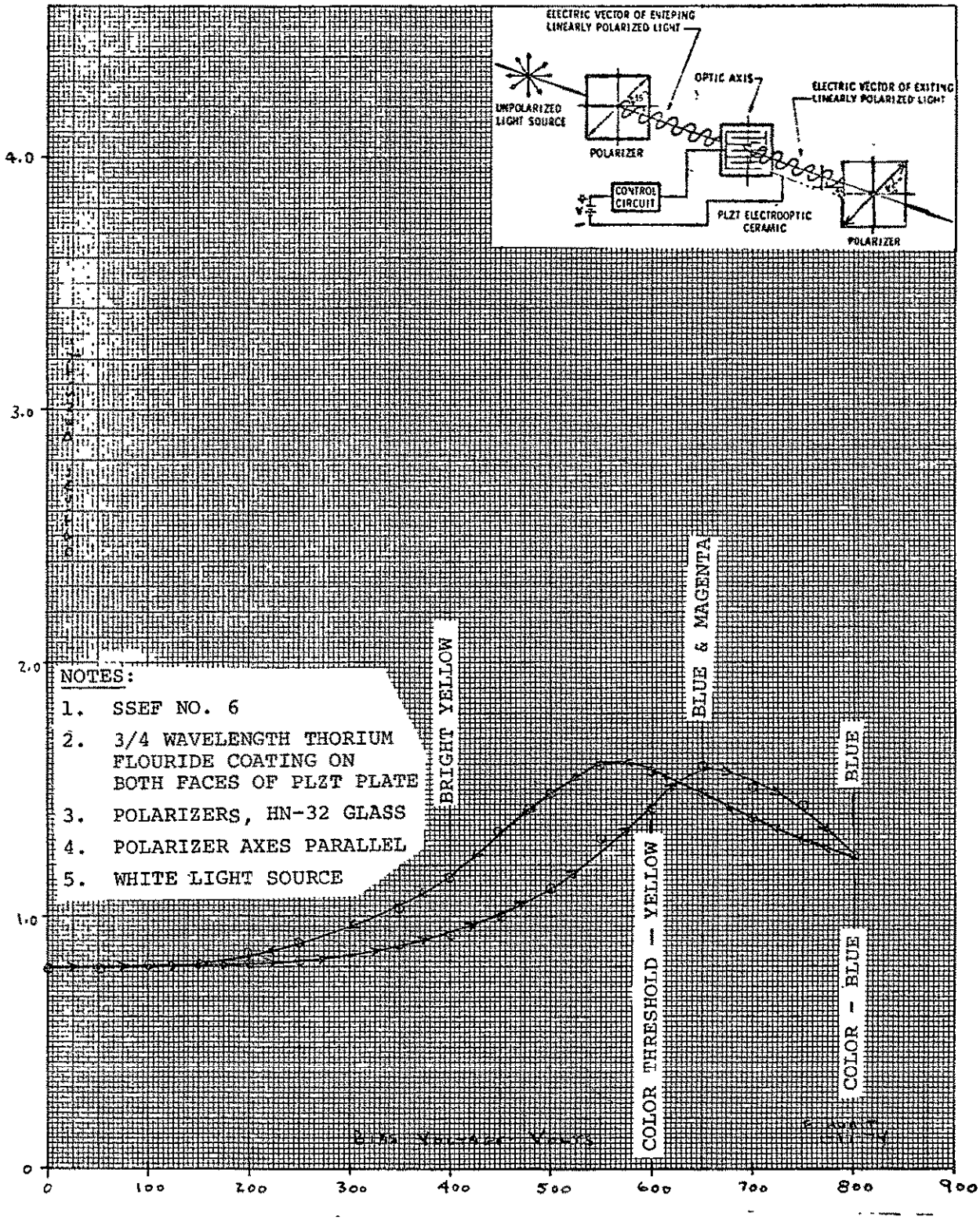

Figure 17. Transfer Curve of PLZT Sample With Parallel (Rather Than Orthogonal) Polarizer Axes

effect was noted which cannot be readily separated from the residual electrode interface problem. Since the light source used was achromatic, a restricted density range was obtained. For a monochromatic source the inverse of Figure 15 would be expected.

The maximum transmission for the crossed polar/PLZT assembly with the PLZT biased to $\lambda/2$ retardation is about 14% which agrees very closely with the predicted value. The density range starting from an unpoled state more than meets the objective range of 2.15. In fact, the range after degradation by the white lines nearly meets the specification. A small improvement in the electrode contacts would thus ensure an adequate dynamic range in the device.

With regard to the maximum transmission, improvement can result from obtaining better polarizers. The present units are equivalent to f/4.5 for the polarizers alone. The combined polarizers and PLZT are equivalent to an f/5.1 system, which is slightly poorer than the stated objective. Other available polarizers such as HN-38 do provide increased transmission, but at the penalty of reduced extinction (crossed axes).

3. Temperature Effects

The controlled temperature chamber described in Section II-C-1 was used to obtain data on the density transfer characteristic as a function of PLZT sample temperature.

Data was taken at 10°C plateaus, from 0°C to 60°C. Initial data at 20°C was used as a baseline reference.

Figures 18 through 25 show the transfer curve data obtained at temperatures where changes were significant.* Figure 26 shows the results obtained at 20°C, several days after the completion of the temperature testing, and indicates the eventual return to a normalized condition. Curves of density versus temperature, for several fixed control voltage levels, are shown in Figure 27.

Photographs of the full field transmission were also obtained at most of the temperature plateaus. These photographs show white line effects similar to those discussed previously. In addition, at 60°C, an additional defect was noted in one corner of the sample, as shown in Figure 28. The defect consisted of lines extending part way across the plate, intermediate to the normal electrode lines. The exact cause of this defect is not known; however, it was a transient effect, disappearing after return to room temperature.

Several significant effects were noted in examining the results of these tests. As the temperature was increased to +60°C, the density for a fixed voltage increased slightly. Conversely, as the temperature was reduced to 0°C, at 500 volts the density increased slightly while for lower voltages significant decrease

*Note the returns through the (nominal) 20°C reference.

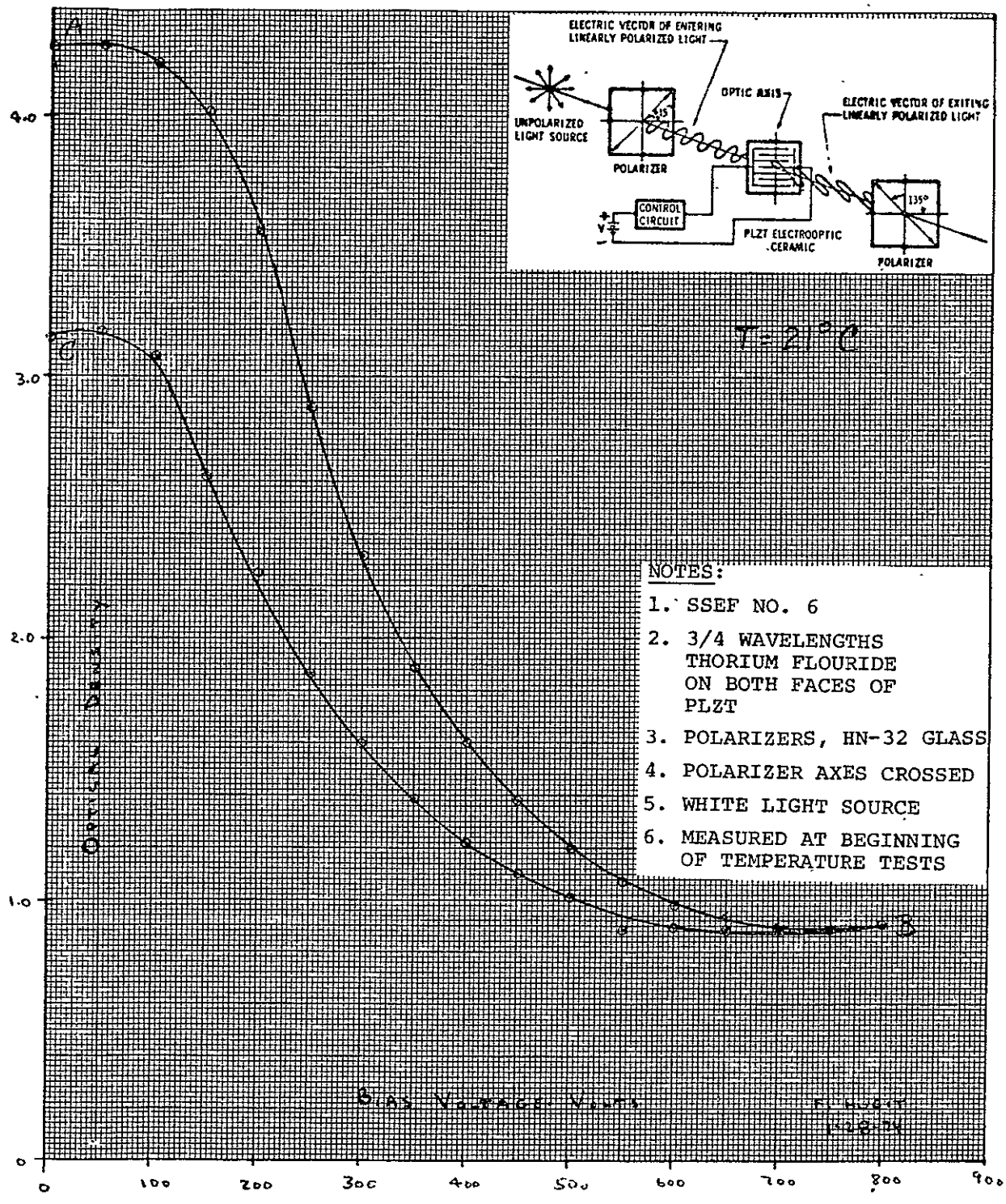

Figure 18. Density Transfer Characteristic as a Function of Temperature of PLZT Sample, T = 21°C

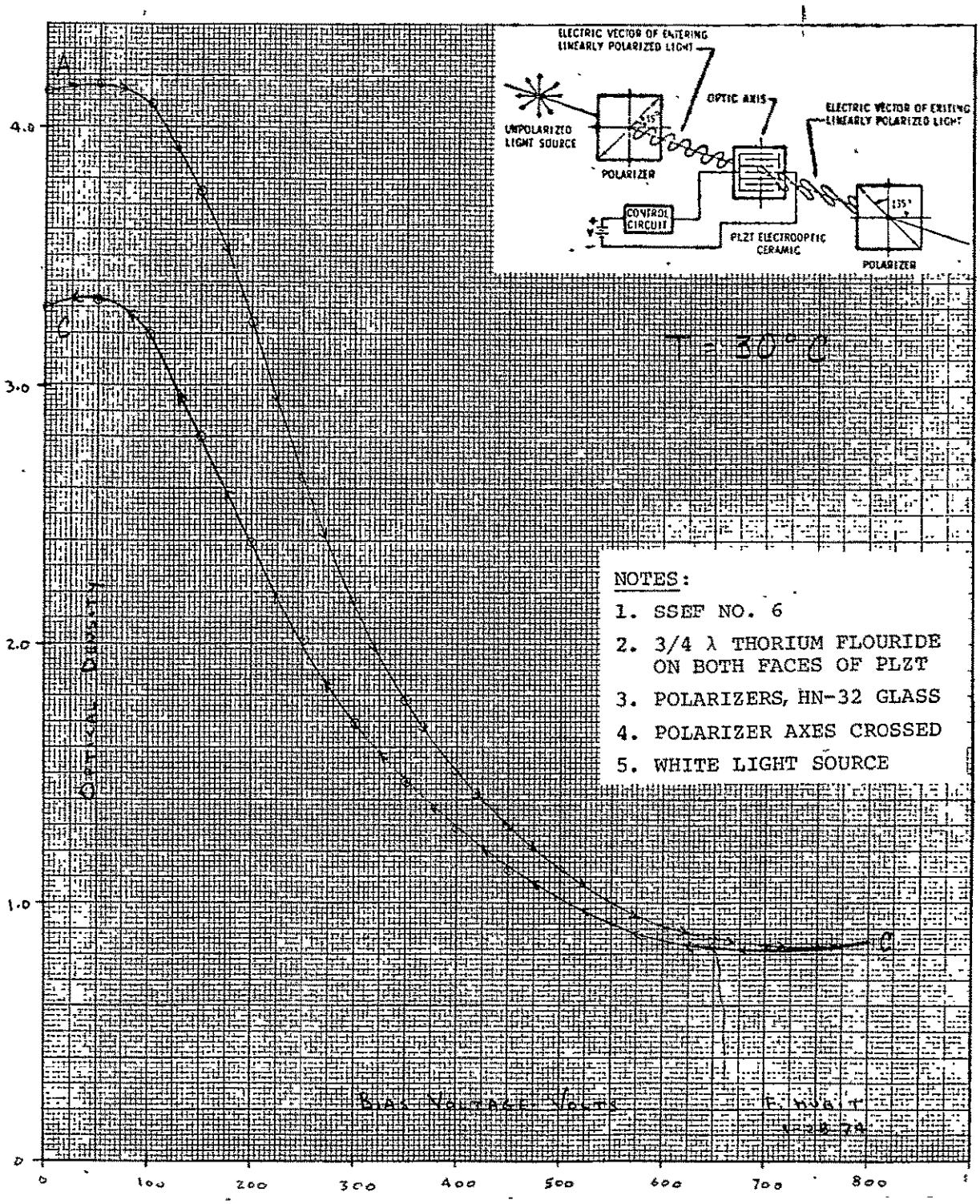

Figure 19. Density Transfer Characteristic as a Function of Temeprature of PLZT Sample, T = 30°C

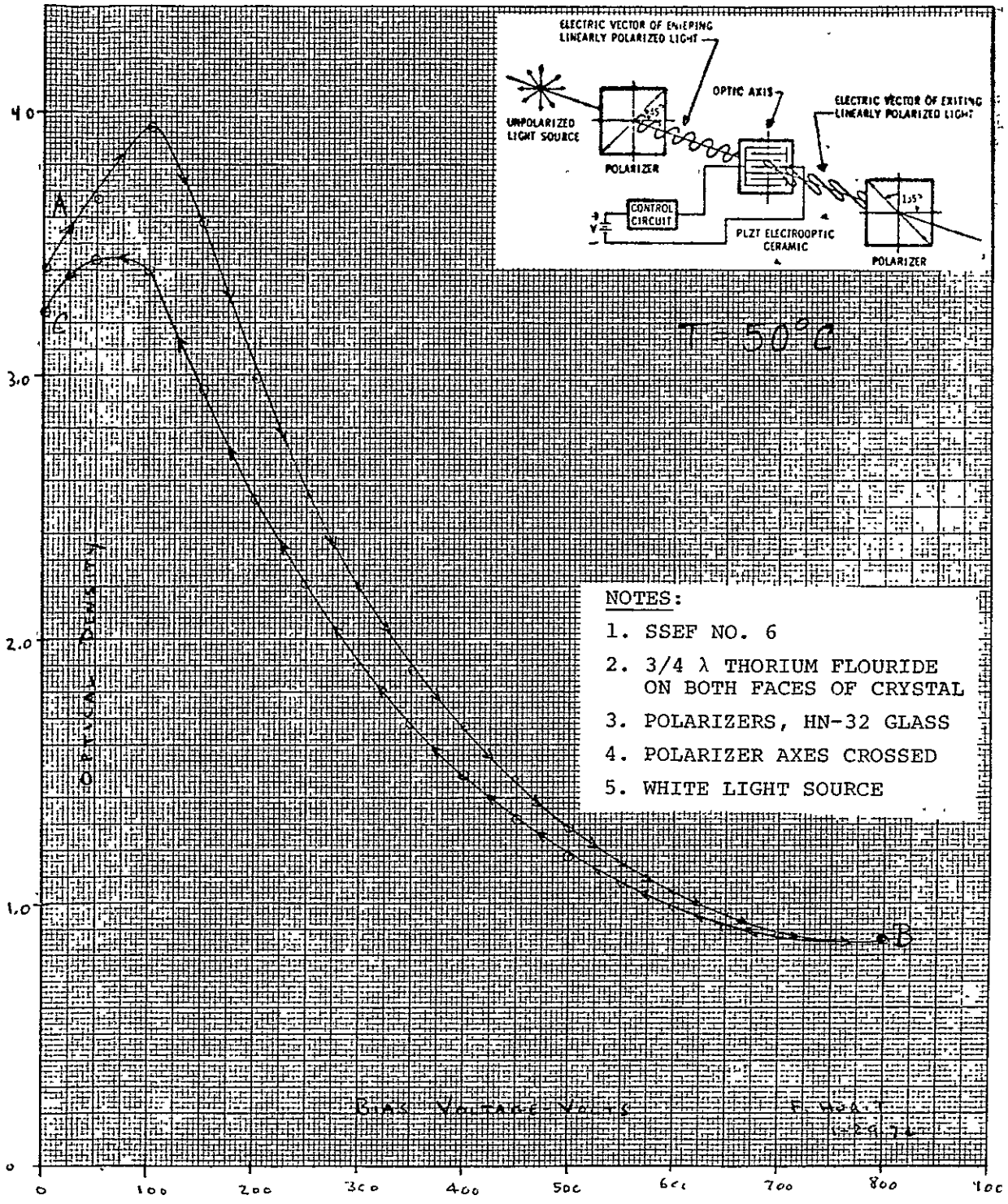

Figure 20. Density Transfer Characteristic as a Function of Temperature of PLZT Sample, T = 50°C

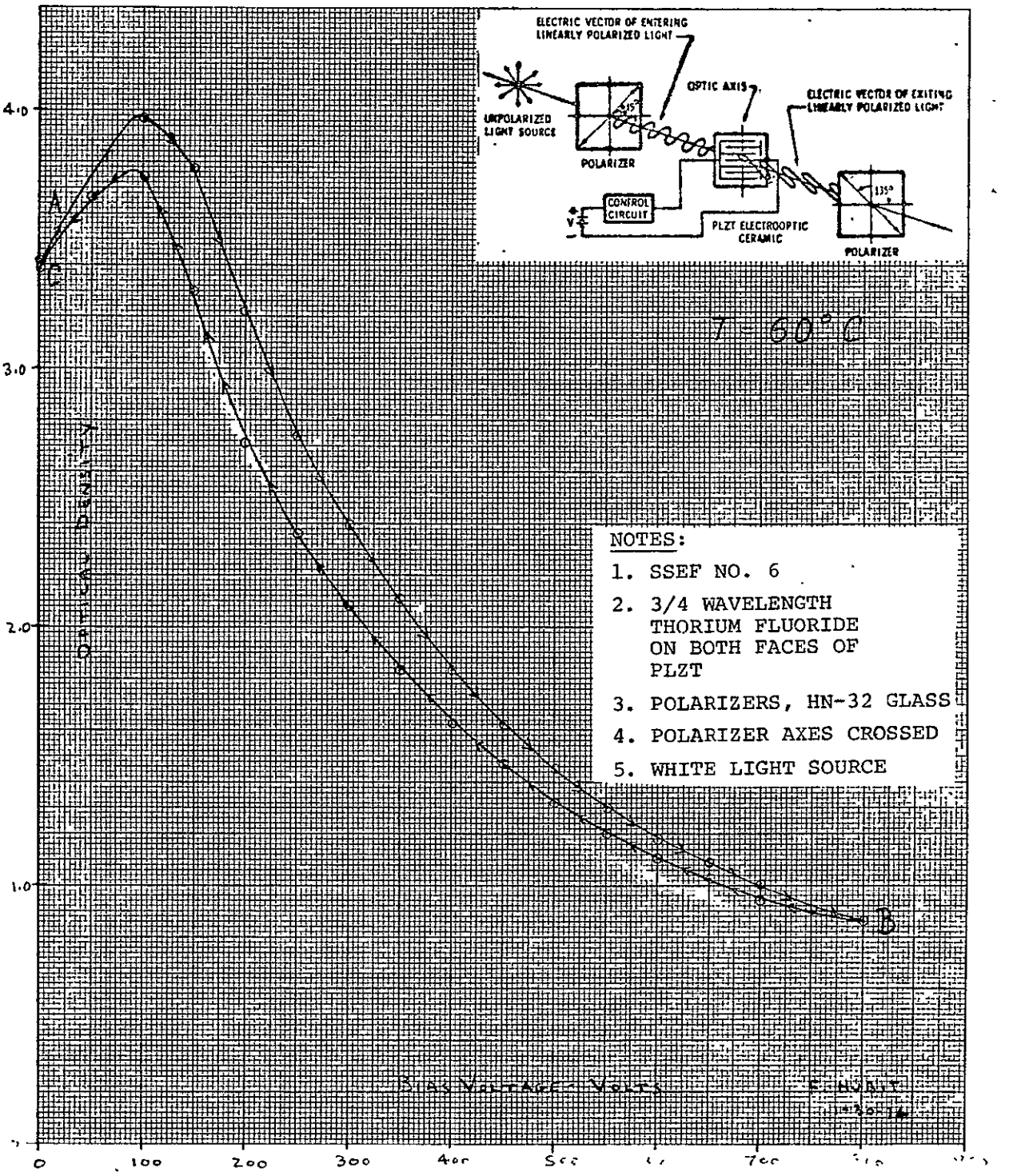

Figure 21. Density Transfer Characteristic as a Function of Temperature of PLZT Sample, T = 60°C

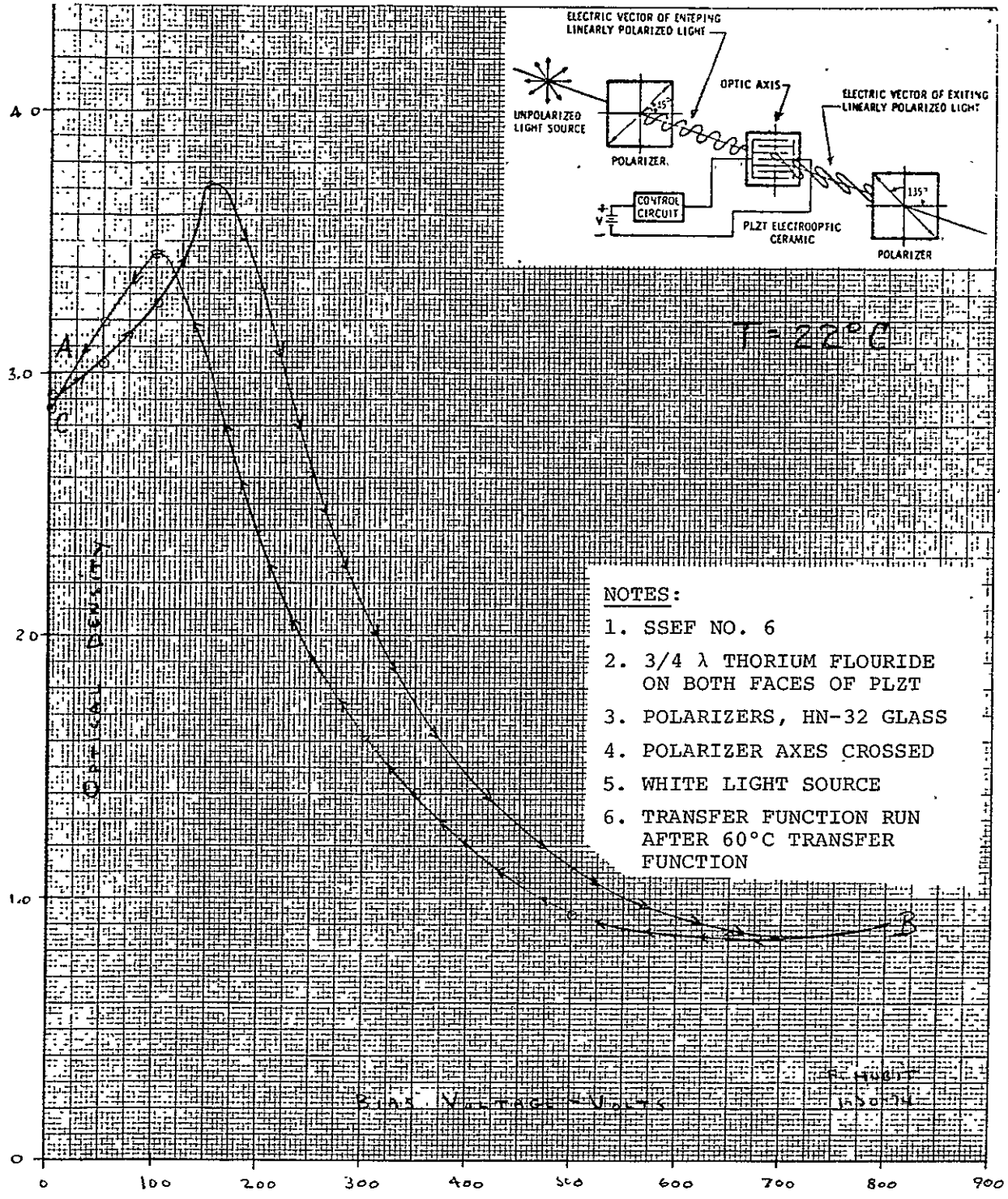

Figure 22. Density Transfer Characteristic as a Function of Temperature of PLZT Sample, T = 22°C

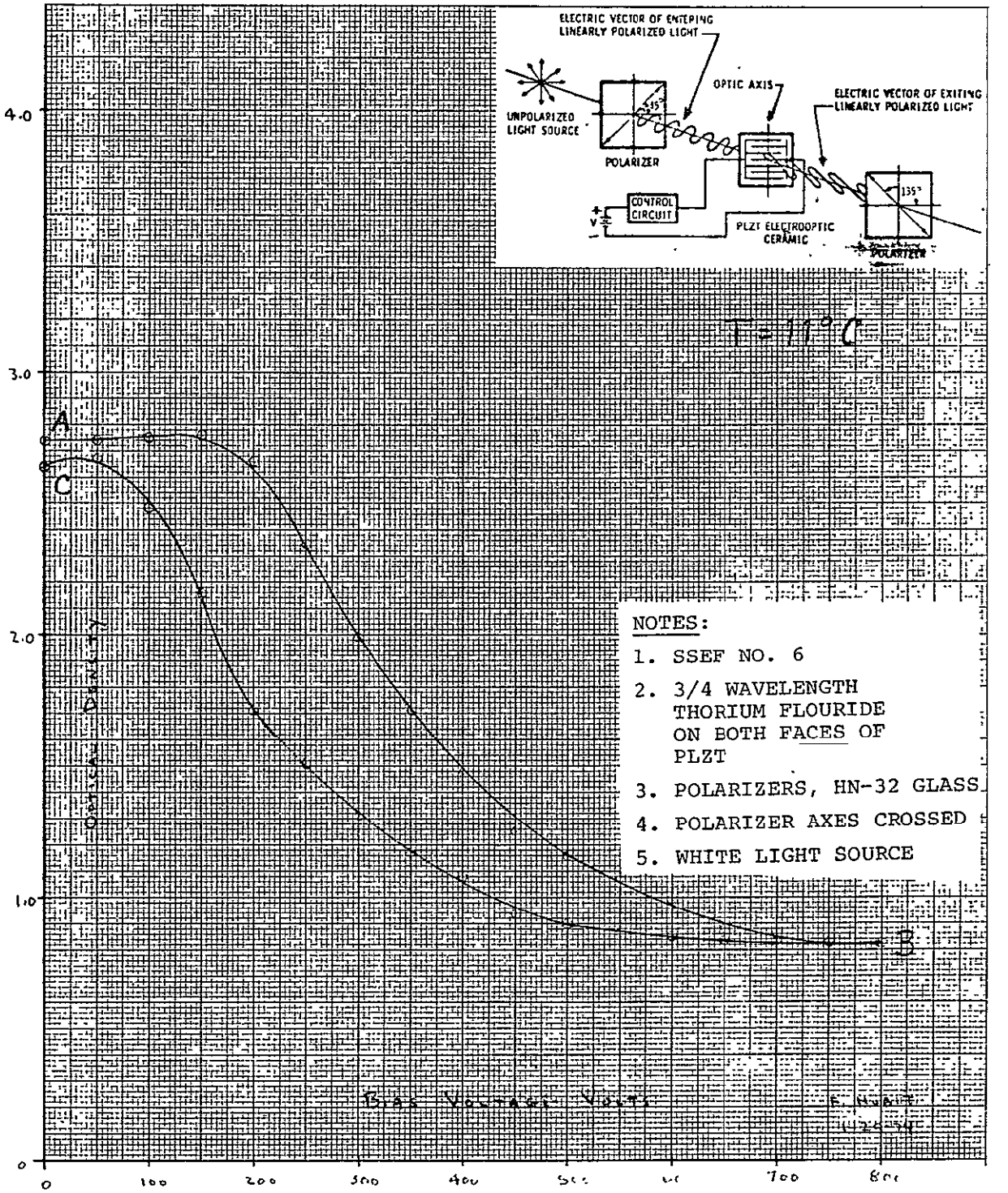

Figure 23. Density Transfer Characteristic as a Function of Temperature of PLZT Sample, T = 11°C

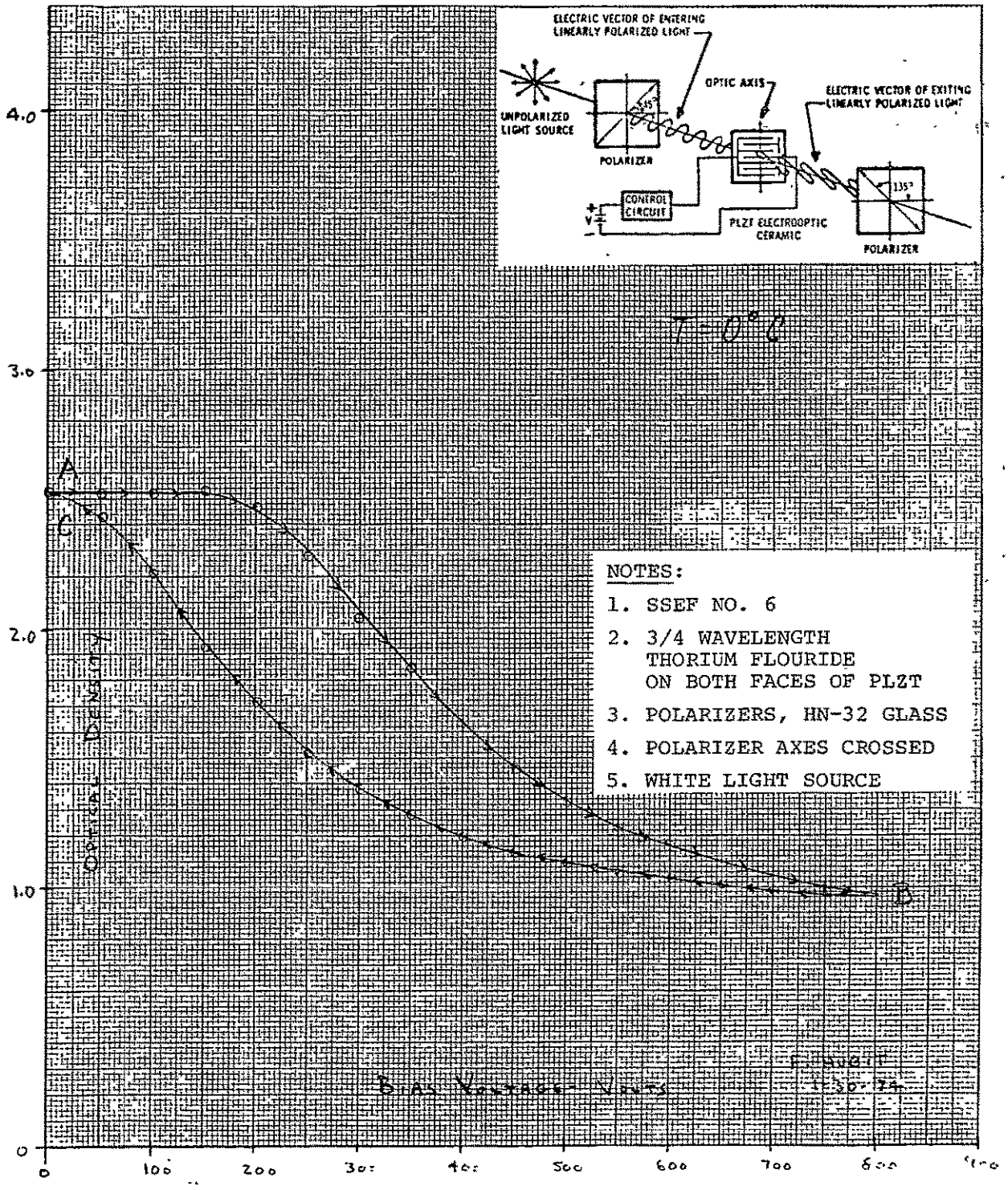

Figure 24. Density Transfer Characteristic as a Function of Temperature of PLZT Sample, T = 0°C

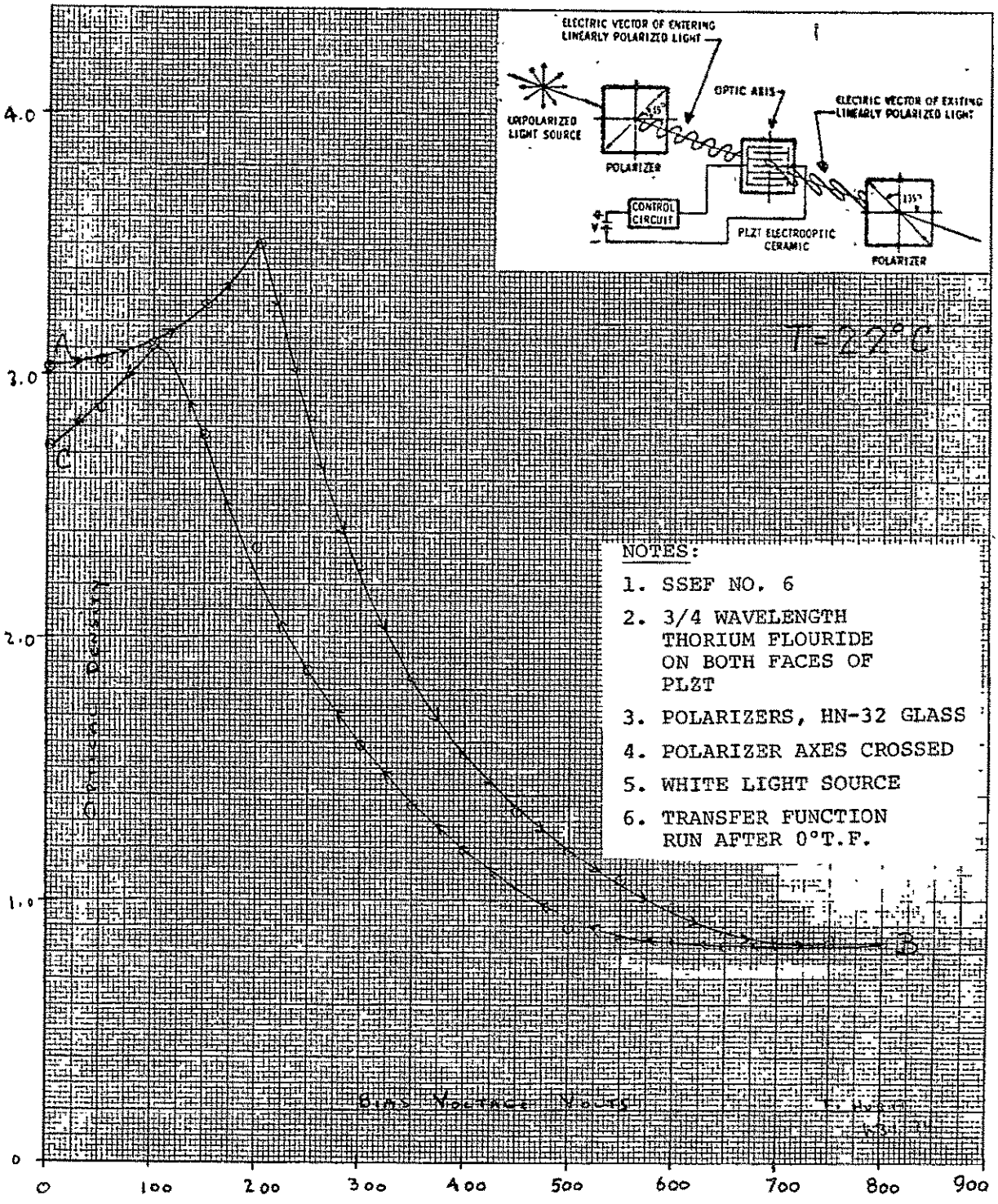

Figure 25. Density Transfer Characteristic as a Function of Temperature of PLZT Sample, T Returned to 22°C

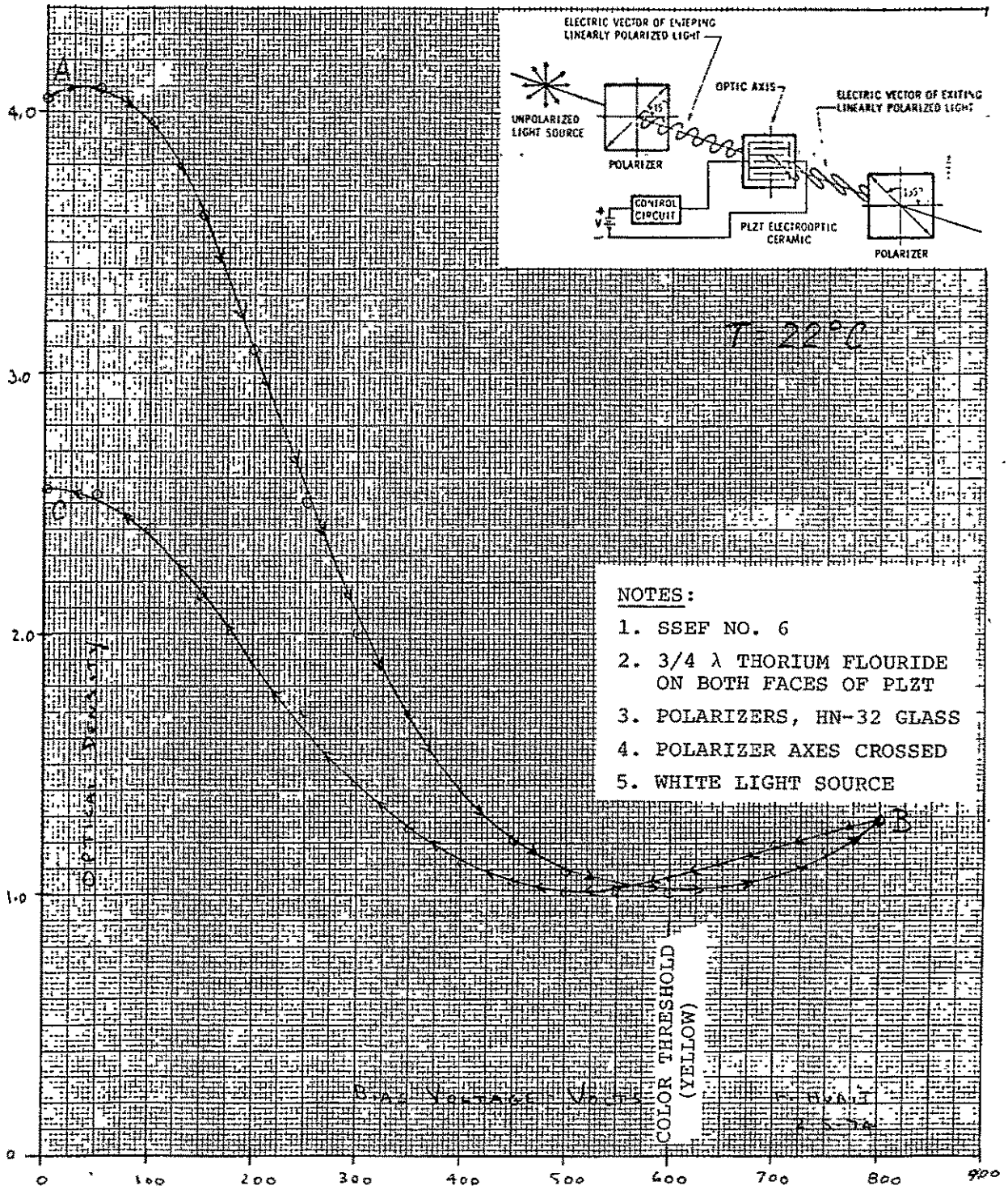

Figure 26. Delayed Measurement of Density Transfer Characteristic of PLZT Sample at Reference (T = 22°C) Temperature

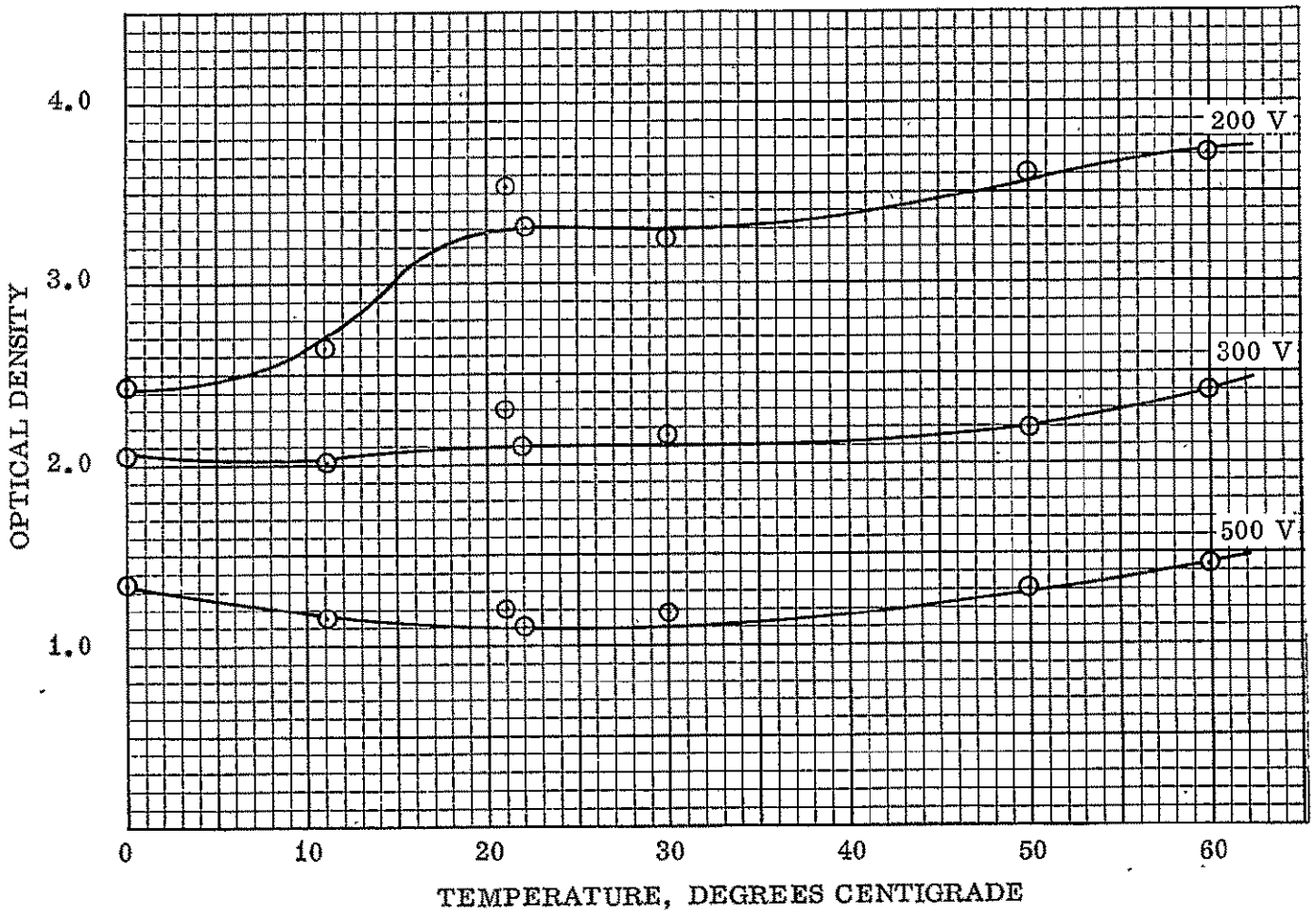

Figure 27. Density Variation With Temperature of PLZT Sample for Several Control-Voltage Levels

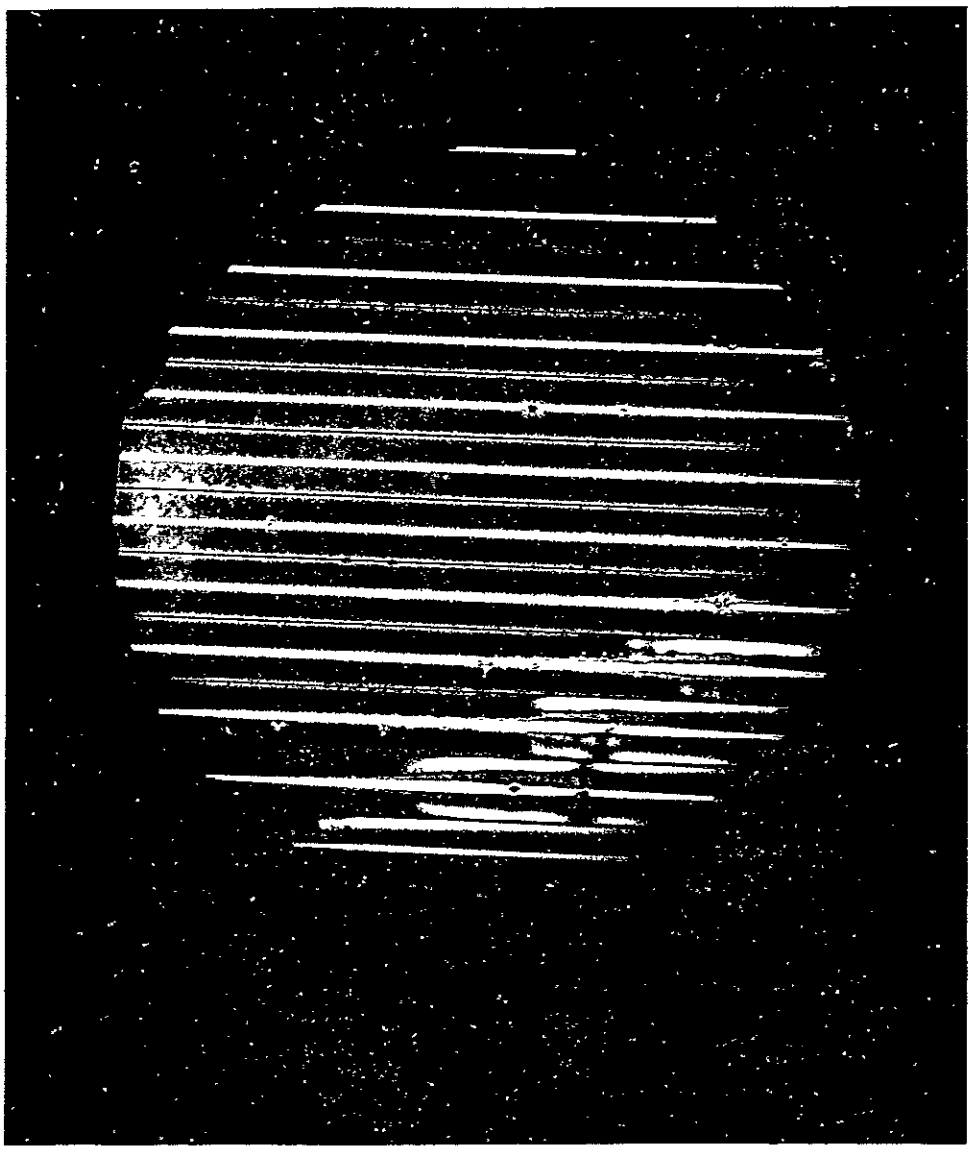

Figure 28. Defect Occurring at 60°C in Full Field Transmission

in density was noted. There was also a severe compression of the dynamic range observed at temperatures approaching 0°C. Also, the threshold of first order colors (light yellow) at 0°C was measured as 600 volts. The corresponding points at 22°C and 60°C were 700 volts and 800 volts, respectively. At 60°C with no voltage applied, the lines disappeared much more rapidly than at 20°C. This is not unexpected as the PLZT is approaching its Curie temperature (85°C).

Although the electrode contact problem tends to obscure some of the data, we can draw the following conclusion with respect to the intended application of the PLZT filter system.

Over a range of temperatures from 20°C to 50°C, operation is nearly independent of temperature. For neutral density applications in a closed loop ALC system the small variations noted will not affect operation. In the spectral filter mode, which is essentially an open loop system, small changes in retardation will affect the spectral hue. For this mode it may be necessary to control the PLZT temperature within narrower limits or to provide temperature compensation of the control voltage.

The compressed range at 0°C was discussed with Dr. Haertling, inventor of the material. He suggests that a small change in material composition such as using 9265 (9.2% lanthanum), rather than 9065, would improve the low temperature performance without adversely affecting other characteristics.

4. Resolution

Using the Air Force 3 Bar Resolution Chart, the optical bench setup, measured without the PLZT/polarizer assembly, yielded system resolution in excess of 400 LP/mm. The PLZT assembly was then installed, and the resolution was evaluated by visual observation of the limiting resolution point. With the voltage adjusted for minimum density, overall resolution in excess of 300 LP/mm was observed. As the voltage was decreased to provide a density of about 1.5, the observed resolution decreased to 200 LP/mm. Further decreasing the voltage to zero (maximum density mode) the apparent resolution was limited to 40 LP/mm; however, the observed brightness was so low at this point that it appears to have limited the measurement. The actual value is believed to be somewhat higher.

Examining the application requirements, for a raster size of 1/2 x 3/8" (typical for 1" sensor), at 300 TV element resolution:

$$\frac{300}{2} \times \frac{4H}{3V} \times \frac{1}{.5 \times 25.4} = 15.7 \text{ LP/mm}$$

From the observed data, the PLZT filter assembly appears to have negligible effect on overall resolution of a system using the anticipated parameters.

5. Angle of Incidence

To observe the effect of off axis incident light, Sample No. 6 was set up as shown in the insert on Figure 29.

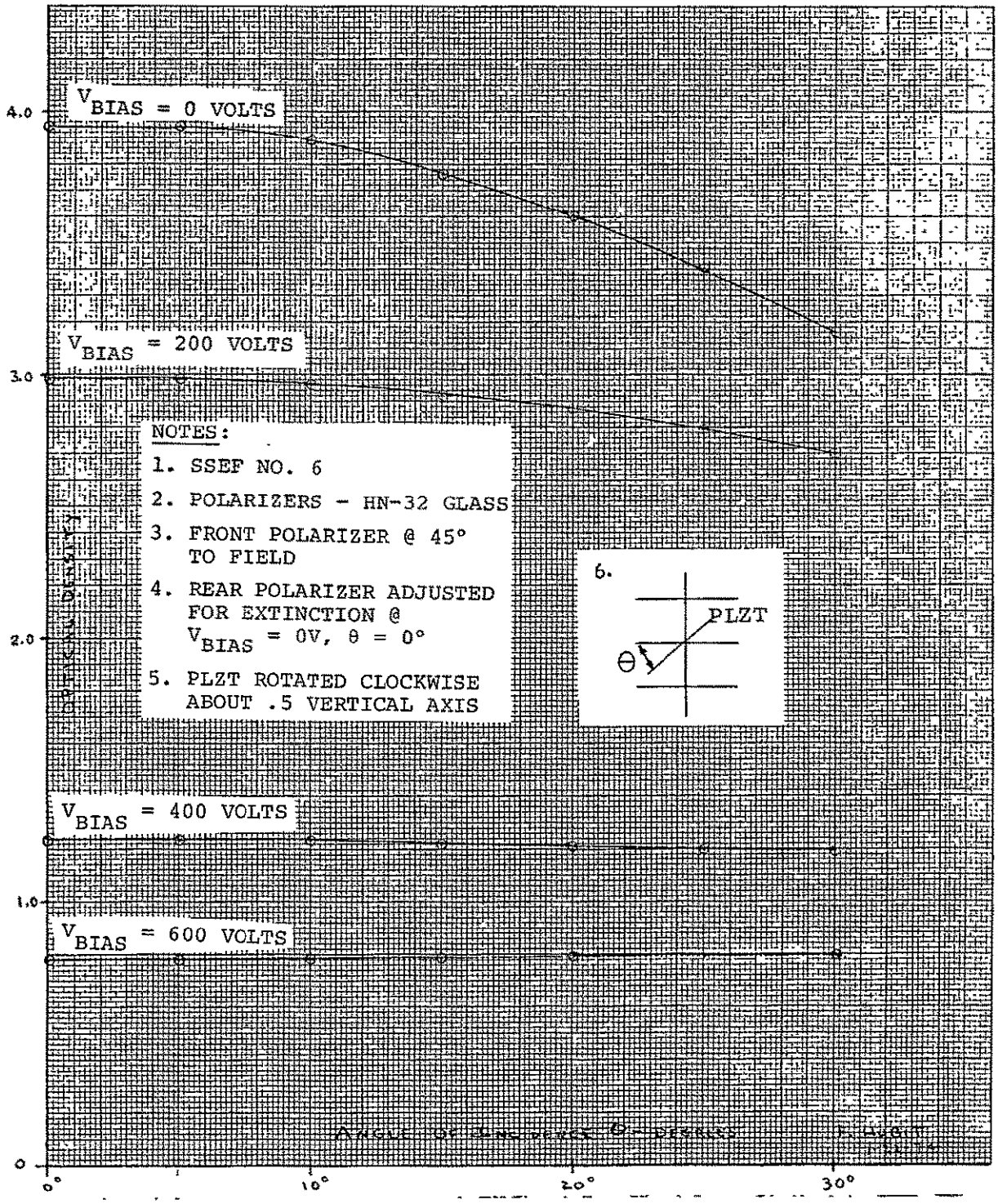

Figure 29. Effect of Off-Axis Incident Light (Normalized Deviations)

Data was taken by varying the PLZT angle from 0° to 30°, and as a function of applied voltage. The data is shown plotted in Figure 29 as normalized deviations, and in Figure 30 as absolute values. The observed performance can be explained by the polarizing effect caused by reflections at the surface of the PLZT. As the plate is tilted, a small polarization rotation occurs which causes a noticeable increase in transmission. This increase should be restoreable by a slight relative rotation of the polarizer/analyzer pair, although this was not tried. When the plate is biased into a birefringent state, the retardation masks the effect of reflection shifts. Similar results have been reported by Cutchen and Harris (Figure 6, Reference 13).

The fact that the sensitivity to incident angle is greatest with 0 volts on the plate can be expected, since at this point the plate is optically isotropic (non-birefringent) and the polar/analyzer axes are at 90°. The transmittance through a pair of polars is proportional to $\cos^2 \theta$, where θ is the angle between the axes. Since the slope of the cosine function is greatest at 90°, small changes in polarization angle will have a much larger effect near 90° than near 0°. When the PLZT voltage is increased from zero, it acts to reduce the effective angle between the polarizers, which is consistent with the observed data.

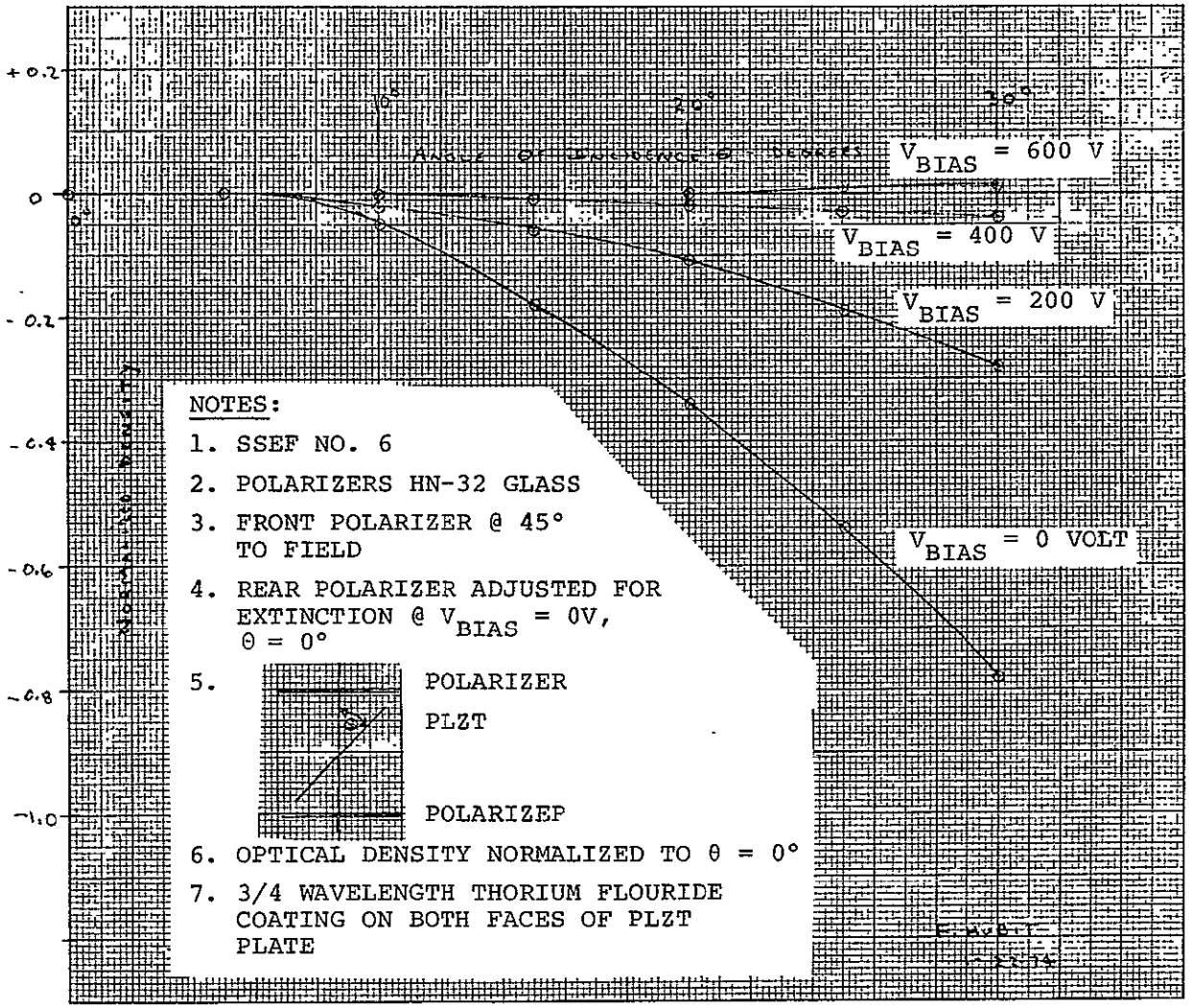

Figure 30. Effect of Off-Axis Incident Light (Absolute Values)

The effects of angle of incidence on the retardation of sample No. 5 were observed by viewing the plate through the conoscopic system of the petrographic microscope as discussed in Section II-C-2. The field-of-view thus observed is a map of the transmission through crossed polars as a function of angle of incidence. The 0.25 numerical aperture objective used in this experiment permits observation over a cone of illumination with 14.5° half-angle. This corresponds to slightly more aperture than f/2 optics. With 900 volts applied to the plate, no variation of the pattern over this cone of illumination could be seen either between crossed polars, or with a first-order red retardation plate inserted. (Application of the voltage in the latter case caused the color of the field to change from violet-red through blue and green to nearly yellow). This relative lack of angular variation is consistent with the other measurements described above, and the theoretical discussion in Section III. It is estimated that the upper limit of the relative change in retardation over the observed field is less than 10 percent.

6. Time Constant

The response time of the PLZT filter is of importance particularly for application as a spectral filter in a field sequential scanning system. When operating in the neutral density mode the response time is of lesser importance since the control loop time constant is generally made purposefully

long (several vertical fields) to maintain color field balance. The reactive power required to switch the PLZT operating point will also be determined by the effective capacitance of the electroded plate.

The dielectric constant for the 9065 composition is known to be nominally 5400; however, an exact calculation of the expected capacitance for the test samples is difficult because of the geometry of the contact fingers. Accordingly, the effective capacitance was observed by subjecting samples to an abrupt change of voltage through a series resistor and measuring the optical response time. Using sample No. 5, before exposure to any other tests, a 1.0 second response time was measured using a 1×10^8 ohm protective resistor. This corresponds to an effective capacitance of 0.01 μfd.

Similar data can be deduced from other published reports. Harris[32] reports 50 μs switching time using a 510 ohm series resistor, with two plates in parallel. This corresponds to an effective capacitance of 0.05 μfd.

Additional experiments were conducted on sample No. 6. Using the rapid switching circuit described in Section II-G, a voltage step was applied to the plate through a 1×10^5 ohm resistor. The voltage rise time, measured at the connections to the PLZT sample with an oscilloscope, indicates an effective capacitance of 0.016 μfd.

In another experiment, the optical response time of sample No. 6 was measured by applying an abrupt voltage step (through a 10 megohm resistor), starting from fixed bias points of 100, 200, and 300 volts. Stabilization time was observed using a photometer which covered an area of four electrode pairs in diameter. A time constant longer than expected was observed, which consisted of an initial rapid response coupled with a long tail (or second time constant) until complete stabilization was reached. It is believed that this second time constant (which represented only a small fraction of the total transmission) is a result of effects adjacent to the electrodes, which are included in the photometer field-of-view. This data is shown tabulated in Table 1.

TABLE 1. OPTICAL RESPONSE TIMES

BIAS VOLTAGE	STEP VOLTAGE	BRIGHTNESS (fL)	STABILIZATION (SECONDS)
100	-	20	0
267	167	130	70
431	331	820	102
200	-	50	0
365	165	430	65
530	330	1400	30
300	-	300	0
464	164	550	90
630	330	2310	30

Additional data on response time, included in the camera measurements described in Section II-H-3, shows the effective rise time in a complete system. The results of the various measurements indicate that it is potentially feasible to achieve full switching of the PLZT plate in a short interval (e.g., horizontal line time, 63.5 μs).

7. RETARDATION VARIATIONS

a. Variation With Applied Voltage

Measurements of the birefringent retardation were made on one Solid State Electro-Optical Filter plate (sample No. 5) as a function of applied (increasing) dc voltage, at a point near the center of the plate approximately halfway between two adjacent electrode fingers. The results of these measurements are plotted on Figure 31. Ascending voltages were used for the measurements. From 0 to 300 volts the retardation varies approximately quadratically with voltage, and above 400 volts the variation is nearly linear.

Subsequent to the initial application of voltage a very small overall birefringence in the absence of applied fields was also noted. The measured value of the retardation arising from this birefringence was about 1 millimicron at the center point being examined, with substantially higher indications noted near to the electrodes.

b. Variation of Retardation Across a Single Electrode Pair

A series of retardation measurements with 500 volts applied was made as a function of position between two adjacent electrode fingers, using the petrographic microscope. Measurements were taken at 100 micron intervals over most of the region, and at 25 or 50 micron intervals near the electrodes. The results are plotted in Figure 32. The difference in behavior

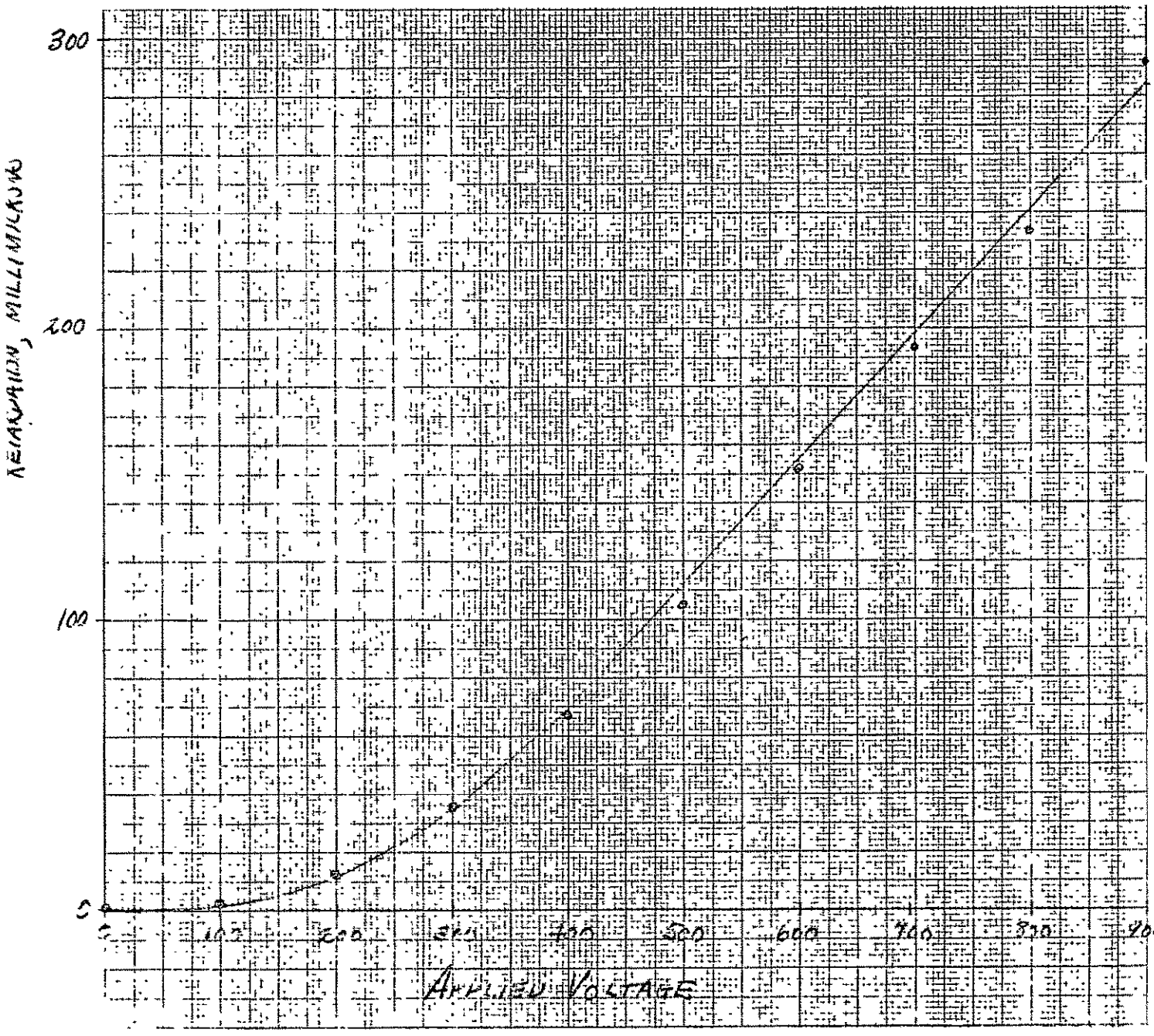

Figure 31. Effect of Increasing DC Voltage on Birefringent Retardation

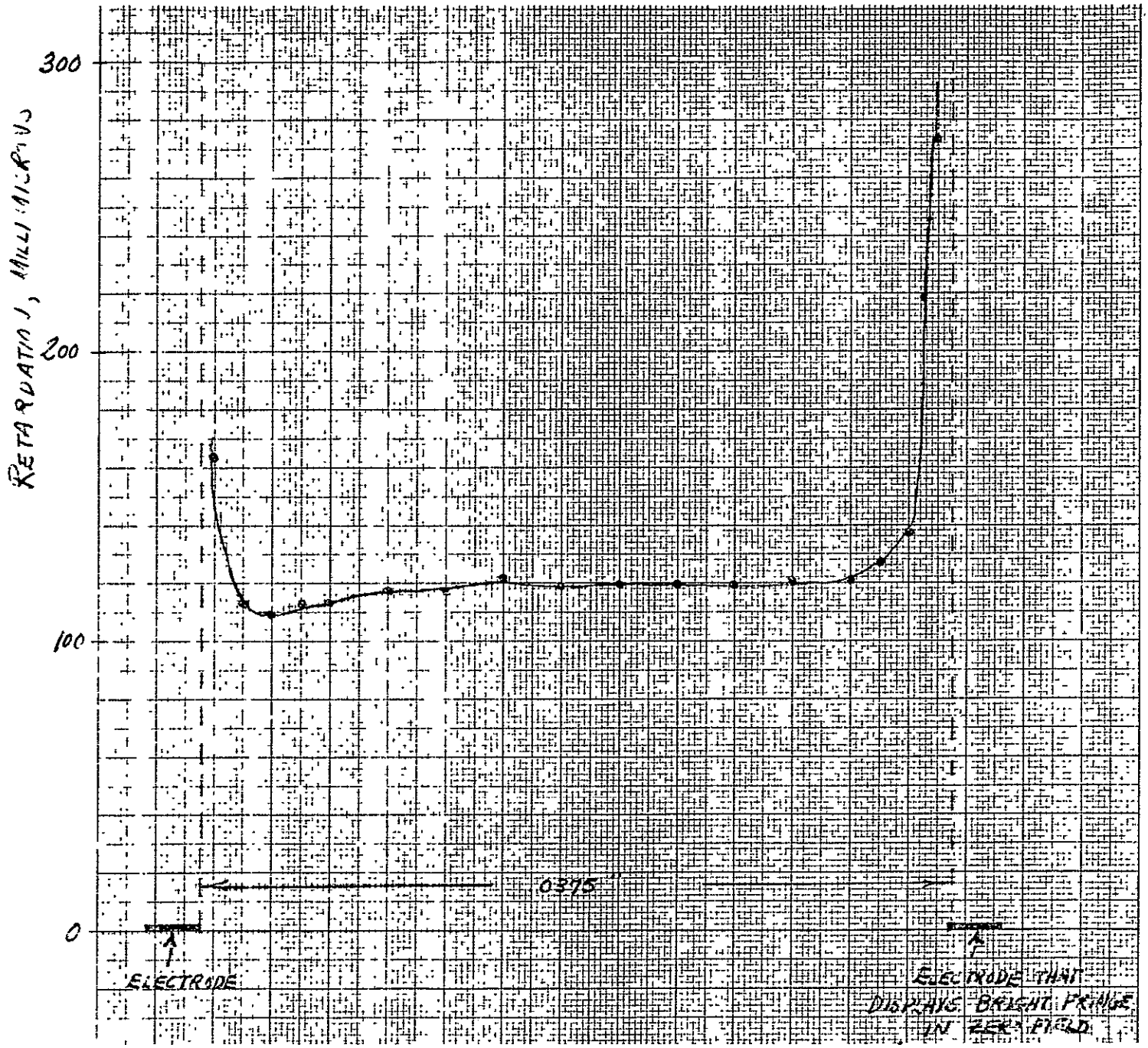

Figure 32. Effect of Position Between Electrode Fingers on Birefringent Retardation

between the two electrodes is real (i.e., definitely not due to random errors); the dip in the retardation that occurs at a small distance away from one electrode may be real.

From an application viewpoint, this non-uniformity is objectionable, but not necessarily intolerable. Since the filter plate is expected to be mounted in the optical path at a point where the electrodes are not in focus, the effect would be to reduce the total dynamic range when operating in the controlled neutral-density mode. In the spectral region of operation, color contamination would occur as a result of the different retardation across the electrode separation. If the non-uniformity were confined to a narrow region adjacent to the electrodes it would be practical to apply an opaque mask to this region and prevent the contamination. Observation of other samples during the optical bench tests shows, however, that the effect with present samples occupies as much as one-half the spacing between electrodes.

These effects, which are believed due to the fact that the contacts between the electrode fingers and the PLZT ceramic are non-ohmic, constitute the most deleterious features observed in the devices studied in this program. What may be still another manifestation of the same phenomenon is the overall variation of retardation with position on the plate with fixed applied dc voltage.

c. Variation With Overall Position

Measurements were made, with 500 volts applied, of the retardation at various widely-separated parts of the disk. The measurements were made at points that were nearly midway between electrode pairs. Because they had to be made with the microscope protruding into the annulus of the holder, the measurements were restricted to a circular region slightly less than 1/2 inch diameter about the center of the plate. The measured retardations are shown in parenthesis as a function of position in Figure 33. The magnitude of this variation is such that it would not significantly degrade the operation of a neutral density filter device but might cause objectionable contamination in a spectral filter mode.

Since the basic PLZT material is electro-optically homogenous, such variations are presumed to result from non-uniformity of the applied electric field. In turn this can be attributed to the previously mentioned electrode contact problem. A less likely cause would be variations in the thickness of the plate in different areas, since

$$r = t\,(n_2 - n_1)$$

where r is the retardation (nm); t is the thickness (nm); and $(n_2 - n_1)$ is the difference between the refractive indices (birefringence).

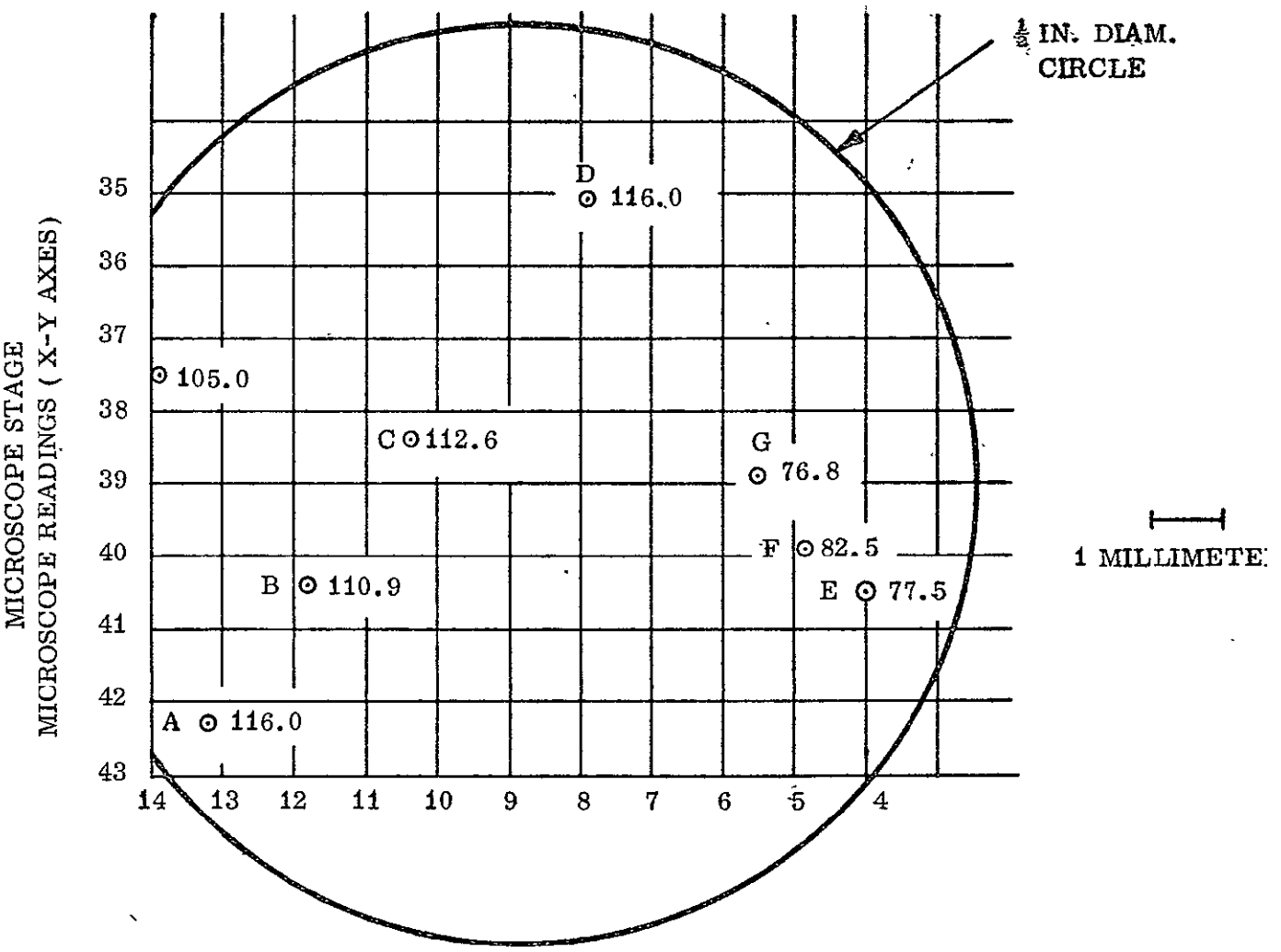

NOTE: VARIATION IN RETARDATION OVER CENTRAL REGION OF DISK, WITH 500 VOLTS APPLIED. RETARDATIONS, IN MILLIMICRONS, MEASURED NEARLY MIDWAY BETWEEN ELECTRODE PAIRS. READINGS A, B, C, AND D WERE MADE BETWEEN A SINGLE PAIR OF ELECTRODES; READINGS E, F, AND G WERE MADE BETWEEN DIFFERENT ELECTRODE PAIRS.

Figure 33. Variation in Birefringent Retardation Over Central Region of Disc (at 500V)

The specified maximum tolerance on surface flatness of the polished PLZT wafers was $\pm$0.001 inch or $\pm$10% of the nominal thickness. From the equation above, this would result in a maximum deviation of $\pm$10% in the observed retardation. The measured deviations were approximately twice this value, or $\pm$20%.

Another possible cause would be errors in the pitch or electrode spacing. Observation of the sample wafers showed that the spacing error was negligible. Thus again the electrode contact problem appears to be the prime cause of the observed problem.

8. Shading

a. Photometric Measurement

The Spectra photometer was used to measure the transmission through the SSEF in the center, and at eight points located symmetrically on a 1/2" diameter circle. The photometer field-of-view covered an area of 12 percent of the PLZT surface. To calibrate out the effects of residual shading from the light source or polarizers, a corresponding set of data was obtained with the PLZT sample replaced by a fixed retardation plate.

The SSEF data was taken with the control voltage set at 440 volts (density ≈ 1.5). The results for this test are shown in Table 2. The SSEF shading, referenced to the retardation plate measurement, ranged from -12.1% to +5.4%. Since the photometer view angle covers the area of four electrodes, the electrode edge effect makes the measured transmission sensitive to small changes in measurement location. To permit evaluation of shading in smaller regions, film negatives were obtained for the two cases (PLZT and retardation plate).

b. Photographic Method

Using the film negatives, the density was measured along a line midway between electrode pairs, using a microdensitometer.

TABLE 2. PHOTOMETRIC SHADING DATA

LOCATION	PLZT (Fℓ) BRIGHTNESS	PLATE (Fℓ) BRIGHTNESS	% SHADING
A	500	500	0
B	472	485	-2.68
C	435	472	-7.84
D	450	489	-8.02
E	435	495	-12.12
F	488	530	-7.92
G	539	535	+0.75
H	526	498	+5.62
I	509	483	+5.38

Data points were obtained from the densitometer plots, at 0.1" increments along the horizontal axis, for a total width of 0.6". These points were measured for the center horizontal line, and for lines between electrodes 6 and 7, and 16 and 17. This data then represents the shading in an area of 0.4" × 0.6". Table 3 shows the measured film densities for the PLZT plate and the reference plate at the 21 intersections defined above.

TABLE 3. FILM DENSITIES FOR THE PLZT PLATE

HOR. REF	LINE 6-7		LINE 11-12		LINE 16-17	
	PLZT OD	REF OD	PLZT OD	REF OD	PLZT OD	REF OD
2	1.72	1.55	1.86	1.73	1.65	1.51
3	1.82	1.67	1.99	1.89	1.97	1.78
4	1.77	1.67	2.07	1.94	2.10	1.95
5	1.71	1.66	2.07	1.96	2.16	1.97
6	1.77	1.67	2.06	1.97	2.16	1.97
7	1.88	1.74	2.09	1.95	2.15	1.94
8	1.84	1.73	2.01	1.90	1.97	1.77

Using the measured density values for the reference plate, we can correct the PLZT plate readings for shading inherent in the light source or polarizers. The corrected readings, expressed as percent shading, are shown in Table 4.

TABLE 4. PLZT PLATE READINGS CORRECTED FOR SHADING

HOR. REF	LINE 6-7	LINE 11-12	LINE 16-17
2	17.4	5.2	7.3
3	11.6	-1.0	25.8
4	-3.5	6.04	13.5
5	-16.4	0	25.5
6	-3.4	-6.3	25.5
7	8.7	10.4	33.6
8	3.0	0.7	29.2

9. Spectral Response

To evaluate the performance available from a single stage PLZT filter assembly, the optical bench setup was used to permit visual observation and photographs of the transmission through the assembly. Operating voltage to the PLZT element was constrained to 800 volts maximum to ensure no damage to the test sample. Fixed retardation plates inserted between the filter and the rear polar analyzer permitted the observation of higher order mode colors. Table 5 shows the combinations of PLZT voltage and retardation plates which were examined.

Photographs of the results for typical combinations are shown in Figures 34, 35 and 36. These correspond to combination Nos. 3, 9 and 11 respectively.

Each of the combinations listed in Table 5 was also examined using a scanning spectrophotometer. To provide adequate amplitude resolution, the instrument's scale factor was increased after calibrating it for uniform response in the visible region. Therefore, the graphs obtained show relative, rather than absolute, values for the spectral transmissions. Figures 37a, b, and c show the resultant spectral response curves for fourteen of the combinations listed in Table 5.

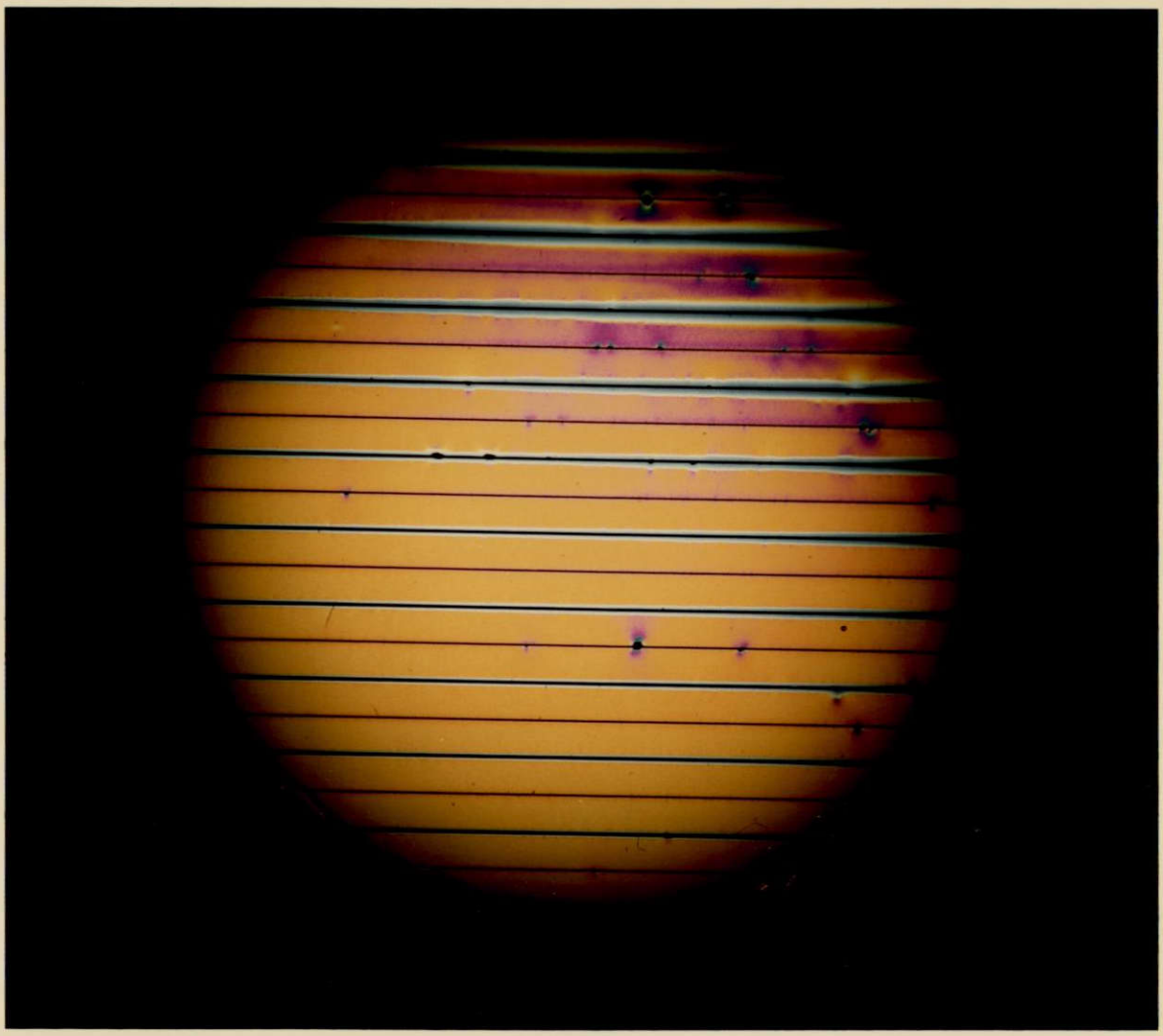

Figure 34. Single-Stage PLZT Filter Assembly Performance, Test No. 3

C-2

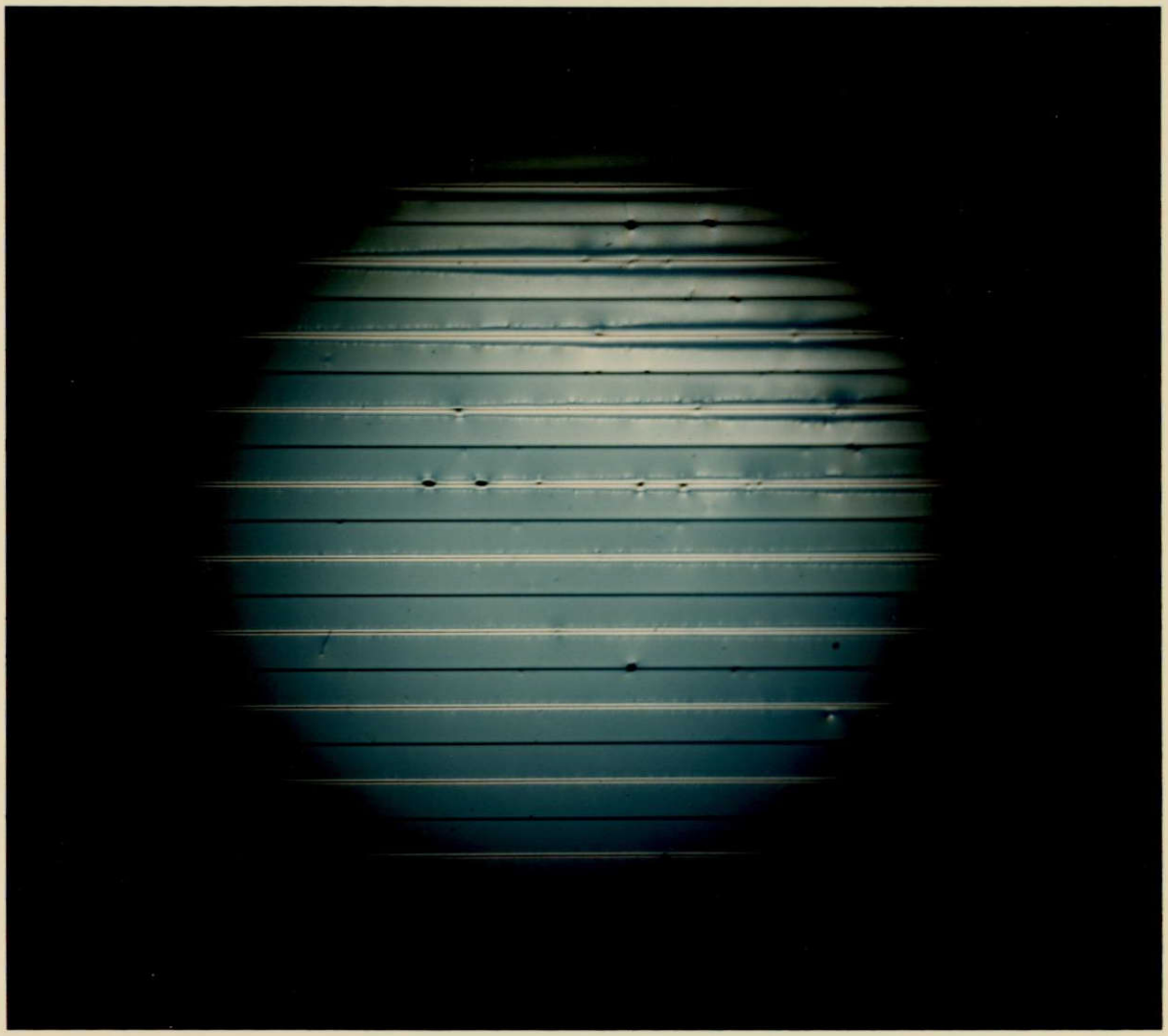

Figure 35. Single-Stage PLZT Filter Assembly Performance, Test No. 9

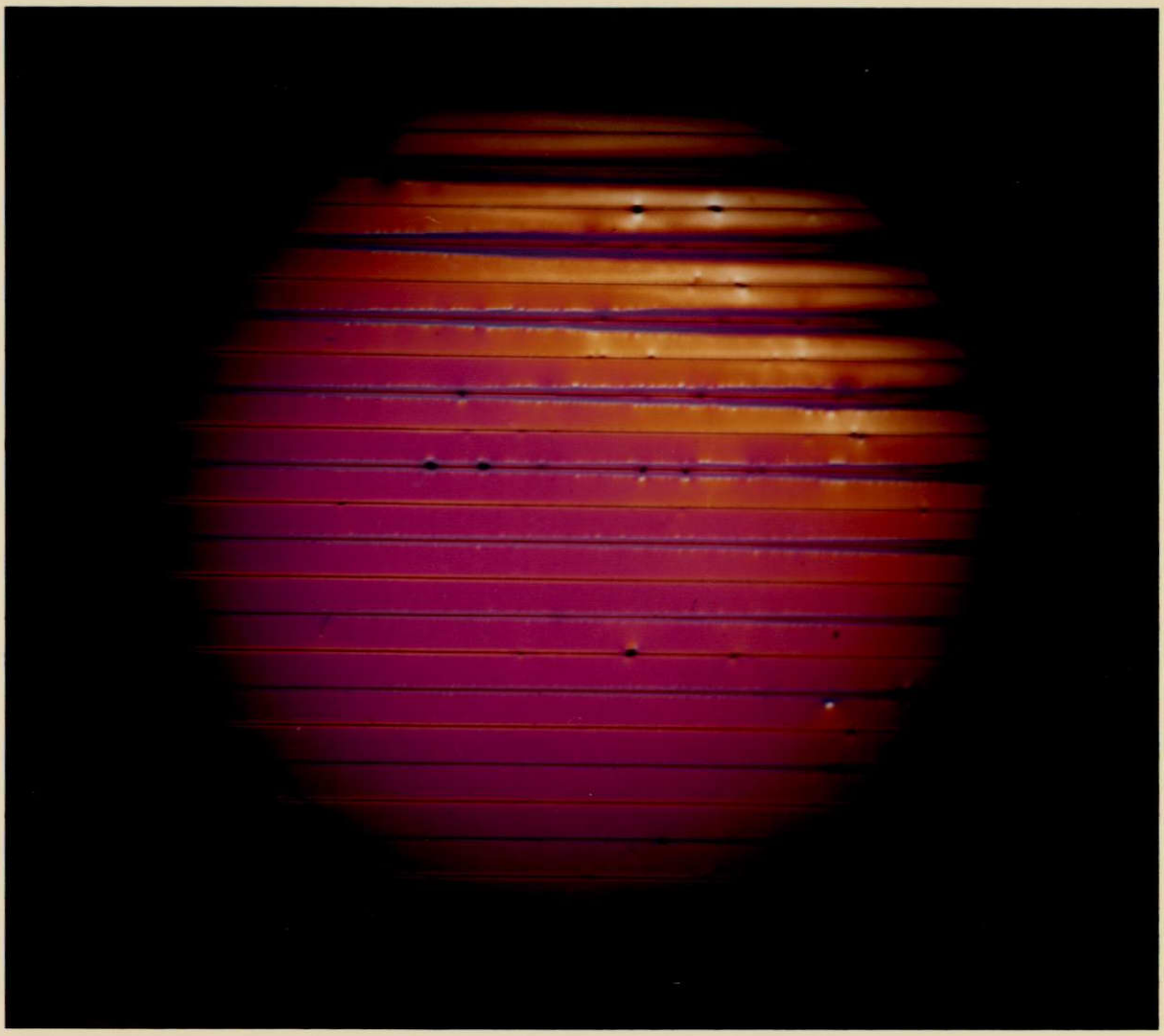

Figure 36. Single-Stage PLZT Filter Assembly Performance, Test No. 11

TABLE 5. RETARDATION PLATE COLORS AND APPLIED VOLTAGES

TEST NO.	VISUAL COLOR	PLZT VOLTS	λ/4(1) PLATE	λ/4(2) PLATE	λ PLATE
1	Pale Yellow	500	-	-	-
2	Bright Yellow	600	-	-	-
3	Yellow Orange	700	-	-	-
4	Red Orange	800	-	-	-
5	Red Orange	700	0°	-	-
6	Yellow Green	800	67° CW	-	-
7	Red (Pale)	800	105° CW	4° CW	-
8	Red/Blue	800	0°	-	105° CW
9	Blue Green	100	0°	0°	-
10	Blue	0	-	60° CW	-
11	Magenta	230	-	60° CW	-
12	Red	290	-	60° CW	-
13	Orange	390	-	60° CW	-
14	Pale Yellow	490	-	60° CW	-
15	Pale Green	697	-	60° CW	-

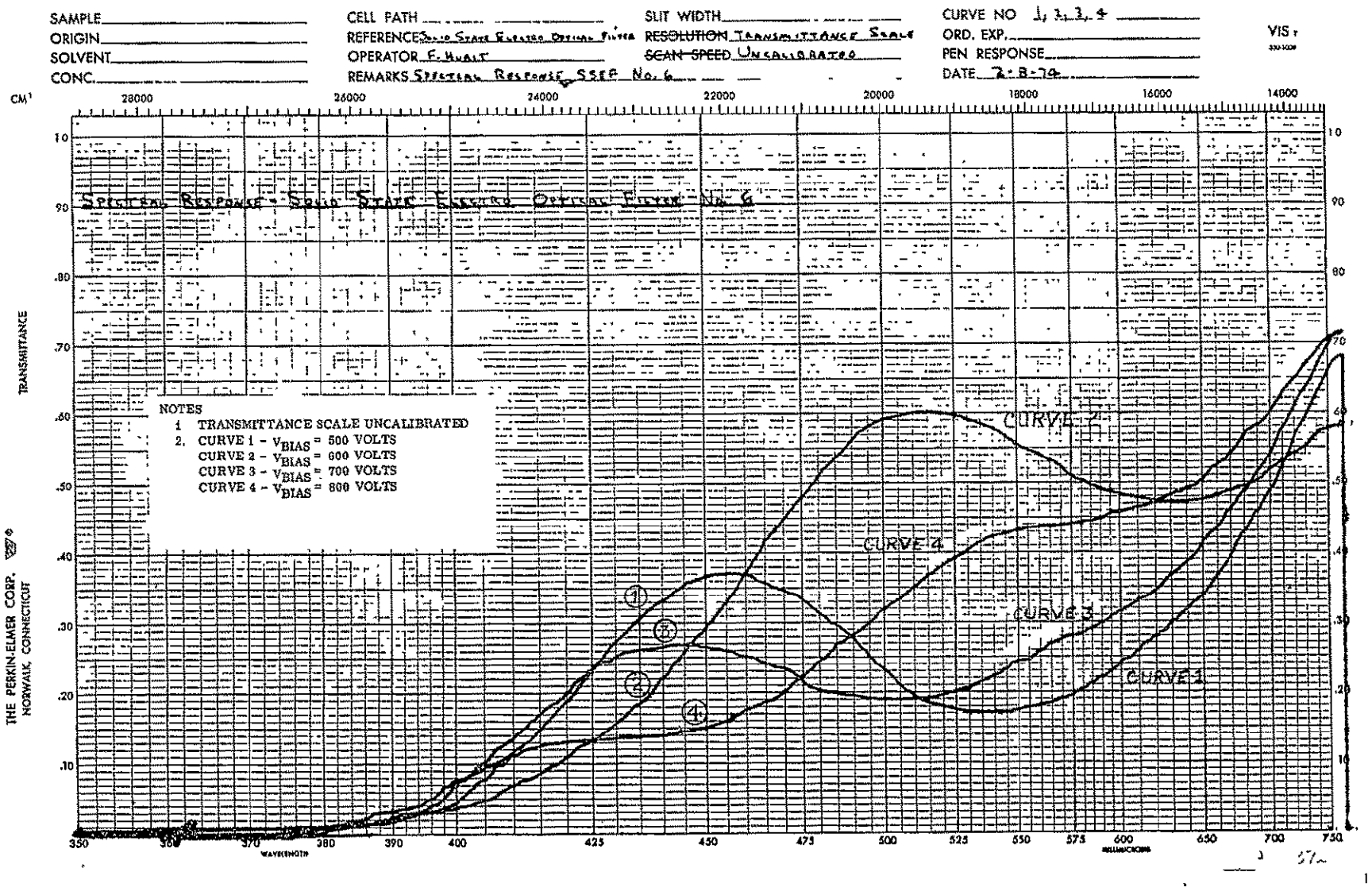

Figure 37(a). Spectral Response Curves Obtained Using the Scanning Spectrophotometer, Test 1 Through 4

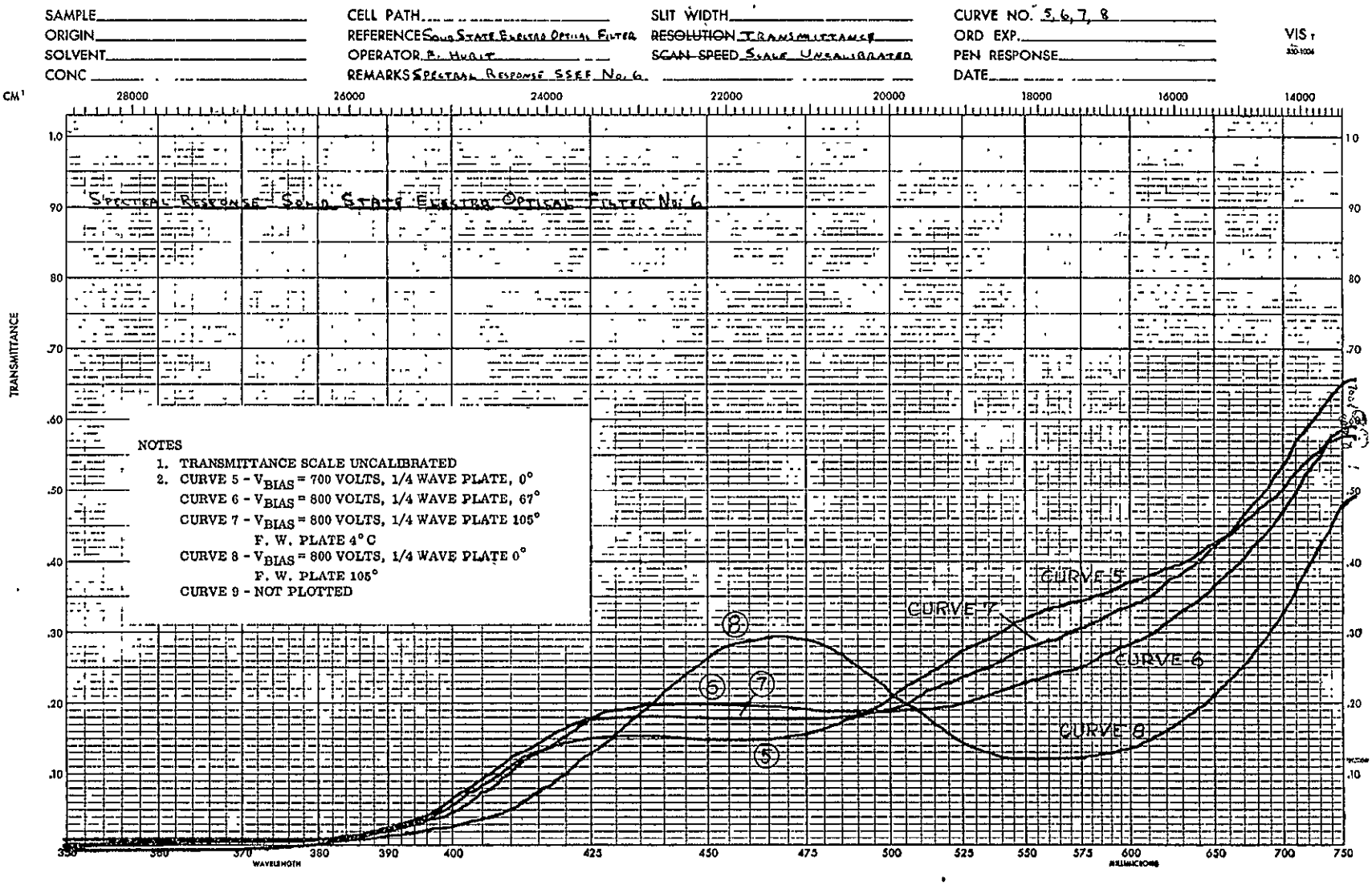

Figure 37(b). Spectral Response Curves Obtained Using the Scanning Spectrometer, Tests 5 Through 8

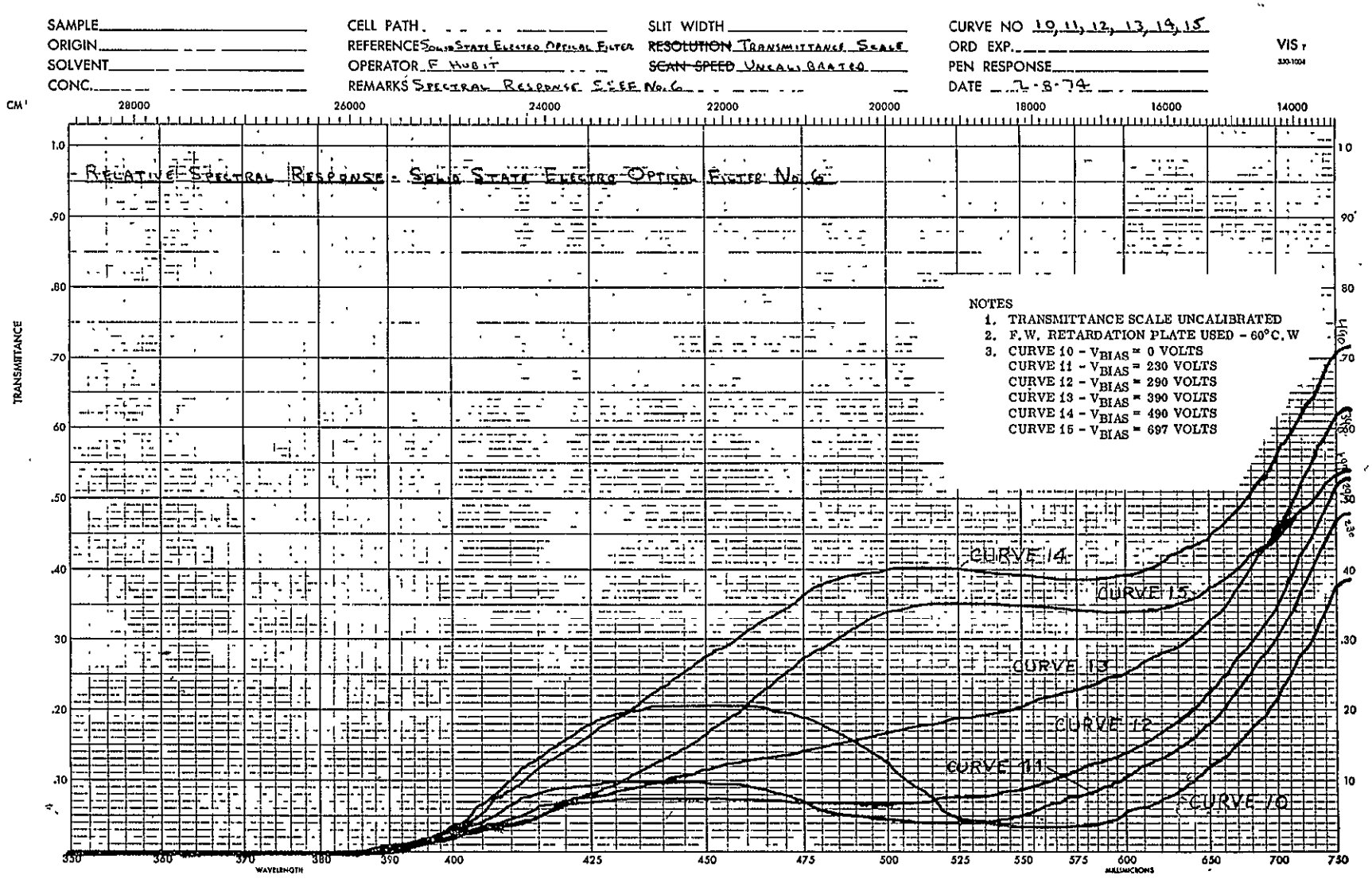

Figure 37(c). Spectral Response Curves Obtained Using the Scanning Spectrometer, Tests 10 Through 15

The photographs show the types of blemishes observed on the samples. The electrode edge effects cause variation in birefringence adjacent to the electrodes. This in turn creates regions of different spectral hue. The effect is not always uniform along the electrode length as seen particularly in the upper right hand corners of the samples. Since the net voltage between electrodes must be constant, when the edge effect dimension increases, the area between electrodes is shifted in spectral response.

Also clearly visible in the photographs are the locations in which electrode repairs were effected. These repairs create small local regions of significantly different birefringence which result in hue shifts.

The scanning spectrophotometer measures the integrated transmission across the entire plate. Therefore, the resultant spectral response curves contain the integrated effects of all of the defects noted. The curves in Figure 37 show the general interference type response expected for a single stage PLZT filter. The non-uniformities in response introduce a bias or spectral dilution into the curves which prevents the null points from returning to zero response. Curves 1, 8, and 10 confirm the expected half bandwidth of 100 millimicrons.

The spectral response data obtained on these initial PLZT samples has not produced optimum results. Clearly the device produces spectral separation but the results are limited by the defects which were previously noted. Improved devices which resolve these defects should provide closer approximations to the desired response.

10. Anti-Reflection Coatings

As discussed in Section II-B, the high index of refraction of PLZT would result in significant transmission loss for uncoated wafers. Several sample coatings were applied to wafers using ThF_4 as the interface material. For these initial applications the coating thickness was selected as a multiple of $\lambda/4$ to provide voltage breakdown protection during testing. More optimum (response uniformity) results will be obtained with $\lambda/4$ thickness where λ is chosen at the midpoint of the visible region. The results obtained, for the various combinations which were prepared, are shown in Figures 8, 38 and 39.

In the application of the PLZT filter to a practical spacecraft system, it is anticipated that the filter will be bonded to provide environmental integrity. The interface to the surface will then be other than the simple air-to-PLZT interface examined here. Selection of an optimum coating material must be performed after, or in conjunction with, the selection of the bonding material. Availability of an optimum refractive index coating material to compensate the cascaded interface may limit the ultimate performance; however, the data already obtained indicates that substantial reductions of the trans-

SAMPLE #5, LR COAT 7/4λ @ 520 NM
ON ELECTRODE SURFACE

ANGLE OF INCIDENCE: NORMAL

FISH-SCHURMAN CORP.
70 PORTMAN ROAD
NEW ROCHELLE, N. Y.

DATE 12/4/73

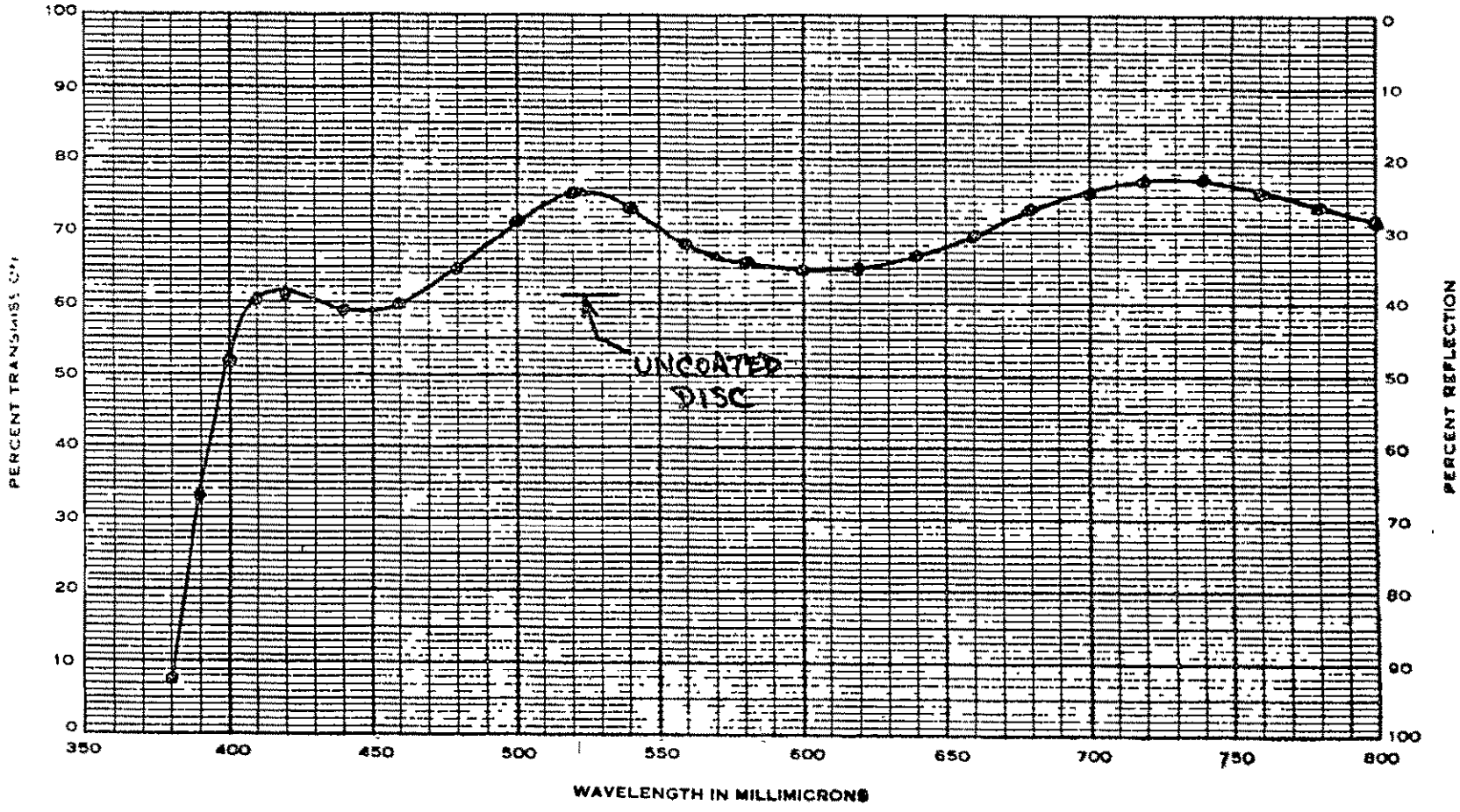

Figure 38. Transmission Loss of PLZT Wafer Across Spectrum for 7/4 λ Coating on Electrode Surface (λ = 520 nm)

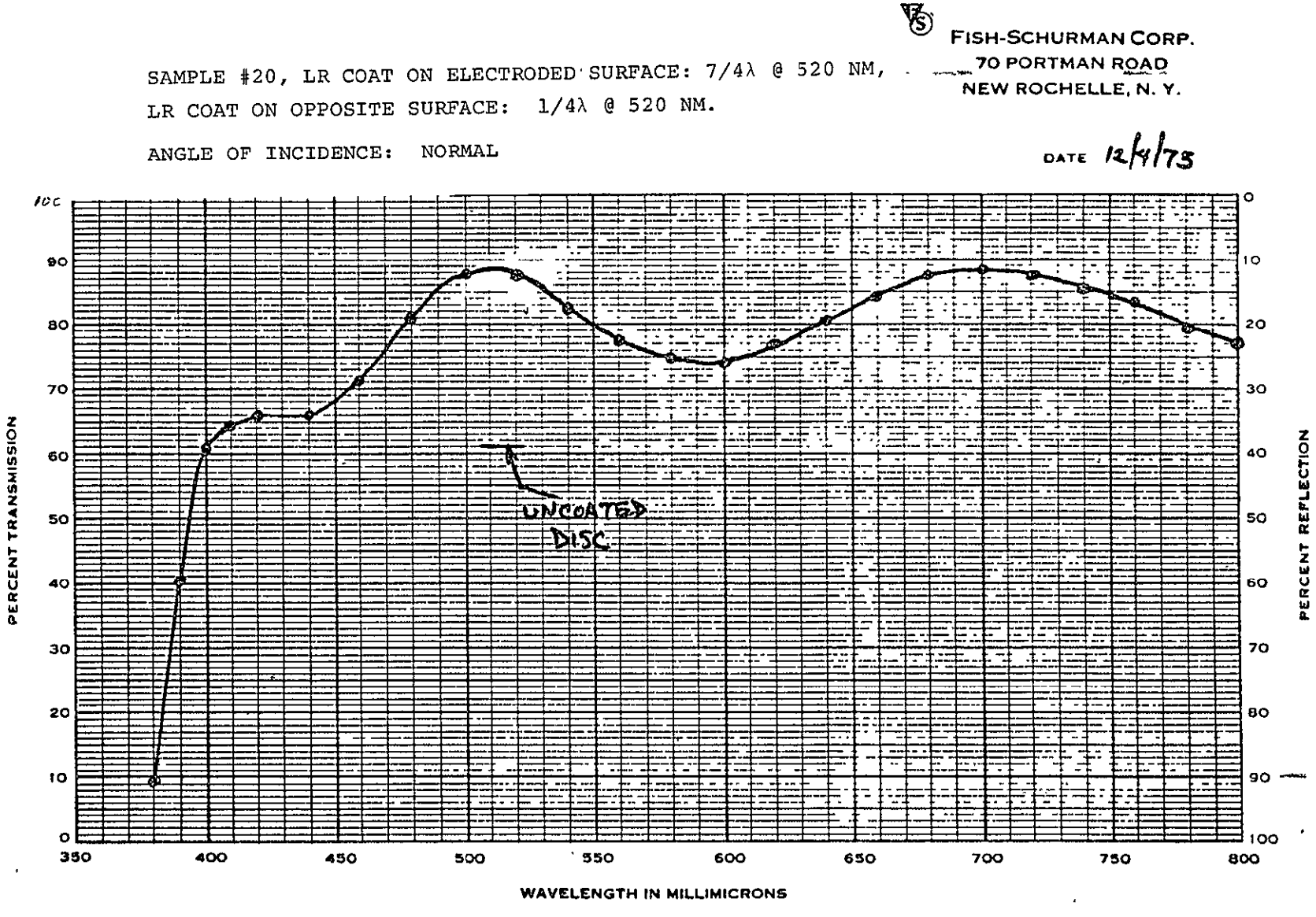

Figure 39. Transmission Loss of PLZT Wafer for 7/4 λ Coating on Electrode Surface and 1/4 λ Coating on Opposite Surface (λ = 520 nm)

G. INTERFACE WITH CAMERA

To permit evaluation of the performance of the SSEF system used with a typical spaceflight camera, an operating model of the Apollo CTV (part of the Ground Commanded Television Assembly) was employed. This camera, provided by NASA/JSC, employs a rotating color filter wheel to provide field sequential video at standard broadcast rates. A Silicon-intensifier-target (SIT) tube is used as the image sensor. Mechanical and electrical modifications were designed to permit replacing the rotating filter wheel and housing with the SSEF assembly. Details of these modifications, together with the applicable design drawings, are contained in the following sections.

1. Mechanical

A phenolic housing was designed to interface between the existing camera housing and the mounting flange of the zoom lens. Dimensions were arranged to permit direct substitution of the SSEF housing for the original color wheel gear housing. Figure 40 shows the housing and zoom lens installed to the camera.

The housing contains machined recesses for installing the front and rear polarizers which can be rotated in place at initial assembly. A ledge is provided for the installation of the PLZT plate. In addition, a slot was provided in the center of the housing to allow installation of passive

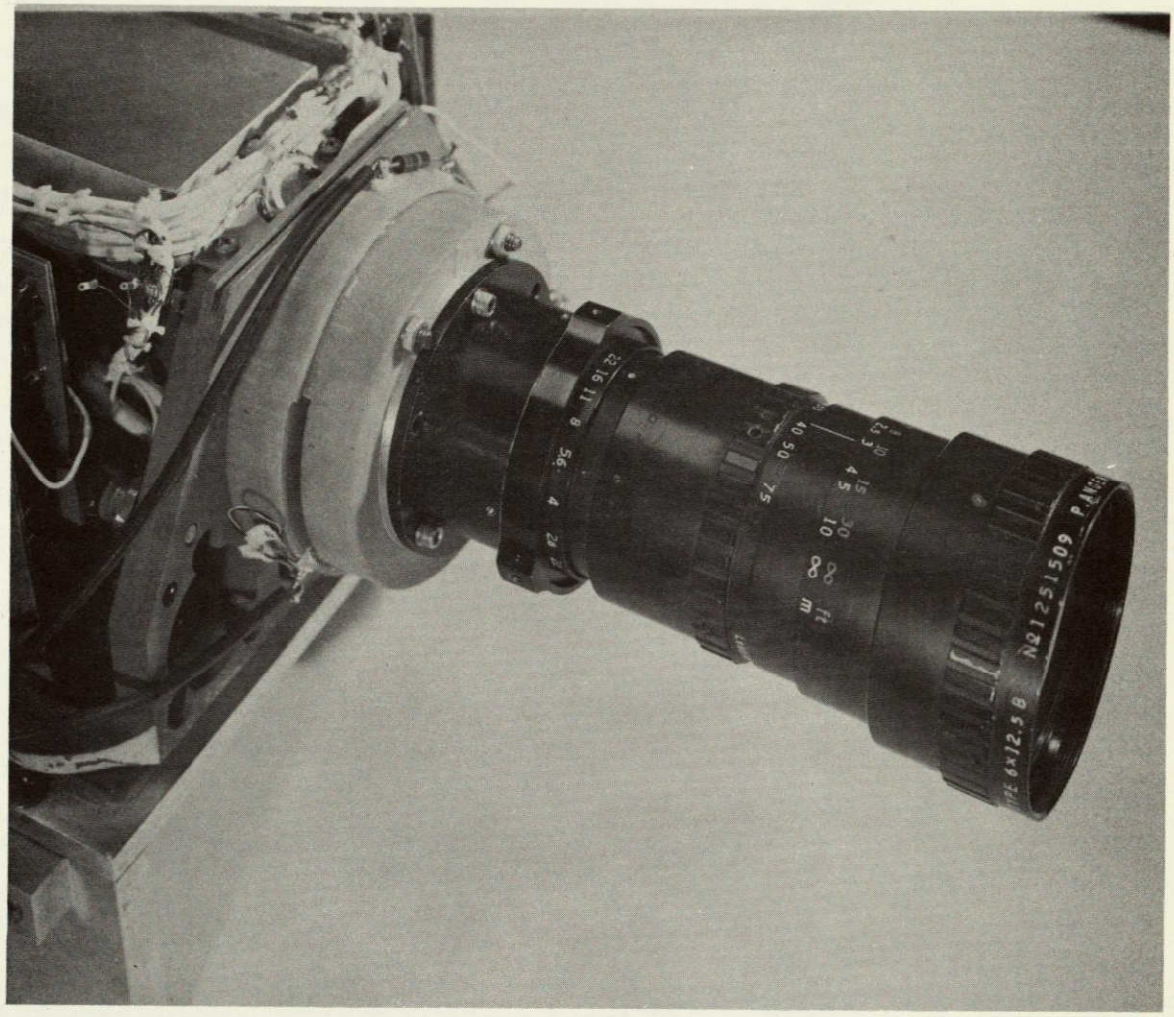

Figure 40. SSEF Housing and Zoom Lens Installed on Camera

retardation plates in the optical path. Drawings of the detail parts of the SSEF holder are shown in Figures 41 and 42. A cross section of the holder and filter elements assembled to the camera is shown in Figure 43.

2. Electrical

To provide the electrical interfaces required to test the SSEF in conjunction with the CTV camera, two special circuits were designed. The first circuit design provides the ability to use the SSEF in an automatic light control (ALC) mode in lieu of, or supplementing, the internal camera ALC system. The second design provides a rapid switching voltage for the SSEF, which can be synchronized to the camera scan rates.

A block diagram of the ALC system interfaced with the camera is shown in Figure 44. As shown, the camera ALC detector signal is routed to external circuits which process the signal and control a programmable high voltage power supply. Also included in the new circuits are independent selection of manual or automatic modes for the internal ALC using control of the SIT intensifier voltage, the internal automatic gain control (AGC) of the video amplifier, and the operating voltage for the SSEF. In any of the manual modes, potentiometers permit setting the operating point of the associated control functions. The control panel provided for selection and operation of the system is shown in Figure 45.

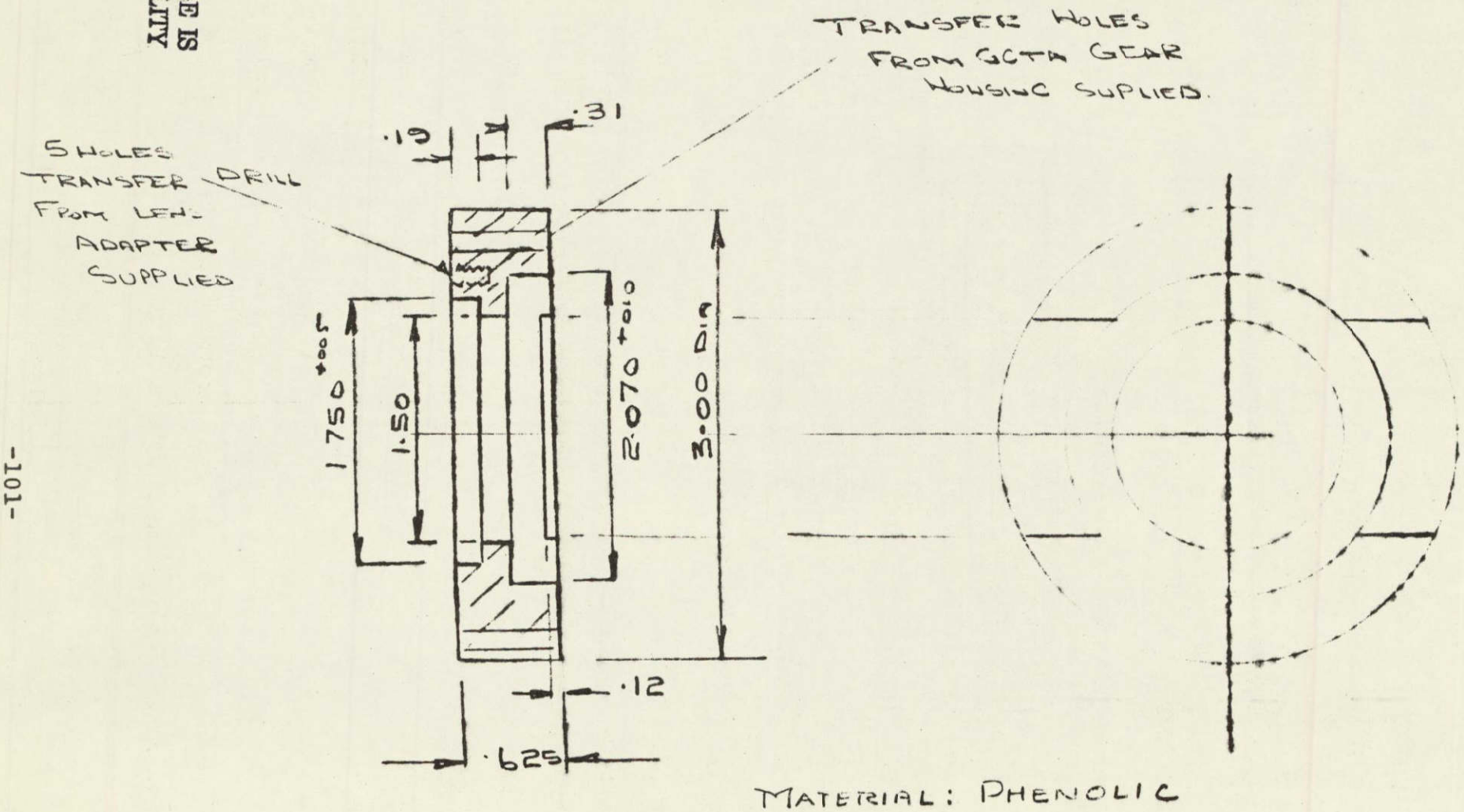

Figure 41. SSEF Holder, Front View

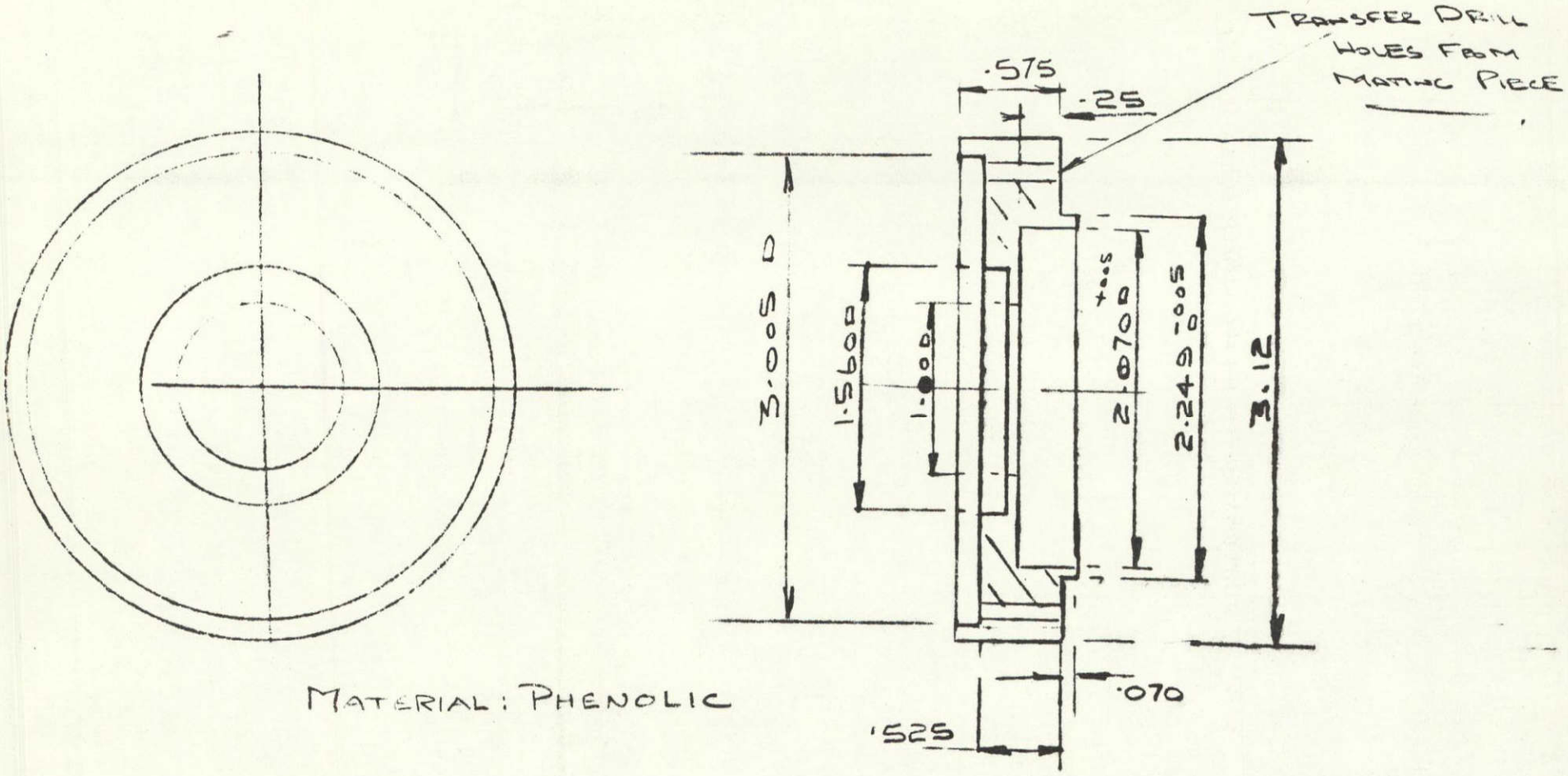

Figure 42. SSEF Holder, Rear View

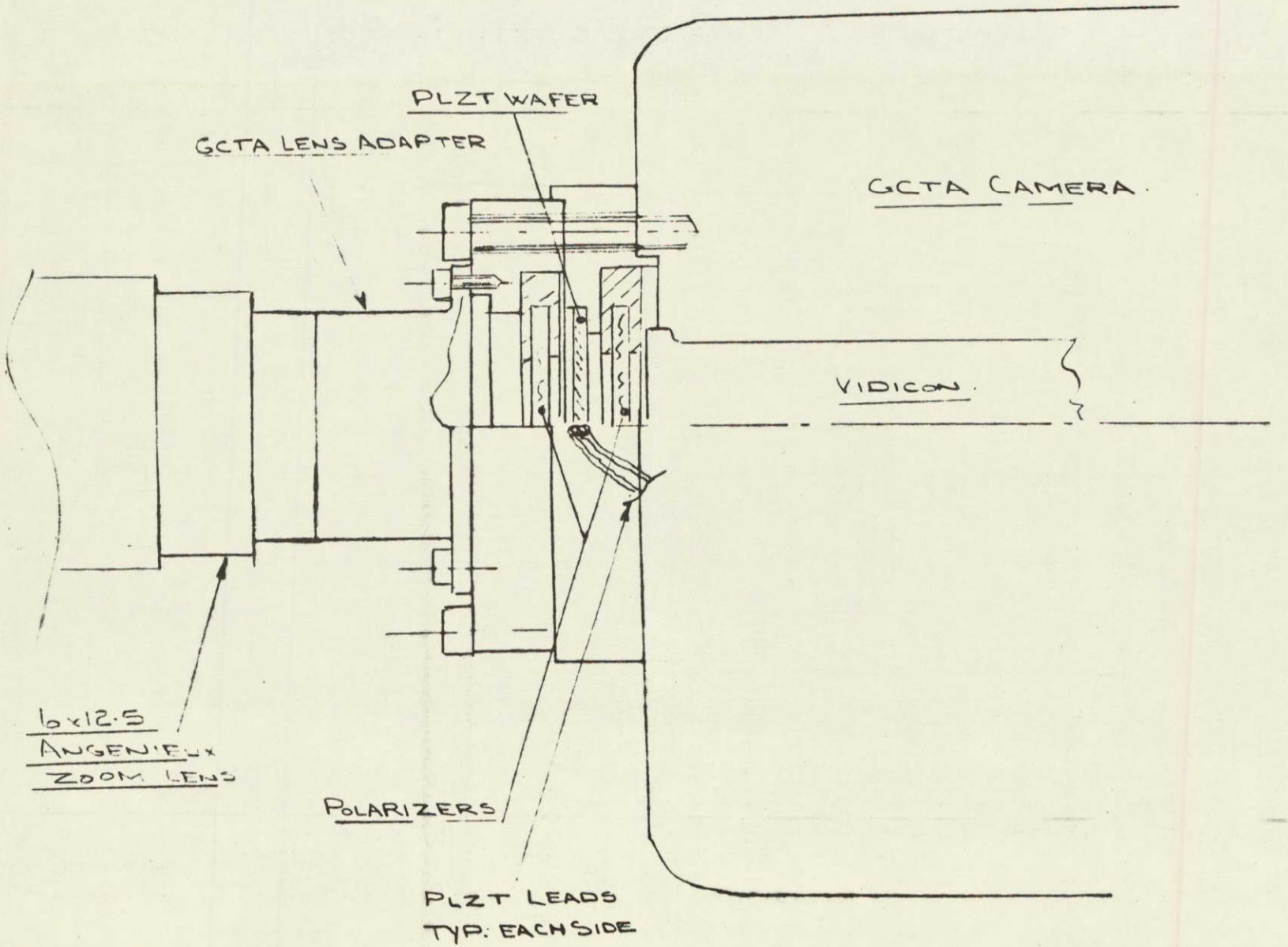

Figure 43. SSEF Holder Assembled to Camera, Cross-Section

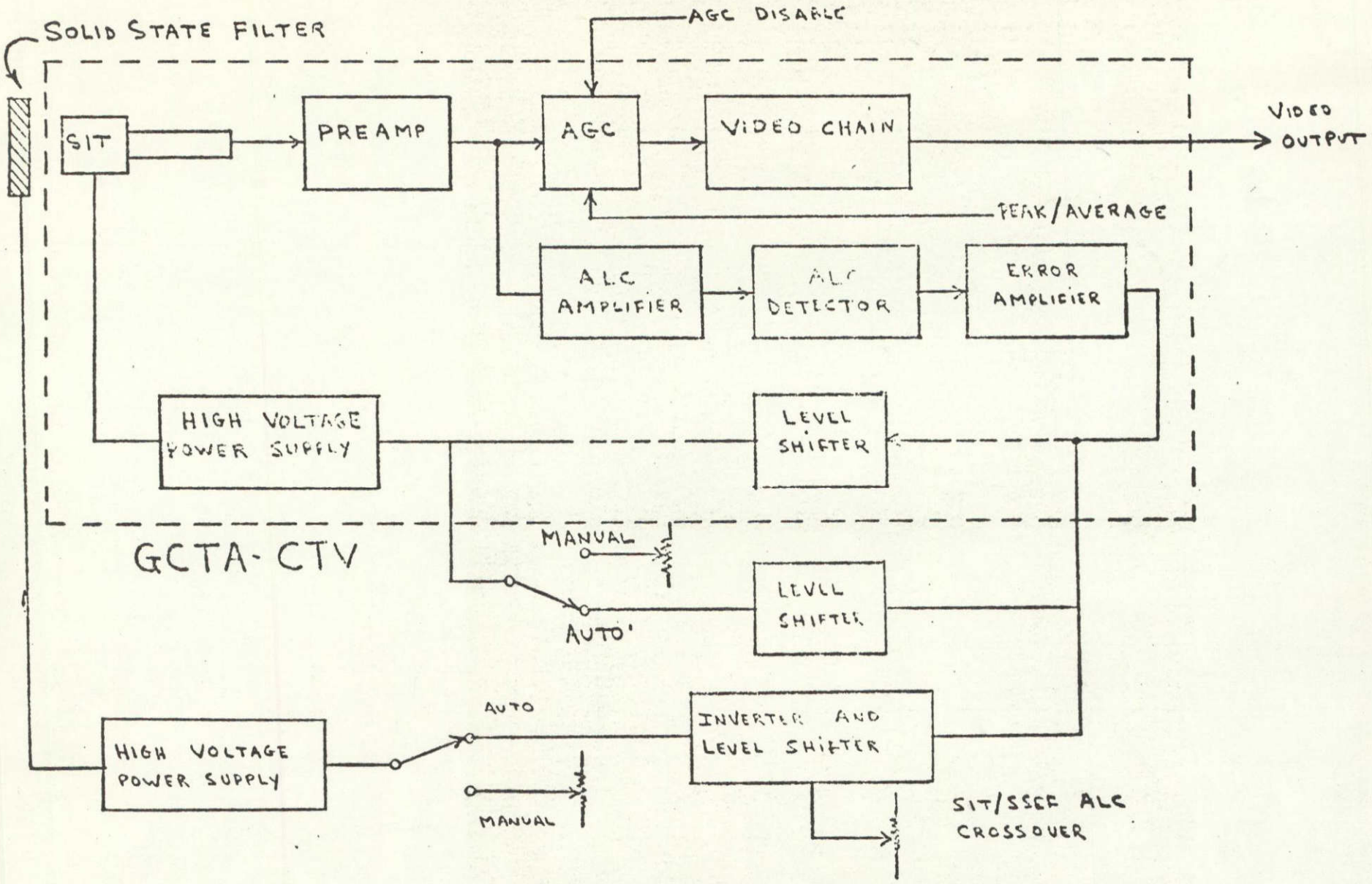

Figure 44. Automatic Light Control System, Block Diagram

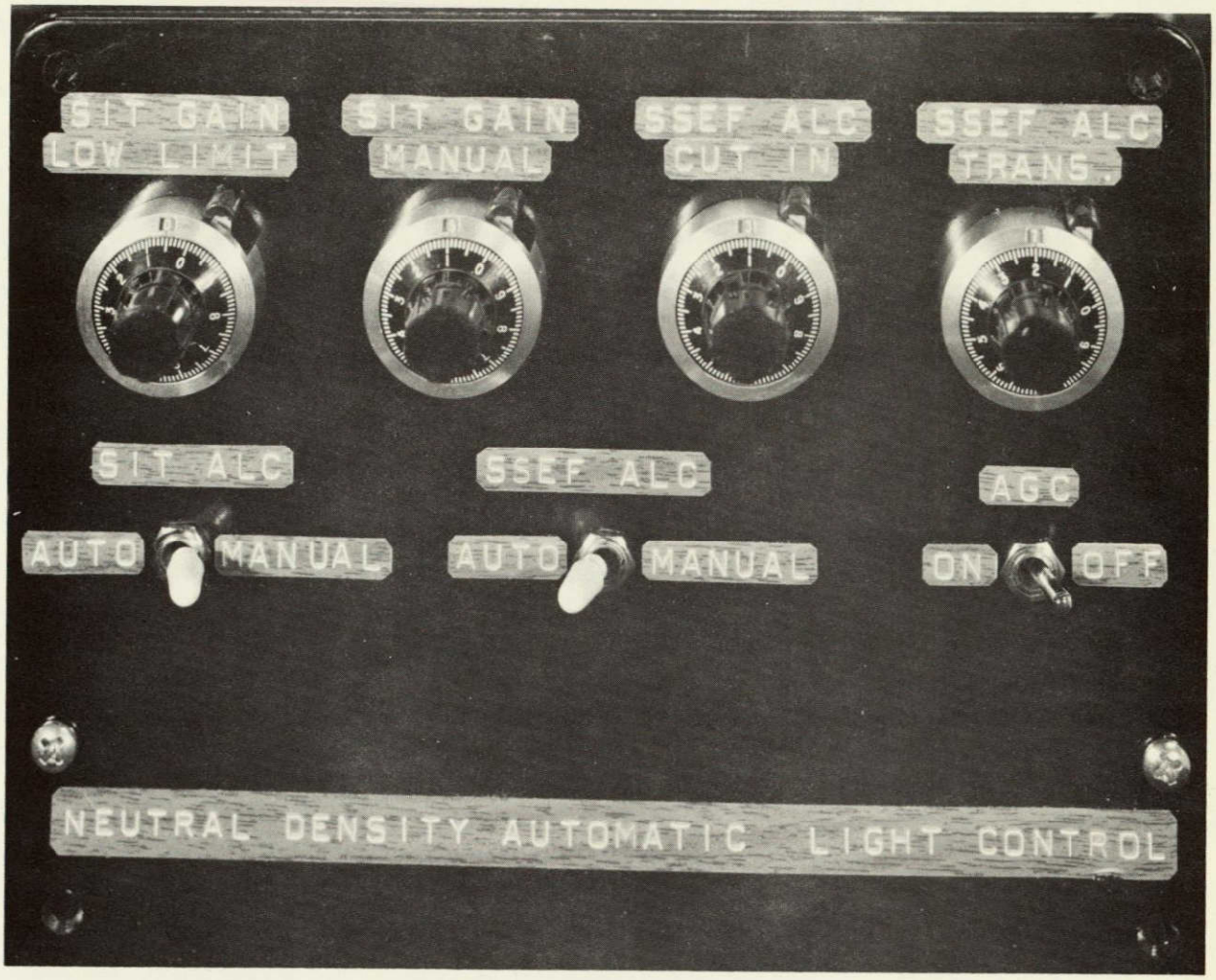

Figure 45. Control Panel for ALC Operation

The detailed circuit schematic diagram, shown in Figure 46, is arranged to minimize the electrical interfaces to the camera circuit boards. Two connections require isolating existing connection points in the camera. All other interfaces are simply attachments to existing circuit board terminals. Components U1 and Q1 replace the original level shifting function, and control the input to the SIT high voltage supply, using either the ALC detector error signal or a manual voltage as a reference.

The AGC channel is controlled by R34 (a simple voltage divider), or the internal camera circuit by switch selection (S3). Components U2, Q2, and U3 perform a similar function for the SSEF channel. This includes signal inversion to match the required control input to the Kepco ABC-1500 power supply which provides operating voltage to the SSEF. The controlled output of this power supply is routed to the SSEF through a series protective resistor located on the SSEF housing. The automatic mode, selected by S2, permits measurement of the SSEF in a closed loop mode. In the manual mode, R9 permits programming the power supply to any fixed operating point within the normal SSEF control range.

The high voltage switching driver design schematic is shown in Figure 47. This circuit is capable of switching from 0 to 1000 volts (10-90% points) in 15 microseconds with no load. With a direct capacitive load of 0.01 μfd (anticipated

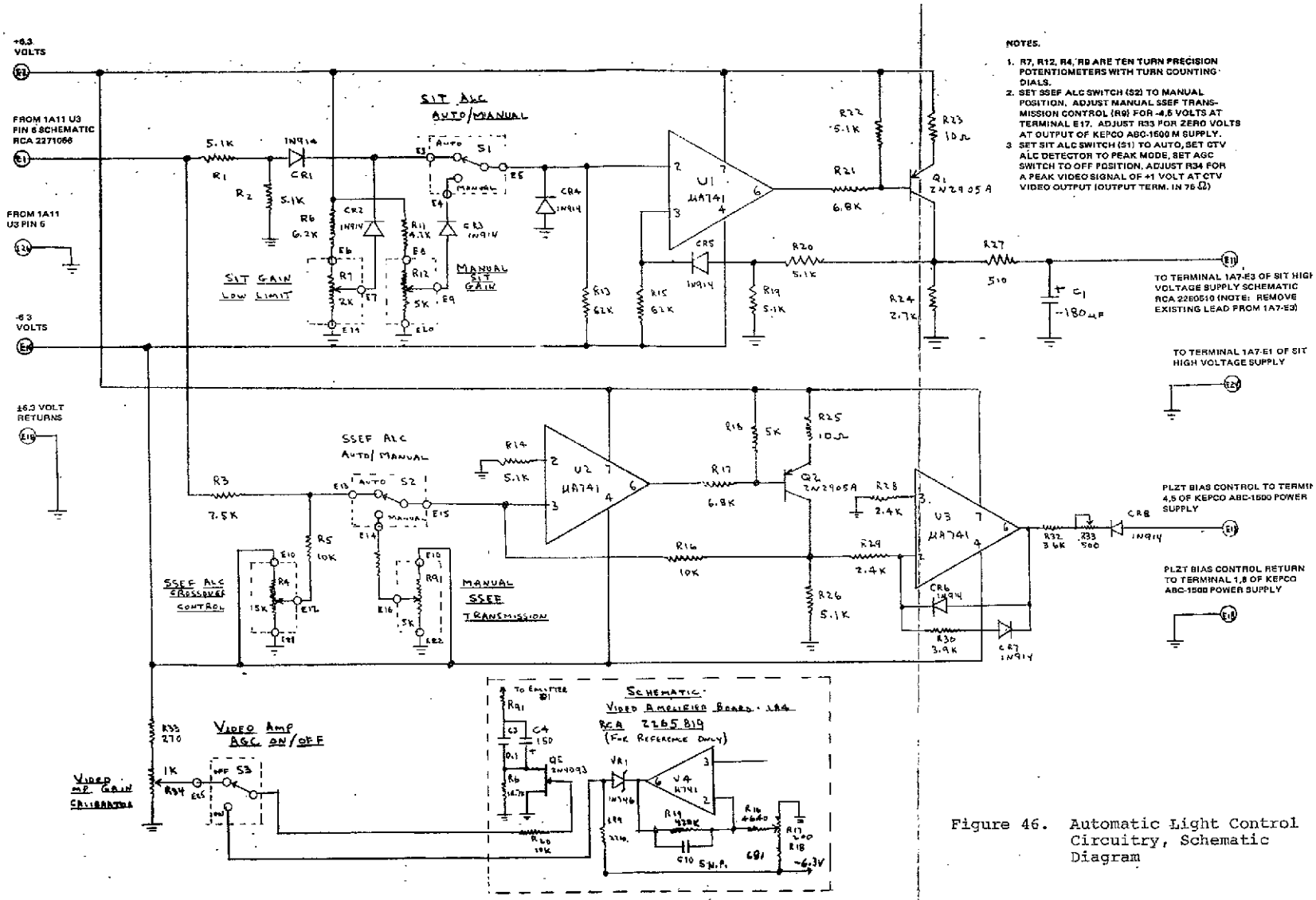

NOTES.

1. R7, R12, R4, R8 ARE TEN TURN PRECISION POTENTIOMETERS WITH TURN COUNTING DIALS.
2. SET SSEF ALC SWITCH (S2) TO MANUAL POSITION. ADJUST MANUAL SSEF TRANSMISSION CONTROL (R9) FOR -4.5 VOLTS AT TERMINAL E17. ADJUST R33 FOR ZERO VOLTS AT OUTPUT OF KEPCO ABC-1500 M SUPPLY.
3. SET SIT ALC SWITCH (S1) TO AUTO, SET CTV ALC DETECTOR TO PEAK MODE, SET AGC SWITCH TO OFF POSITION. ADJUST R34 FOR A PEAK VIDEO SIGNAL OF +1 VOLT AT CTV VIDEO OUTPUT (OUTPUT TERM. IN 75 Ω)

Figure 46. Automatic Light Control Circuitry, Schematic Diagram

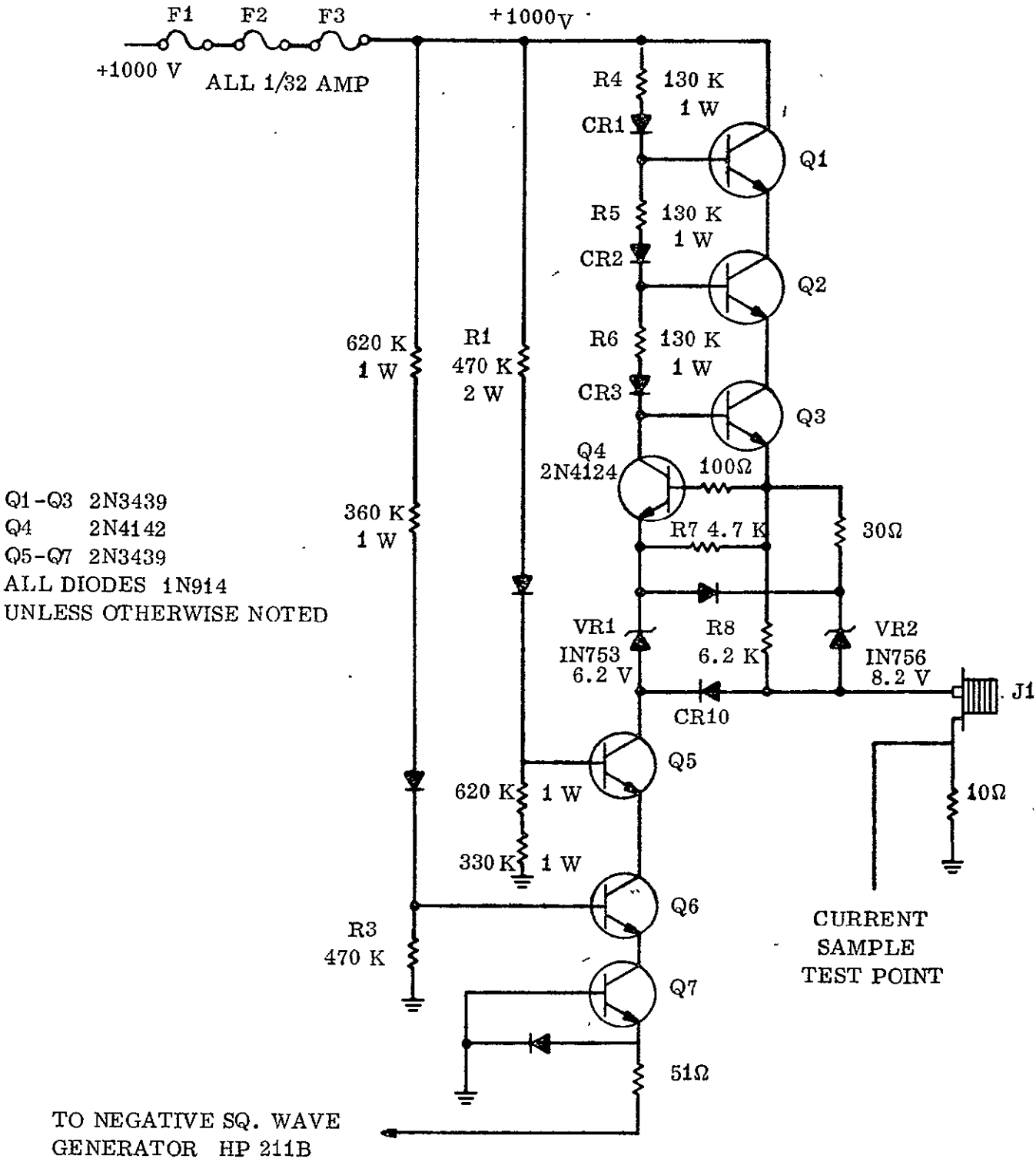

Figure 47. High-Voltage Switching Driver, Schematic Diagram

single PLZT wafer) the rise time from 0 to 1000 volts is about 150 microseconds. The circuit is designed to be driven by an external square wave generator. By using the camera vertical sync to trigger the square wave generator, switching of the circuit (and thus the SSEF operating points) can be accomplished in phase with the camera vertical blanking. Interposing a frequency divider between the sync signal and the generator permits observation of the SSEF at either of two operating points for intervals of multiple vertical fields.

H. TEST RESULTS WITH CAMERA

With the SSEF holder assembled to the CTV camera, several different tests were conducted to study the behavior of the complete system. The dynamic control range was measured using the external automatic control circuitry with the SIT gain and AGC at fixed operating points. Limiting resolution was observed on the monitor display using a standard RETMA test chart. Response time was observed by using the rapid switching circuit described in Section II-C-2. Spectral filter mode operation was examined by obtaining "A" scan photograph for different static SSEF operating points while observing a test pattern containing standard color test chips.

Figure 48 shows the SSEF assembled to the camera in operation during the resolution measurements. The monitor can be seen displaying the camera video output with the resultant "A" scan presentation as viewed on the oscilloscope face.

1. ALC Operation

Several measurement runs were made using the SSEF as the neutral density control element in the ALC system. Highlight scene brightness was varied while monitoring the ALC control loop voltage to the SSEF. As a result of the charging effect at the electrodes, the performance obtained depended strongly on the recent history of the PLZT sample. Best results (largest dynamic range) were obtained when the PLZT

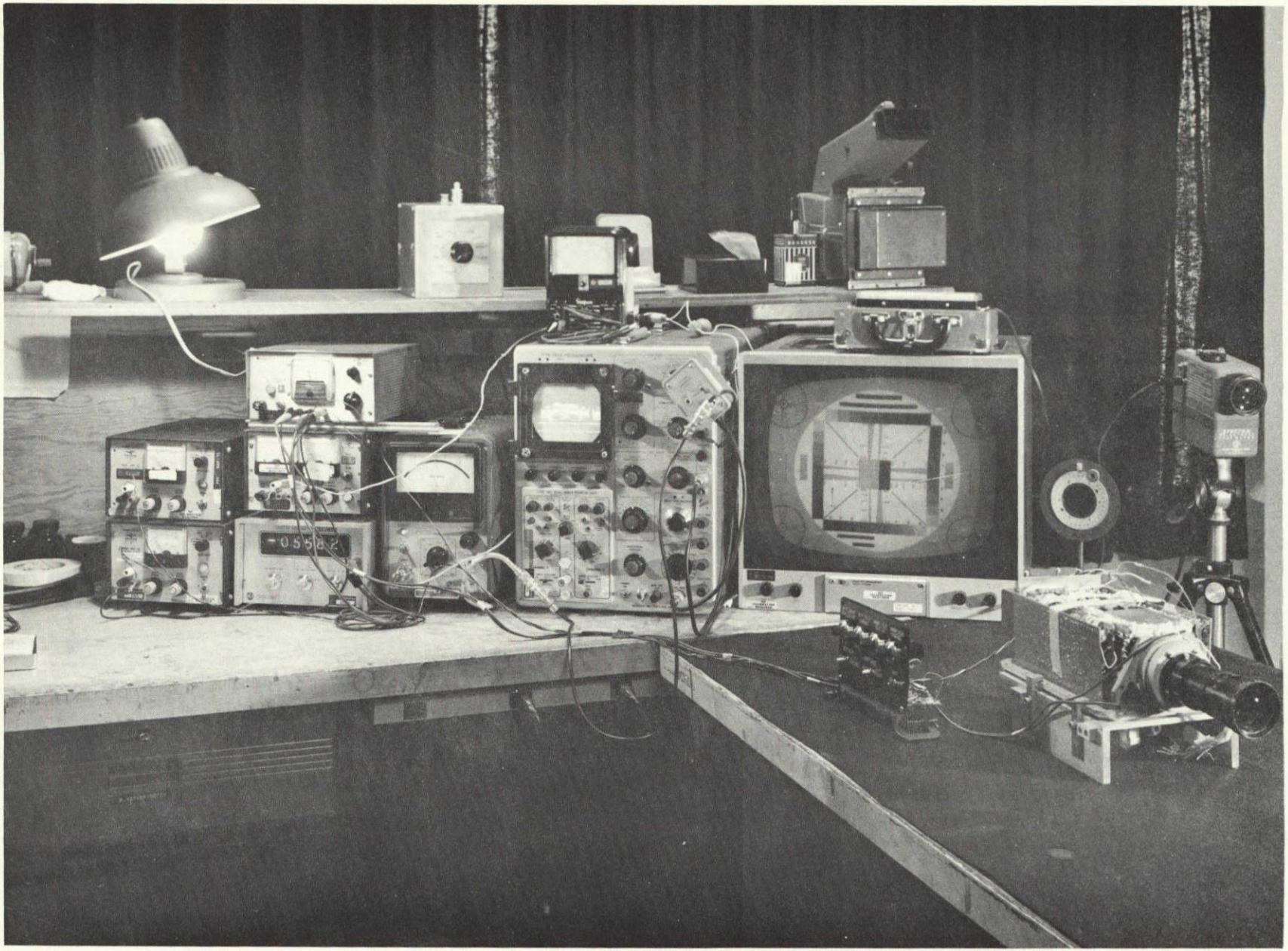

Figure 48. Overall SSEF/CTV Test Set-Up

device was allowed to stabilize at zero potential for a number of hours before starting a test run. Figure 49 shows a typical camera transfer curve obtained after such a stabilization period.

For this curve, the control voltage was manually adjusted to maintain a constant video output level as the highlight brightness was varied. The curve in Figure 49 shows a dynamic range in excess of 225:1. For other runs where no stabilization time was permitted, a reduced range was obtained as a result of electrode charging.

In the automatic mode the operation of the SSEF was smooth and well behaved, giving strong evidence of its potential usefulness in such an application.

2. Resolution

The limiting resolution of the system, with the SSEF installed, was measured to be in excess of 350 TV lines using the monitor display. The SIT gain was manually adjusted to maintain constant video level output while the PLZT voltage was varied to provide minimum and maximum transmission. No apparent change in resolution was noted over the entire range, confirming the resolution measurements performed on the optical bench.

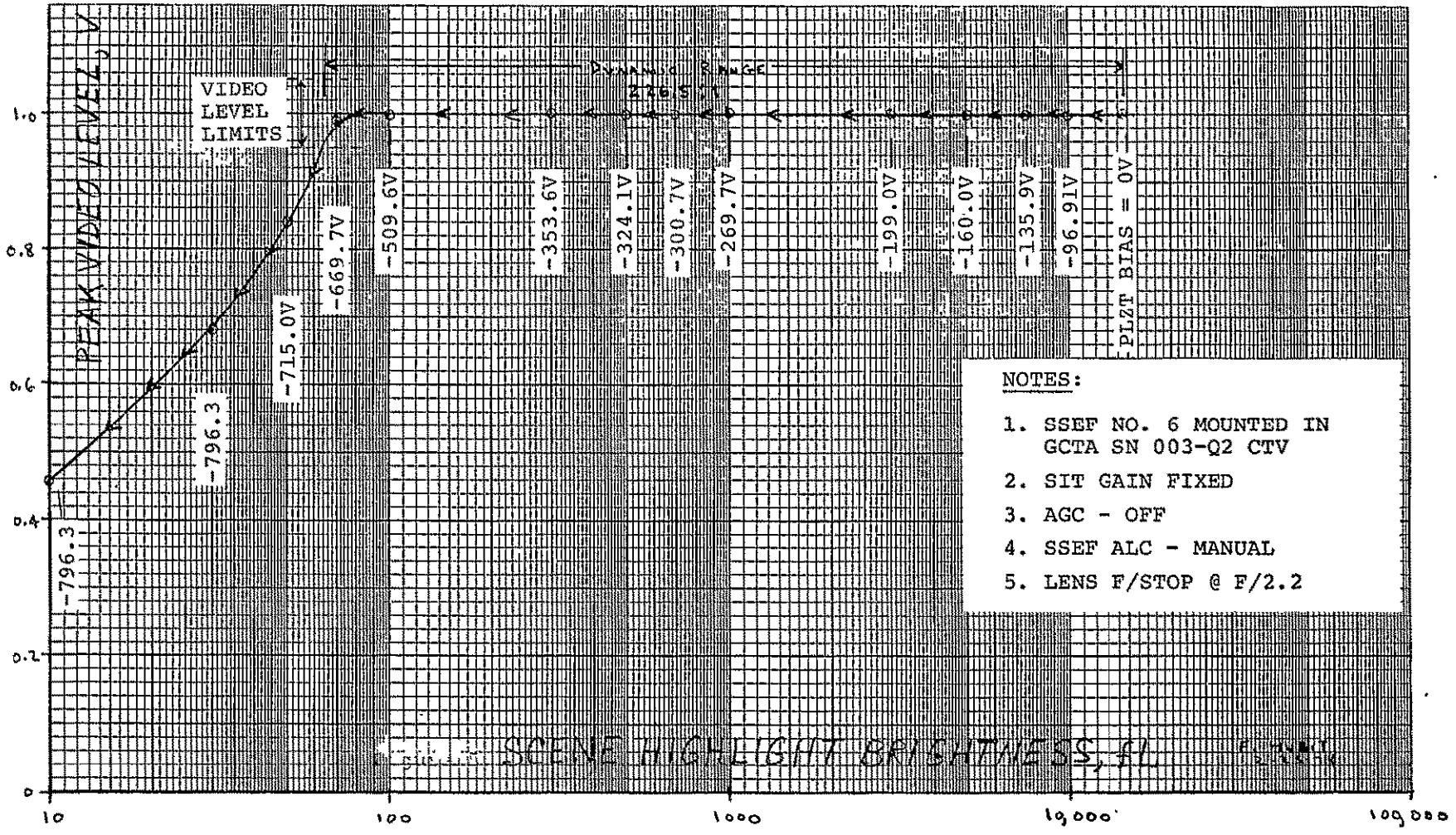

Figure 49. Dynamic Range of SSEF With CTV

The resolution measurements were performed with the lens aperture set at f/2.2. The monitor display was also examined as the lens aperture was stopped down to f/22. At f/2.2, the overall transmission was relatively uniform. As the lens was stopped down, interference bands, projected from the electrode spreading effects grew progressively more intense. In a practical application, the lens system will probably be operated at maximum aperture (to compensate for the SSEF insertion loss); however, the banding still represents an undesirable effect. Improved electrode contacts are expected to greatly minimize the magnitude of this effect.

3. Response Time

The high voltage drive circuit was applied to the SSEF through a 100 kilohm limiting resistor. Switching was synchronized with the leading edge of the vertical blanking pulse. "A" scope photographs of the applied switching voltage and camera video output signal are shown in Figures 50 and 51 for the on and off transition respectively. Approximately three vertical field periods are observed before nominally constant output is obtained. Since some of the signal buildup and decay can be attributed to integration and lag characteristics of the sensor, an additional test was performed using a photodiode to measure the transmission through the SSEF in response to the switching voltage.

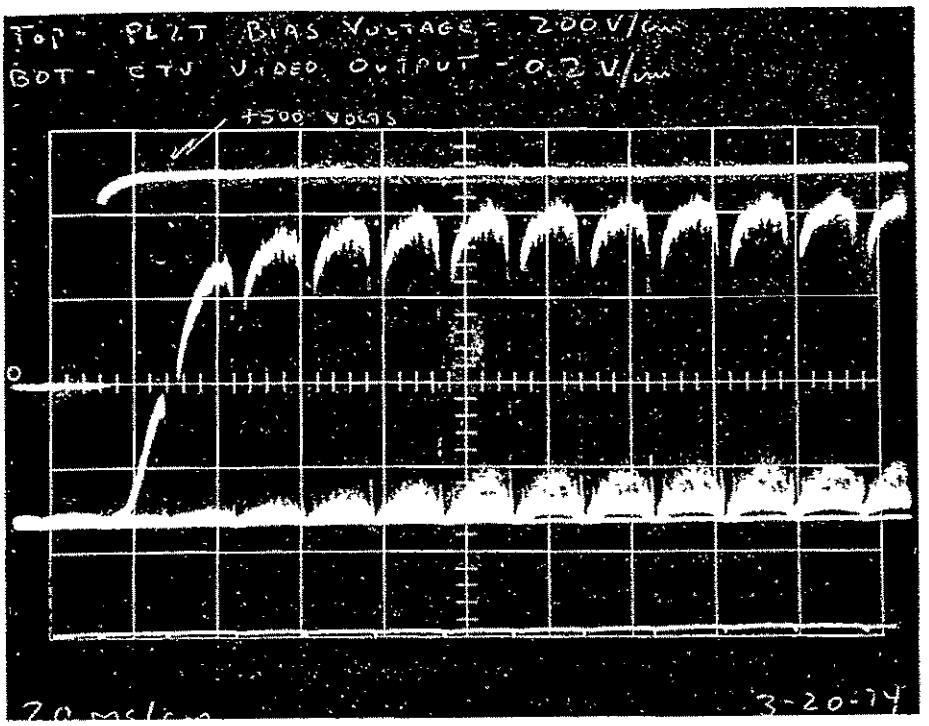

Figure 50. Video Output, SSEF Switched On

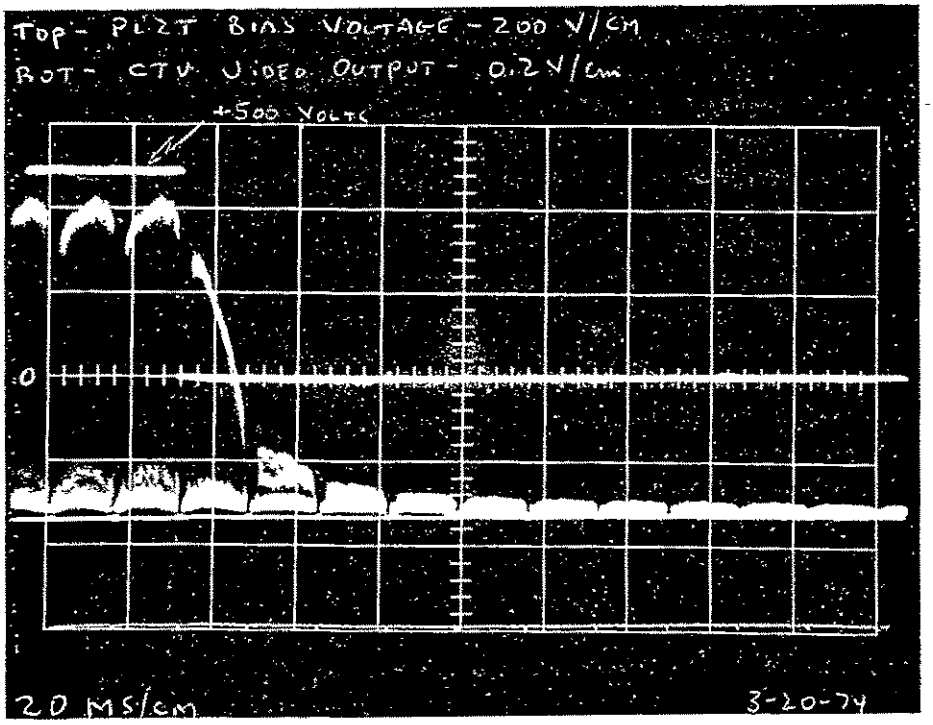

Figure 51. Video Output, SSEF Switched Off

The results for this test are shown in Figures 52 and 53, while the applied voltage step is shown in Figure 54. The voltage step, through the limiting resistor, approaches full amplitude in about 10 milliseconds. The corresponding optical response times observed on the photographs are nearly identical, indicating that the time constant problem associated with the use of an SSEF in a rapid switching application (such as spectra separation filtering) will relate to the circuit design rather than the limiting properties of the SSEF device.

4. Spectral Filter Observation

The spectral filter separation characteristics of the SSEF were observed, using the CTV camera, for the same operating points which were evaluated on the optical bench (Section II-F-9).

The color reference chart consisted of six color chips plus a black and white reference. The colors on the chart were red, blue, green, cyan, yellow, and magenta (three primaries plus three complements). For each test condition (PLZT voltage and retardation plate), the SIT gain was manually adjusted to provide a constant signal level from the white reference. The video signal level from each chip was measured at each test condition. To provide a common reference, the data obtained was normalized to the reference values in the neutral density mode, as shown in Table 6.

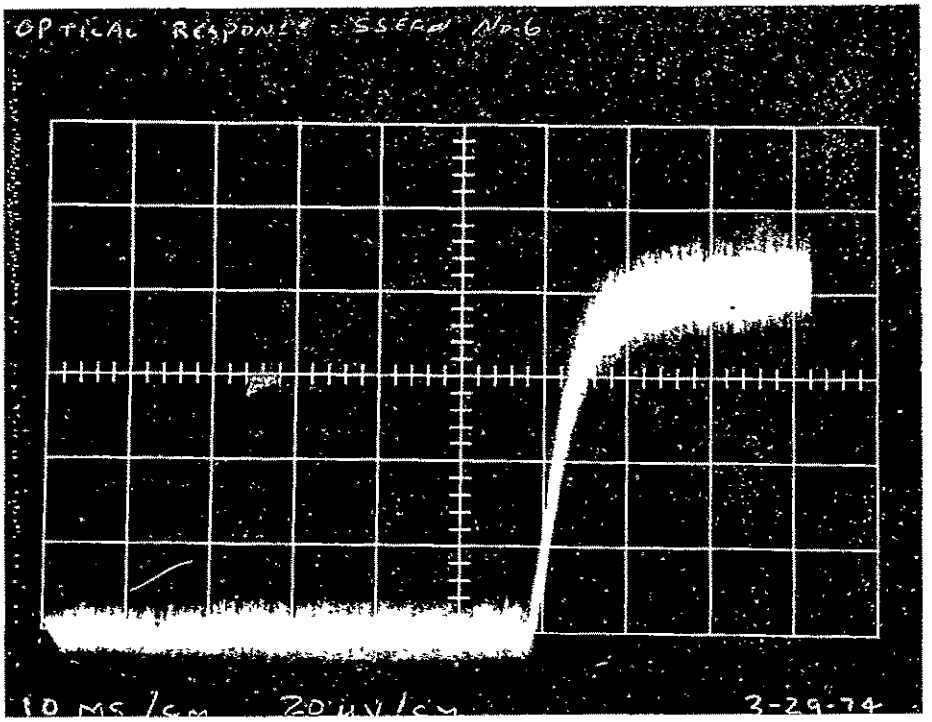

Figure 52. Photodiode Output, SSEF Switched On

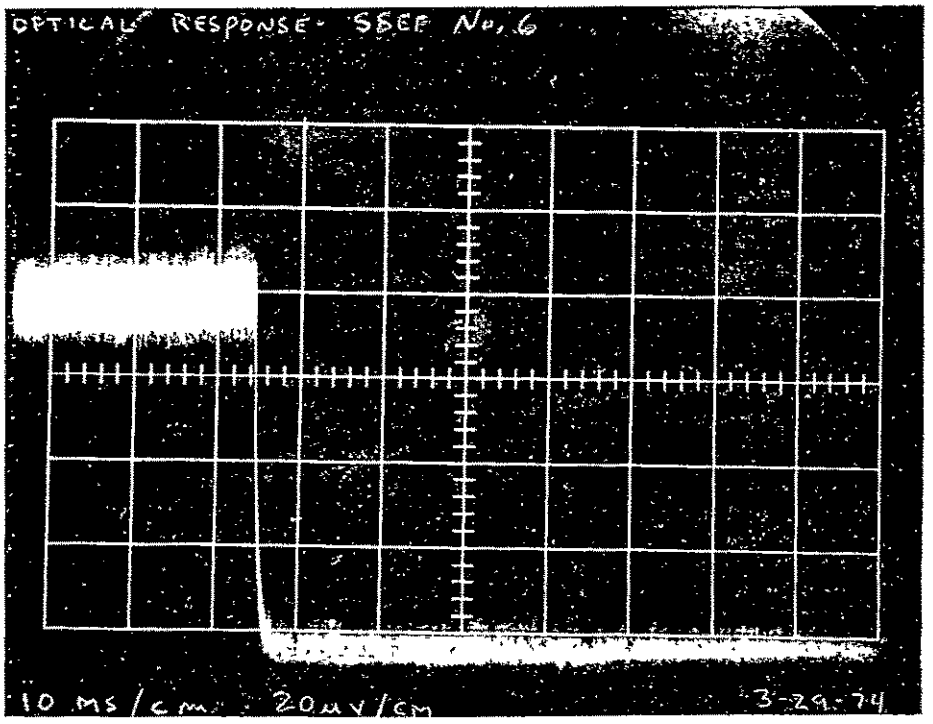

Figure 53. Photodiode Output, SSEF Switched Off

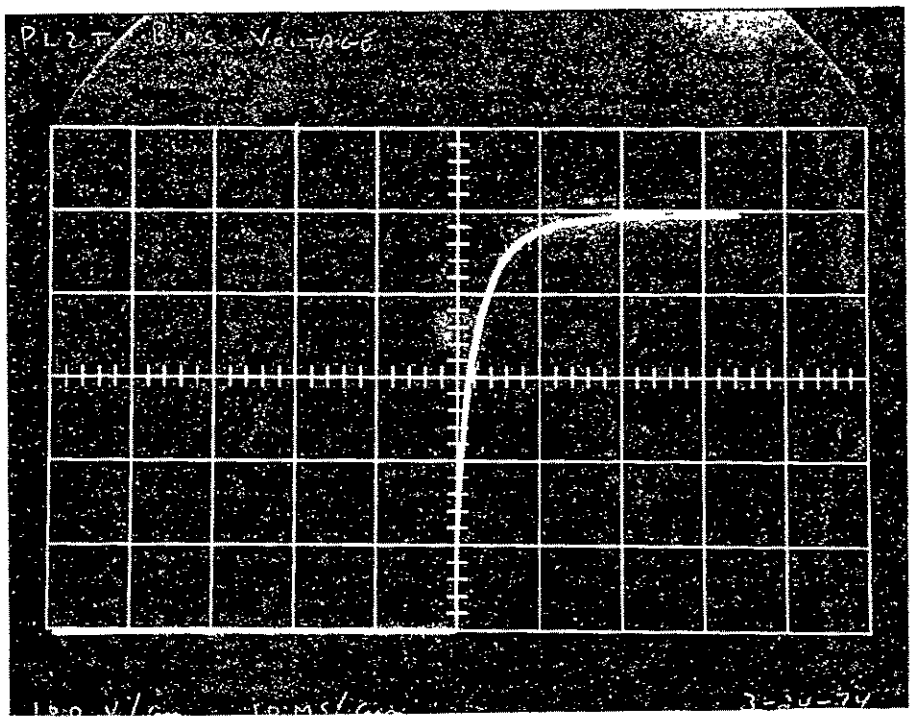

Figure 54. SSEF Applied Switching Voltage Step

TABLE 6. NORMALIZED COLOR CHIP MEASUREMENTS

TEST	RED	MAGENTA	BLUE	CYAN	GREEN	YELLOW	VISUAL COLOR
*	.19	.31	.34	.44	.33	.24	Neutral
1	1.21	1.03	.94	.86	.97	1.17	Pale Yellow
3	1.79	1.29	.94	.68	.73	1.17	Yellow Orange
10	1.37	1.29	1.26	.86	.79	1.0	Blue
11	1.89	1.61	1.21	1.0	.24	1.0	Magenta
12	2.11	1.68	1.21	.5	.30	1.08	Red
13	2.11	1.55	1.06	.59	.55	1.25	Orange
14	1.79	1.35	1.03	.73	.79	1.25	Pale Yellow
15	1.47	1.16	.94	.70	.85	1.17	Pale Green

* Reference neutral density mode scale values.

The resultant spectral amplitude responses for the three primary colors at each test condition are shown in Figure 55. The solid lines shown connecting the plot points convey no information; they serve merely to tie together points of a common color. The relative responses at each test condition can be compared to the observed visual transmission through the filter which is listed for reference in Table 6.

This relatively simple test is not meant to represent the final system operation; rather, it serves merely to indicate the potentially useful spectral separation properties of the SSEF.

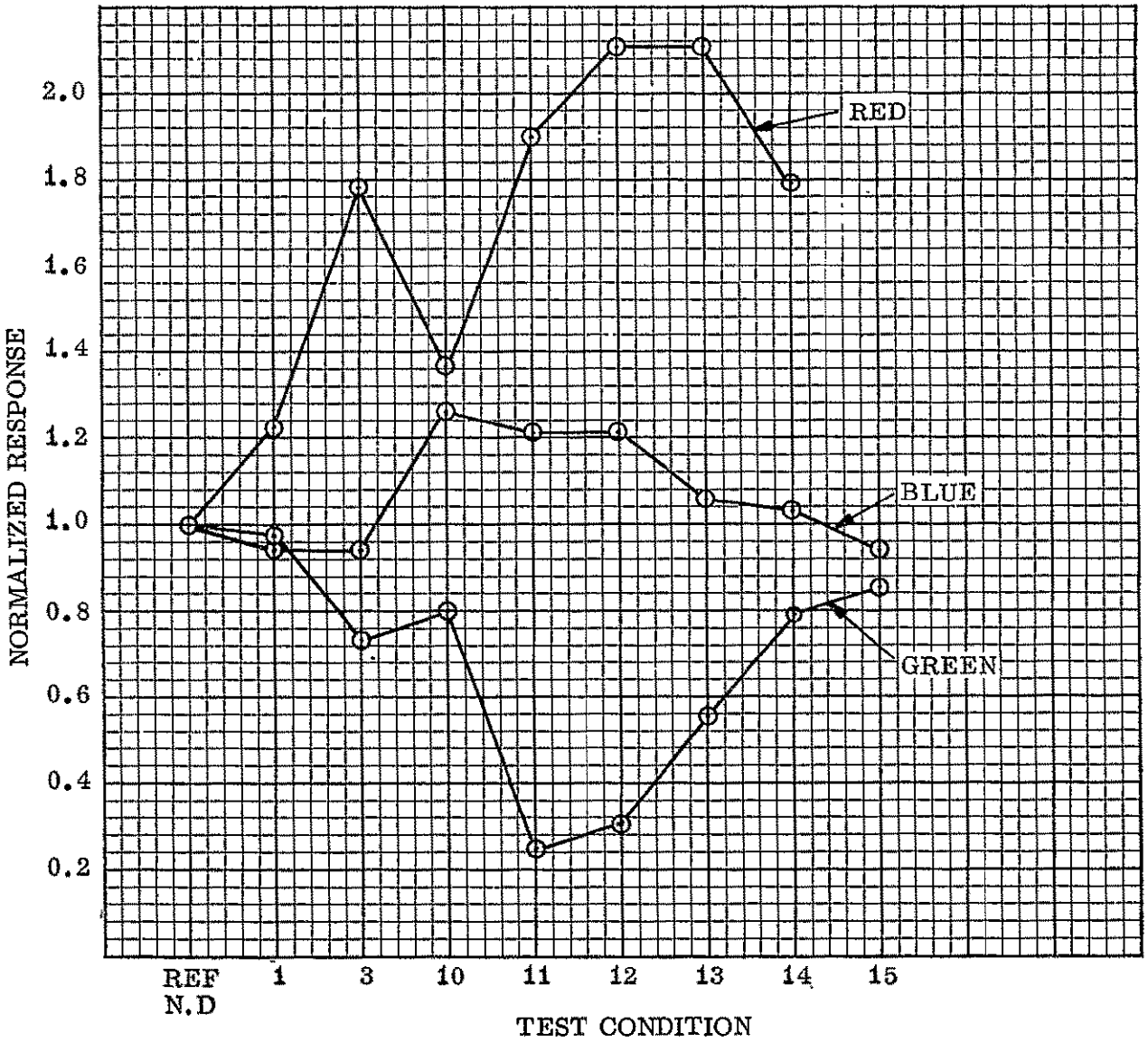

Figure 55. Normalized Response to Color Sample Chips

SECTION III

THEORETICAL ANALYSIS

A. GENERAL

This section contains theoretical analyses which were performed during the course of this study for certain aspects of the PLZT filter system which can be treated mathematically. An analytic approach to the performance with non-normal incident light is presented in Section III-B. The performance which may be expected using a synthesized optical network, rather than the straightforward polarizer/PLZT/ analyzer assembly, is analyzed in Section III-C. This analysis is based on the work reported by Chang, Amman, and Harris[8], and should be further experimentally verified in future application work.

B. ANGULAR APERTURE OF SOLID-STATE ELECTRO-OPTICAL FILTER DEVICES

The transmission at each wavelength through a Solid-State Electro-Optical Filter (SSEF) depends on the birefringent retardation of the active ceramic element (or elements) of the device. Ideally, this retardation should be independent of the angle of incidence of a beam of light upon the device. The reason for this is that at any point in any real optical system, light is incident over a finite range of angles. (This range of angles increases with increasing "speed" of the system,

i.e., with increasing numerical aperture or decreasing f-number.) If the birefringent retardation varies with angle of incidence then the wavelength corresponding to peak transmission at one angle of incidence will be different from that at a different angle of incidence. The net effects for light incident over a range of angles will be to decrease the spectral purity in the case of a color filter, or decrease the maximum permissible throughput in the case of a neutral density filter.

In this section, quantitative expressions for the variation of birefringent retardation with angle of incidence are obtained; the effects that such variation will have on the operation of SSEF devices are assessed; and methods (if required) for reducing the variation are discussed. The PLZT ceramic used in SSEF devices is an optically isotropic (i.e., non-birefringent) medium in the absence of electric fields. When an electric field is applied, the ceramic becomes optically uniaxial, with the optic axis parallel to the electric field direction. We observe in this case that except for non-basic nonuniformities discussed elsewhere in this report, the active SSEF plate behaves like a homogeneous uniaxial medium with its optic axis parallel to the plane of the plate and perpendicular to the direction of the electrode fingers.

The birefringence exhibited by the plate will in general vary not only with the angle between the light beam and the plate-normal but also with the azimuthal direction of the light

beam, i.e., the angle between the optic axis and the projection of a light ray onto the plane of the plate. We have derived expressions for the transmission of such a plate situated between crossed polars that are exact, except for the following three approximations: (1) that anti-reflection coatings on the surfaces of the plate make losses and phase-shifts at the interfaces negligible, (2) the birefringence is sufficiently small that the refraction processes can be treated with a single refractive index, and (3) that the polarizers behave ideally. The derivation is complicated, and the final expression for the transmission retains any semblance of compactness only if it is presented in the form of a series of substitutions involving different variables that finally lead back to the original physical parameters of the problem. This is exactly the situation that is most readily treated by modern computer techniques. For this reason the expression for the transmitted intensity was derived in the form of a Fortran PI (Princeton Interactive) program. The explicit program and its derivation are included as Appendix A to Monthly Report No. 5.

Expressions for the angular variation of the birefringent retardation can be obtained in vastly simplified form if the treatment is restricted to the two cases shown in Figure 56 that the azimuthal orientation of the light beam is such that the projection of the ray direction onto the plane of the plate is either (1) perpendicular or (2) parallel to the optic axis of the ceramic. These cases are especially significant

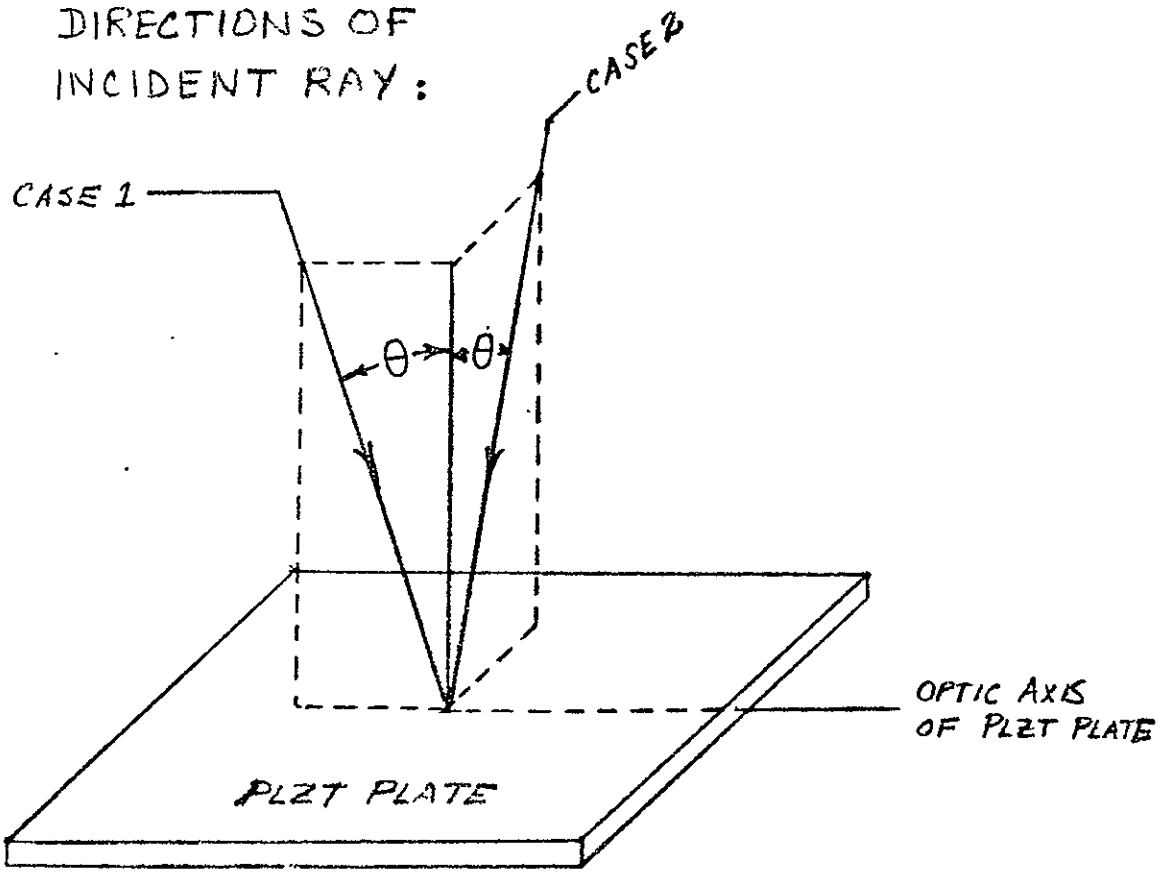

Figure 56. Special Cases for Directions of Incident Light Rays

because they represent the worst-case behaviors as the direction of the beam deviates from normal incidence upon the plate. The results in these cases are sufficiently simple that they convey physical understanding of how various factors can influence device performance.

Case (1) above will be treated first. In this case the direction of the light, even after refraction into the ceramic plate, is normal to the optic axis. Let θ be the angle between a light ray and the normal to the faces of the plate. Under these circumstances, the Fresnel ellipsoid-of-wave-normals construction [86] dictates that the refractive indices for the two orthogonal polarizations are simply n_ε and n_ω, independent of θ, the principal extraordinary and ordinary refractive indices of the plate. The variation of birefringence with θ arises in this case entirely from the variation with angle of incidence of the effective optical path length through the plate. This variation can be calculated with the aid of Figure 57. The light ray IOAB is incident at angle θ upon the plate of thickness t. The optical path length $\overline{OA}$ through the plate is:

$$\overline{OA} = t/\cos\phi = t/(1 - \sin^2\phi)^{1/2} \qquad (1)$$

Since from Snell's law:

$$\sin\phi = \frac{1}{n}\sin\theta\ , \qquad (2)$$

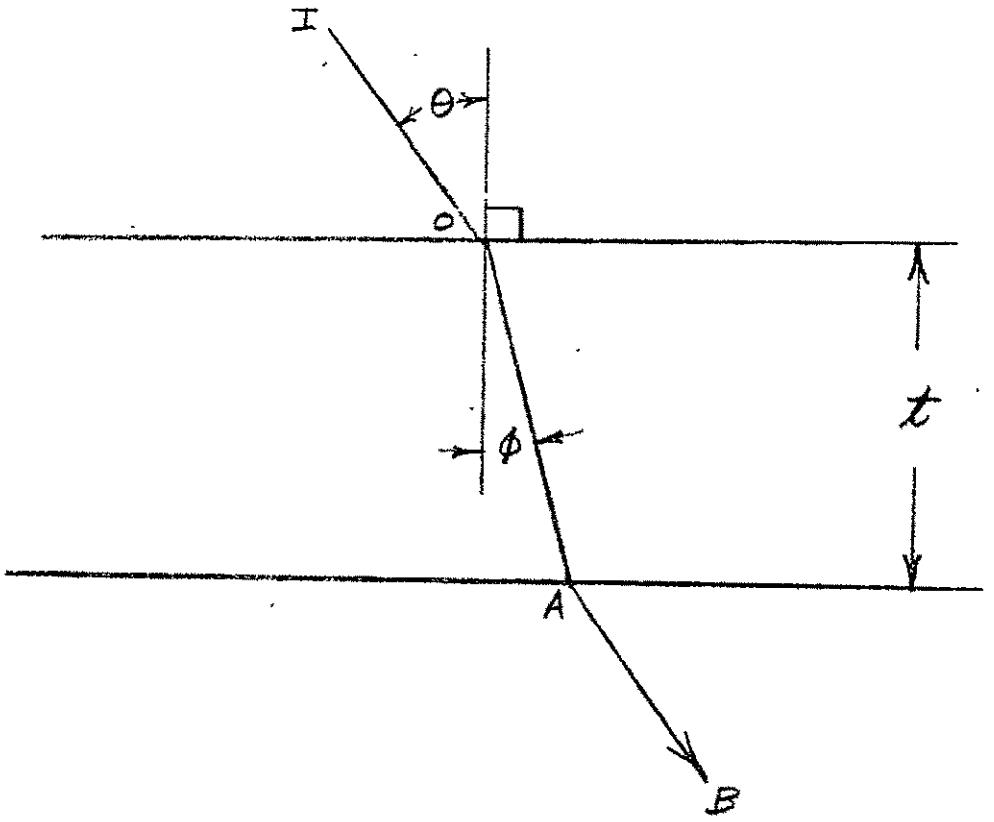

Figure 57. Transmission of Light Through PLZT Plate

where n is the (mean) refractive index of the plate, and the birefringent retardation $\Gamma_1(\Theta)$ is the product of $\overline{OA}$ and the difference between the refractive indices for the two orthogonal polarizations, it follows that

$$\Gamma_1(\Theta) = \overline{OA}\left(n_\varepsilon - n_\omega\right) = t\left(n_\varepsilon - n_\omega\right) \Big/ \left(\frac{1 - \sin^2\Theta}{n^2}\right)^{1/2} . \qquad (3a)$$

For small values of Θ, an approximation to this result can be obtained by expanding Equation (3a) and retaining only the lowest-order term in Θ:

$$\Gamma_1(\Theta) \approx t\left(n_\varepsilon - n_\omega\right)\left(1 + \frac{\Theta^2}{2n^2}\right) \qquad (3b)$$

The change $\Delta\Gamma_1(\Theta)$ in retardation is equal to the difference between the retardation at angle of incidence Θ and that at normal incidence $(\Theta = 0)$:

$$\Delta\Gamma_1(\Theta) = \Gamma_1(\Theta) - \Gamma_1(0) \approx t\left(n_\varepsilon - n_\omega\right)\frac{\Theta^2}{2n^2} \qquad (4)$$

Case (2), in which the projection of the ray direction onto the plane of the plate is parallel to the optic axis of the ceramic, will now be discussed. The optical path length through the plate is the same as in Case (1), and is given by Equation (1).

The refractive indices for the two orthogonal polarizations in this case are n_ω, and a value $n_i(\theta)$, intermediate between n_ω and n_ε, that depends on the angle θ. According to the ellipsoid-of-wave-normals construction, the index n_i is given by the length of line segment $\overline{OC}$ in Figure 58, where $\overline{AO}$ is parallel to the ray direction, $\overline{OB}$ is normal to the faces of the plate, $\overline{OD}$ is parallel to the optic axis, and the curve is an ellipse whose principal axes $\overline{OB}$ and $\overline{OD}$ are equal in length to n_ω and n_ε respectively. It follows from the above and from the basic equation for an ellipse that n_i is given by:

$$n_i(\theta) = n_\varepsilon \left[1 + n_\varepsilon^2 \sin^2 \phi \left(\frac{1}{n_\omega^2} - \frac{1}{n_\varepsilon^2} \right) \right]^{-\frac{1}{2}} \qquad (5)$$

When Equation (2) which relates ϕ to θ is inserted into Equation (5), and the result is expanded to lowest order in θ and in the small quantity $(n_\varepsilon - n_\omega)$ (which is equal to zero in the absence of an applied electric field), the following approximate form for n_i is obtained:

$$n_i \approx n_\varepsilon - \frac{(n_\varepsilon - n_\omega)}{n^2} \theta^2 \, . \qquad (6)$$

The retardation $\Gamma_2(\theta)$ is given analogously to that in case (1) as:

$$\Gamma_2(\theta) = \overline{OA} \left(n_i - n_\omega \right) \approx t \left(n_\varepsilon - n_\omega \right) \left(1 - \frac{\theta^2}{2n^2} \right)$$

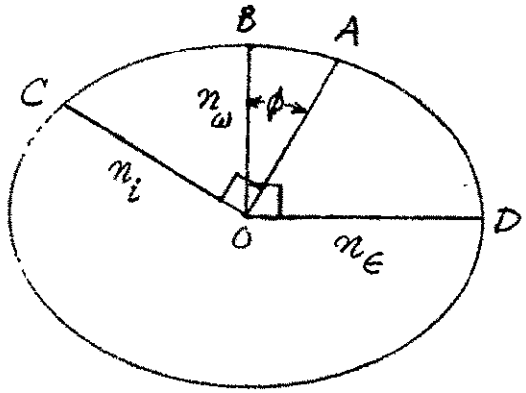

Figure 58. Fresnel Ellipsoid-of-Wave Normals Construction for Determining n_i

It follows that:

$$\Delta\Gamma_2(\Theta) = \Gamma_2(\Theta) - \Gamma_2(0) \approx -t\left(n_\varepsilon - n_\omega\right)\frac{\Theta^2}{2n^2} \quad . \tag{8}$$

Comparison of Equations (4) and (8) shows that to these approximations, $\Delta\Gamma_1(\Theta)$ and $\Delta\Gamma_2(\Theta)$ are simply negatives of one another.

These equations imply that the retardation mapped in projection as a function of direction of incidence might be expected to have the form of a symmetrical saddle. This is precisely what is observed for birefringent plates by conoscopic methods, which are described in Section II-C-2. For azimuthal angles intermediate between Cases (1) and (2) the change in retardation assumes values intermediate to those given by Equations (4) and (8). For an azimuthal angle exactly halfway between the two cases (i.e., when the projection of the ray direction onto the plane of the plate is at an angle of 45° to the optic axis) the retardation is observed to be essentially independent of Θ.

Because the retardation for normal incidence is $t\,(n_\varepsilon - n_\omega)$ it follows from either of Equations (4) or (8) that the magnitude of the relative change in retardation in the worst case is simply $\Theta^2/2n^2$. For $\Theta = 0.245$ radians, which corresponds to f/2 optics, and $n = 2.5$, this relative change is 4.8×10^{-3}, or 0.48%. The relative insensitivity of the retardation of

PLZT ceramic to direction of incidence is due to its high index of refraction n.

There are a number of ways of keeping the variation of retardation with angle within even closer limits than those implied above. One method[98] is to use two identical retardation plates rotated 90° with respect to one another, interspersed by a half-wave retardation plate. A drawback of this scheme is that a half-wave plate functions rigorously as such only at a single wavelength. A number of other schemes, involving arrays of optically biaxial (rather than uniaxial) media have been advanced[96,98]. A scheme that provides at least partial compensation over an essentially unlimited range of wavelengths, and that is applicable to uniaxial media such as PLZT ceramic, is discussed below.

A second uniaxial plate, with its optic axis oriented as shown in Figure 59, is introduced. The thickness of this compensating plate depends upon its principal refractive indices (n_ω and n_ε), and upon the principal refractive indices and thickness of the primary retardation plate. If the primary and compensating plates are of the same material (with the same values of n_ω and n_ε at all wavelengths), then the compensation is obtained for all wavelengths, and the appropriate thickness of the compensating plate is exactly one-half that of the primary retardation plate. It is shown in Appendix B to Monthly Report No. 5 that for directions of incidence of

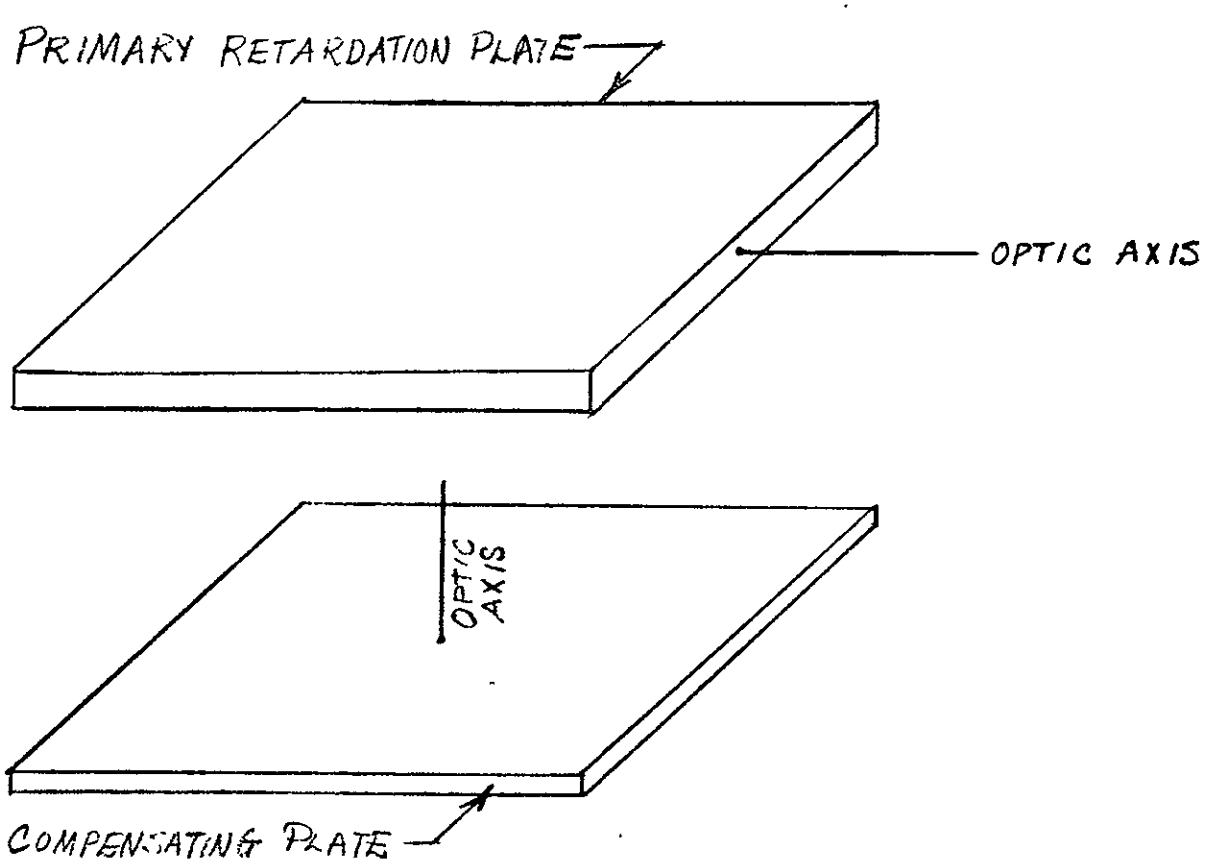

Figure 59. Compensation Scheme for Decreasing the Variation of Retardation With Angle of Incidence (Exploded Drawing)

light as in Cases (1) and (2) above, this array has a net retardation that is independent of θ to order θ^2. It was mentioned above that for an azimuthal angle halfway between Cases (1) and (2) the simple retardation plate has a retardation that is essentially independent of θ. For such an azimuthal angle, the principal directions of the additional birefringence introduced by the compensating plate are parallel to the polarizer axes, and therefore have no effect on the optical behavior of the system. The net result is that the optical behavior of the array shown in Figure 59 is independent of θ to the order θ^2 for all azimuthal angles that are multiples of 45°, and is more independent of θ than a simple birefringent plate for intermediate azimuthal angles.

C. SPECTRAL RESPONSE OF SOLID-STATE ELECTRO-OPTICAL FILTERS - OPTICAL NETWORK SYNTHESIS

It is convenient to discuss the spectral response of birefringent devices in terms of the wave number, $\bar{\gamma}$, of the incident light. The wave number is simply the reciprocal of the vacuum wavelength of the light, and is proportional to the optical frequency. The intensity I transmitted by a birefringent plate between parallel polars is given by:

$$I = I_o B \cos^2 \pi (n_1 - n_2) t \bar{\gamma} \qquad (9)$$

where I_o is the incident intensity, B is a factor that is essentially independent of $\bar{\gamma}$, n_1 and n_2 are the refractive indices for the two orthogonal polarizations in the medium, and t is the thickness of the plate. For crossed instead of parallel polars, the cosine function in Equation (9) is replaced by the sine function. The intensity I expressed in Equation (9), when plotted as a function of $\bar{\gamma}$, represents the spectral response function of the array. Note that there are many ways that this function can be made to have a maximum at any desired wave number $\bar{\gamma}_o$. This can be achieved if the thickness and/or the birefringence of the plate are adjusted so that:

$$(n_1-n_2)\ t = m/\bar{\gamma}_o \qquad (10)$$

where m is any integer. The particular value of m that is used to make an array with a transmission maximum at $\bar{\gamma}_o$ is called the order of the birefringent interference filter. Filters having large values of m have the desirable property that their transmission decreases rapidly as $\bar{\gamma}$ departs from $\bar{\gamma}_o$. However, they suffer from the drawback that the adjacent maxima are more closely spaced than with filters with lower orders. The colors produced by simple filters of this sort are actually quite different from pure spectral colors. It is interesting to note that, when attempting to approximate the visible spectral hues with a simple filter whose value of $\bar{\gamma}_o$ can be "tuned" over the range of visible wavelengths, the best subjective impression is obtained with a filter having parallel

polars and $m = 2$. For $m = 1$ the transmission peak is too broad and for $m = 3$ and higher the adjacent transmission peaks in the visible produce unsaturated colors. The colors produced by an $m = 2$ filter are found subjectively to represent the visible spectrum fairly well, with the exception that a really satisfactory green is not obtained.

It is possible to make filters whose transmission decreases rapidly as $\bar{\gamma}$ departs from $\bar{\gamma}_0$, without degradation from closely-spaced adjacent maxima, if more than one birefringent element is employed. Arrays of many parallel polarizers, interspersed by birefringent plates whose retardations increase in a powers-of-two series, have been used as monochromatizing filters with a very narrow spectral passband.[98] The presence of many polarizers in an optical system may introduce excessive losses. Narrow passband filters have been described [96,97] that utilize a multiplicity of birefringent plates and as few as two polars.

It is possible in fact to produce a low-loss filter that closely approaches any desired spectral response by incorporating a sufficient number of birefringent plates between two polars. The techniques by which such filters are designed are termed optical network synthesis. A wide variety of spectral responses can be obtained by using a number of identical birefringent plates[8]. If N such plates, each with birefringence (n_1-n_2)

and thickness t are used, then a spectral response function:

$$I = I_o A^* A \tag{11}$$

can be produced, where the asterisk denotes the complex conjugate, and

$$A = \sum_{j=0}^{N} a_j e^{2\pi i j (n_1 - n_2) t \bar{\gamma}} \tag{12}$$

The a_j's can have any desired set of values, subject merely to the constraint imposed by the principle of conservation of energy that A^*A may not exceed unity. From the form of Equation (12) it follows that if the dependence of the birefringence (n_1-n_2) upon $\bar{\gamma}$ is ignored, then A is a periodic function of $\bar{\gamma}$. The periodicity (spacing of successive equivalent maxima) is in fact the same as that of a simple filter composed of a single plate of birefringence (n_1-n_2) and thickness t, whose spectral response is given by Equation (9). The spectral response is not, however, restricted to the sine or cosine function of the simple filter. The function A is a finite Fourier series. As more birefringent plates are incorporated (N increased), more terms are allowed in the Fourier series, and subject to the constraint mentioned above, the spectral response can approach any desired function, as long as its periodicity is that which is dictated by the thickness and birefringence of the individual plates.

If the birefringence (n_1-n_2) of each plate in the network is changed by the same amount, then the shape of the spectral response function is retained but the periodicity is changed, so that the positions of the transmission peaks are shifted. The coefficients a_j in Equation (12) are determined by the angles between the birefringent plates and the polars in the network. The reverse process, that of deducing the angles that correspond to a given desired set of a_j's, is performed by the methods of optical network synthesis.[8]

We now examine further the case of an interesting compromise between the simple filter and complex networks, which is a filter consisting of two identical active plates. One possible set of a_j's when there are two birefringent plates is $a_0 = a_1 = a_2 = \frac{1}{3}$. The corresponding spectral response function is

$$I = \frac{I_0}{9}\left[3 + 4\cos 2\pi (n_1-n_2)\, t\,\bar{\gamma} + 2\cos 4\pi (n_1-n_2)\, t\,\bar{\gamma}\right] \quad (13)$$

This response function has the narrowest principal peak that is allowed for a two-plate filter, but it is not as free of subsidiary maxima as are other allowed functions. Even though this is an extremely simple optical network, the computation of the angles between the elements is fairly involved. The detailed calculations are given in Appendix C of Monthly Report No. 5, and the results of the calculations are depicted in Figure 60.

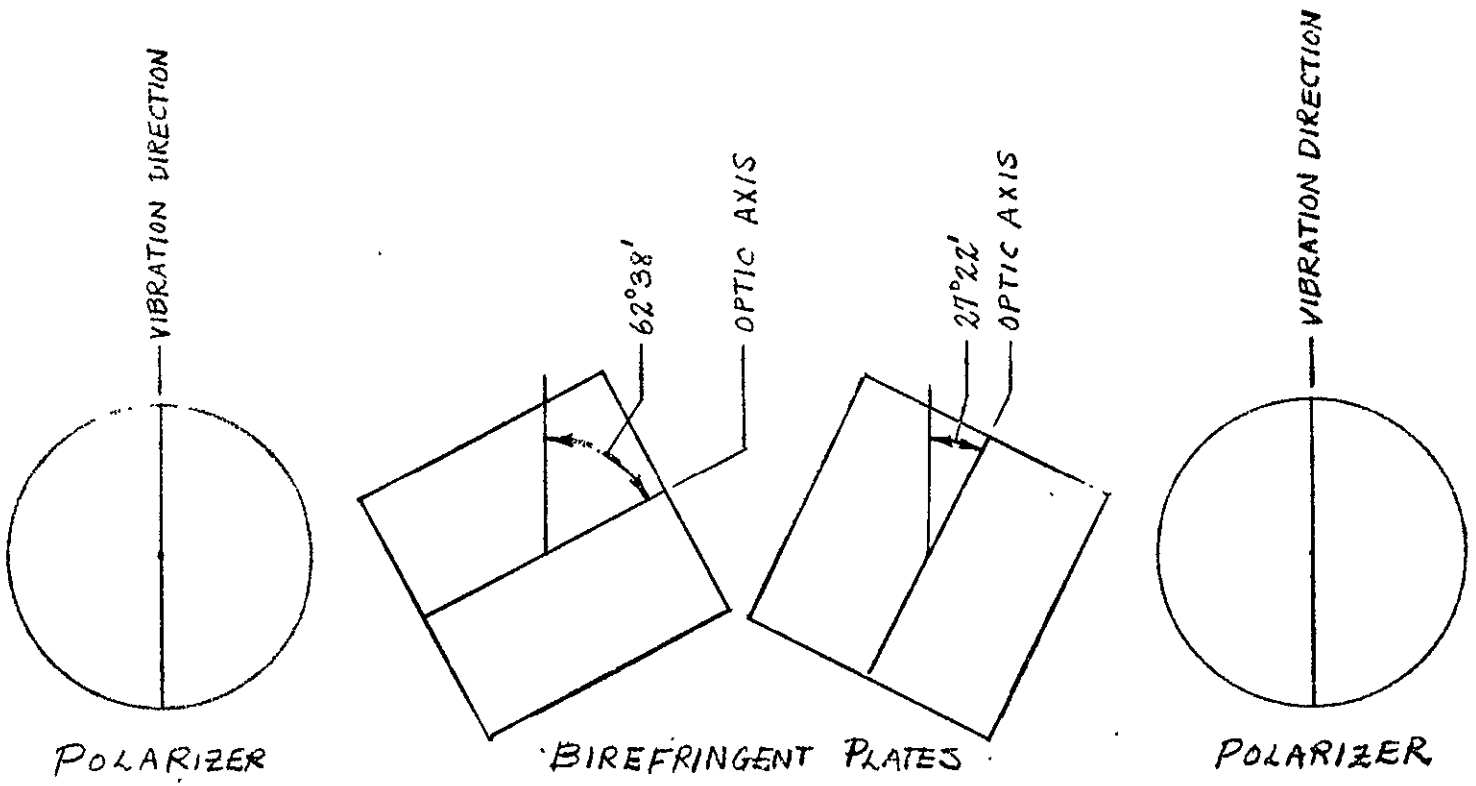

TWO-PLATE OPTICAL NETWORK WITH SPECTRAL RESPONSE FUNCTION

$$I = \frac{I_o}{9}\left[3 + 4\cos 2\pi (n_1 - n_2)\, t\tilde{\nu} + 2\cos 4\pi (n_1 - n_2)\, t\tilde{\nu}\right]$$

DISASSEMBLED REPRESENTATION. THE FOUR FLAT ELEMENTS ARE STACKED UPON ONE ANOTHER IN THE ORDER AND ORIENTATION SHOWN.

Figure 60. Disassembled Representation of Optical Network

Experiments to confirm the predicted results were performed with passive birefringent elements each having a retardation $(n_1-n_2)t$ equal to 1.071×10^{-4} cm. When one such element is placed between parallel polars it constitutes a simple filter with a second-order ($m = 2$) transmission peak at an optical wavelength of 536 nm (green). It was mentioned previously that the simple filters that subjectively most closely approximate spectral hues are those with $m = 2$ between parallel polars, but that adequate greens are not obtained in this manner. Indeed, the color obtained with the single birefringent element could most nearly be described as "olive drab". This is because the transmission peak for the simple filter is indeed at 536 nm, but there is excessive subsidiary transmission at longer wavelengths. An optical network was constructed as shown in Figure 63 from two such birefringent elements and two polars. This network is expected to exhibit a second-order transmission peak at the same optical wavelength, 536 nm, as the simple filter, but with the subsidiary transmission repressed. The subjective hue perceived through the two-plate network was observed to be remarkably different from that found with the simple filter, and could be described as a fairly saturated green.

From this initial analysis, it appears that a filter with two identical, electro-optically variable birefringent plates, made according to the scheme shown in Figure 63, would

produce a satisfactory array of hues for either camera or display devices. Further detailed analyses should compare the results obtained with other combinations of birefringent plates in terms of actual spectral bandwidth, shape factor, insertion loss, and tolerance to errors or changes in the operating characteristics of the plates.

SECTION IV

SYSTEM PERFORMANCE AND FUTURE RECOMMENDATIONS

A. ANTICIPATED SYSTEM EFFECTIVENESS

The primary goal of this program (investigation and characterization of the performance parameters of PLZT Solid-State-Electro-Optical Filters) has been successfuly accomplished. Limitations in the quality of the samples available for test, particularly as related to the electrode contacts, restricted some of the measured parameters. However, sufficient data was obtained to show that the PLZT filter system can be successfully applied to a spacecraft television system.

Comparisons of measured performance with system requirements were discussed in some detail in connection with the reported measurements. The system requirements are summarized here, with measured comparative data, to permit assessing the anticipated system effectiveness. It is tacitly assumed in these comparisons that the observed electrode contact problems can be resolved through further investigation.

1. Neutral Density Filter Operation

The two most significant parameters for applying the SSEF as a controllable neutral density filter are the insertion transmission loss, and the available control range. The stated

system goals for these parameters are 30 percent transmission (f/4 equivalent), and 140 to 1 control range.

The measured performance for the present components is about 14 percent transmission. This data was obtained using HN-32 polarizers with a measured 20 percent transmission (axes parallel). The indicated PLZT transmission for this case is, 0.14/0.20, or 70 percent. From this, the opaque electrodes are subtracted giving an indicated transmission based on surface reflection loss and inherent opaqueness of the PLZT, of 0.7/0.94 or 75 percent. (This value is also confirmed by measurements during the anti-reflection tests).

Improved polarizer performance can be expected to yield transmissions of 30 percent for the parallel polars. For example, HN-32 catalog data[91] predicts 25 percent transmission. Also available is type HN-38 which should provide 30 percent transmission at the possible penalty of slightly reduced maximum density range. Further improvements in polarizer performance may be achievable through development work. For calculating the predicted system effectiveness, we will simply assume the availability of polarizers meeting the HN-38 specification. Electrode line widths of 1.5 mils at the present spacing will reduce the masking to 4 percent (96 percent transmission). The anti-reflection test data indicates that at least 85 percent transmission should be achievable for the PLZT wafer. Thus the anticipated transmission is:

Polars × Masking × PLZT,

or 0.3 × 0.96 × 0.85 = 0.25,

or: 25 percent

The small difference from the goal of 30 percent should not be significant in terms of system operation. Achieving higher performance will depend primarily on improved polarizers rather than the PLZT device, since the polarizers are the predominant loss in the system.

With regard to control range, the ultimate range for the present system components is set by the crossed/parallel transmission range of the polars. For the HN-32 filters this was measured as a density range of 0.8 to 4.1, or a transmission change of 1900 to 1. The corresponding system measurements with the PLZT sample installed provided a transmission control range of 1600 to 1, which is far in excess of the stated goal of 140 to 1. This excess control range can be considered as a tradeoff factor in improving the insertion loss of the SSEF, such as by using the HN-38 polarizers. It should also be noted that the measured control range exceeds the GCTA specification of 1000 to 1.

Resolution degradation, introduced by the presence of the SSEF, was shown by the optical bench and camera measurements to be negligible for Apollo type spacecraft cameras. A system effectiveness consideration is the effect on depth-of-field of the

optical system. When the lens iris is stopped down to provide exposure control (larger f numbers) the depth of focus is increased. When the SSEF is similarly used to control the exposure, the depth-of-focus remains constant. Since the camera lens can, and probably will, be supplied with a focus adjustment this is not in itself a negative factor; it should simply be recognized.

Temperature related data shows the PLZT filter to be somewhat less tolerant to temperature changes than the Apollo type design. Particularly in the range from 0°C to 20°C, restricted performance was obtained. This may be more a function of the particular composition which was evaluated, rather than being fundamental to the basic system. Discussions with Dr. Haertling have indicated that a small change in composition would provide more uniform characteristics down to 0°C. Based on the present data; however, it may be required to actively control the PLZT temperature, or restrict the operating temperature range to provide uniform performance.

The observed time constant performance in the camera system appears to be quite adequate for application to a closed loop automatic light control where the system response time is normally set to be at least several vertical field periods. Similarly, small hysteresis effects in the transfer characteristic are accommodated by the closed loop control; large effects could reduce the total dynamic range and are therefore undesirable.

Angle of incidence effects with the measured samples were shown as being relatively small for an f/2 optic system (14° half angle). For low density settings the observed change as a function of angle was negligible. At the highest density settings ($\simeq$ 4.0) the maximum change as a function of angle approached 30 percent. At the density corresponding to an adjustment range of 140 to 1, the maximum change as a function of angle was under 10 percent. This effect would represent a small change in the image shading as a function of SSEF density and will not significantly degrade the television picture quality.

2. Spectral Filter Operation

The spectral filter performance of the SSEF was examined during this program in terms of the simplest implementation, i.e., a single PLZT plate between crossed polars. As discussed in Section III-C more elaborate techniques give promise of improved performance. The parameters of prime importance in studying the application of an SSEF to spectral separation in a spacecraft camera are:

- Color Saturation (Spectral Purity)
- Speed of Response
- Uniformity Across Field
- Field Sequential Adaptability

For a standard system using three primaries, the half-bandwidth response of each color filter is nominally about 100 millicrons. Crosstalk caused by response of one filter within the passband of the others must be minimal to maximize the purity.

The measurements (Section II-F-10) of the single PLZT filter system show that appreciable color separation can be obtained. The bandwidths shown on the spectrophotometer curves do not presently meet the system objectives in terms of crosstalk and spectral separation; however, this is not unexpected for the single stage filter. Additional stages are required to suppress

out-of-band responses. Preliminary calculations for such multi-stage systems (as in Section III-C) indicate that performance approaching the stated objectives can be achieved. This discussion has assumed that a standard three color (R,B,G) system is a basic requirement. Other specialized applications which utilize spectral discrimination may be satisfied by the existing characteristics of single state devices.

The speed of response in achieving the transition from one spectral response to another is directly related to the rate of change of retardation in the PLZT device. As with the neutral-density mode of operation, the limiting factor presently appears to be the switching capability of the driving circuit. Switching of the PLZT retardation between two fixed states appears to be feasible in a time interval comparable to one horizontal line (63.5 μs), although the present measurements were purposefully lengthened by a series protective resistor. The response time does not appear to be a significant limitation in achieving field-to-field color transitions.

Uniformity of color hue across the area of the PLZT surface, as shown in the photographs (Figures 34, 35, and 36), is seen to be quite good except for two effects associated with the electrodes. The first is a relatively narrow region adjacent to each electrode, which displays a different birefringence (and resulting hue shift). The second, seen in one corner of

the plate, is a tapered field distribution between several of the electrodes. This is created when the contact efficiency decreases, resulting in a non-uniform field between the electrodes. The first effect could be tolerated by masking with an opaque overlay at the cost of a small loss in throughput. Both of these effects are expected to be resolved by improved electrode contacts. From the above observations, the uniformity of hue is expected to be adequate for the proposed application.

For field sequential applications using electron beam scanning sensors (such as the SIT or silicon vidicon), current techniques have utilized a rotating color filter wheel to provide field-to-field color separation. Optimum operation is obtained with this type of system when the opaque area between color segments is designed to track or mask the vertical motion of the scanning beam. An analogous application of the SSEF would suggest implementing a "window shade" control of the PLZT retardation. This could conceivably be achieved by separating the common junctions of the present electrode pattern and supplying control voltages to each electrode independently, so that the operating points can be shifted down the electrode array. If the shifting is synchronized with the camera vertical scan, this would then provide the equivalent of the color wheel operation. Considering the problems associated with the present electrodes, the difficulties anticipated in making isolated attachments to each electrode, and the problems which are related to the shifting voltage source, such a technique does not appear attractive.

Another method which could be applied would be to utilize only the vertical blanking interval for exposure of each color field (as in a shuttered operation). In this case, no modification to the electrodes is required, and the circuit adaptation is straightforward. There is however a significant loss in efficiency since the exposure interval for each color field is limited to 10 percent of the total field time. For the sensors in current use (SIT, silicon, etc.) we therefore conclude that the effectiveness of the SSEF as a field sequential spectral separator is limited in efficiency.

Recent developments in sensor technology indicate that other devices may be expected to displace the electron beam scanning sensors in spacecraft cameras. The advent of the charge coupled device (CCD) and the anticipated implementation of the device in a practical TV camera, suggests the use of SSEF elements as a desirable adjunct.

Typically a field transfer CCD camera can integrate the optical image for a full field time. During the vertical blanking interval, the information contained in the sensing area will be rapidly transferred to the temporary storage region. During the subsequent exposure interval the stored data is shifted, line-by-line, to an output register for readout.

As a consequence, the spectral shift from color-to-color can be implemented once per field, during the vertical blanking

period, with the exposure maintained for the full active scan time. This method of operation provides a very good match to the SSEF operating characteristics. In fact, in this mode the SSEF can provide greater throughput efficiency than a rotating wheel. This is because the mask between wheel segments must be large enough to project an opaque image of the scan beam with the lens optic angle considered. For typical spacings of color wheel to image plane this efficiency rarely exceeds 50 percent. Conversely for the SSEF, 90 percent efficiency can be anticipated. The expected small volume of a camera utilizing a CCD sensor further suggests that the advantages of an SSEF device would be best utilized with this type of sensor.

B. RECOMMENDATIONS FOR FUTURE EFFORT

The present phase of SSEF measurements has provided evidence of the potential usefulness of this device in spacecraft television imaging systems. Continued effort is recommended to improve area where deficiencies have been noted. Following the correction of deficiencies, further effort can be directed towards optimizing the application usage. The recommended effort should be considered as several program phases, with the present program representing Phase 1. During Phase 2 the effort should be concentrated on resolving the major operating limitations which were observed. Succeeding phases would then refine the application usage. The recommended investigations are described in the following paragraphs.

1. Phase 2

The most striking shortcomings of the PLZT samples investigated up to now have been those associated with the electrode-substrate interfaces. The variation of the field-induced retardation in the vicinity of the electrode fingers, and the existence in the same region of birefringence after the field has been turned off detract considerably from the performance of the device. In preliminary experiments performed at RCA Laboratories it was found that the undesirable phenomena described above that were observed with the initial PLZT samples could be eliminated, or at least greatly reduced, if either gallium-indium electrodes were applied directly or chrome-gold electrodes were applied using an evaporation mask.

It is recommended, therefore, that the electrode contact problem be addressed by considering the use of various types of material for the contacts, such as chrome-gold, indium oxide, or copper interfaces. This investigation should be coupled with examining different surface cleaning treatments such as solvents, or a dc or rf glow discharge to prepare the material for electroding. Also to be considered should be the difference in results using evaporation masks as opposed to photoresist methods.

To support the electrode investigation, additional material samples will be required. Optoceram, Inc., is a company recently formed by Dr. Haertling, dedicated to the production of high quality PLZT for electro-optic use. They have full facilities for performing the compositional control and hot-pressing techniques required to prepare PLZT samples in the quantities required. To permit evaluation of this commercial source of supply, it is recommended that the new test samples be procured from Optoceram. Initial samples should be of the same 9/65/35 (La/Zr/Ti) composition as the present devices to provide comparative data. Other compositions can be examined in successive phases.

The PLZT filter substrate is a hard, quite brittle, ceramic compound having a tensile strength similar to crown glass; however, it is more susceptible to cracking through bending or local stress concentrations. The mounting holders developed in the initial program phase were designed to accommodate these

characteristics in a manner suitable for ground data evaluation. A different technique is required to develop a holding method compatible with the environment anticipated for flight qualification. It is recommended that this be investigated during Phase 2 by utilizing two clear glass plates with a bonding medium between the plates which uniformly supports the substrate. The supporting medium should have a low modulus of elasticity which will avoid transfer of clamping strains into the PLZT substrate. These glass plates may also mount or provide the required polarizers. For optimum performance, each of the interface surfaces should be considered during the investigation in terms of applicable anti-reflection coatings to maximize throughput. Selection of the bonding material and dimensions can also address the problem of providing increased high voltage properties to the finished assembly.

With regard to the network analysis technique for assessing cascaded filter performance, this effort should be continued to provide firm recommendations and tradeoffs in performance for different combinations of filter elements. The conclusion of this analysis would be the assembly and spectral test of the recommended network, using improve samples resulting from the electrode experiments.

In light of the application advantages of an SSEF when coupled to a CCD sensor, preliminary analysis of such a system should be started. This should include an optical layout to determine the optimum lens/SSEF/CCD geometry, and an analysis of the residual electrode structure,which can provide recommendations for required electrode mask dimensions. This information will permit better assessment of the field-sequential performance and recommendations for future development.

2. Succeeding Phases

Satisfactory completion of the Phase 2 tasks will permit addressing other SSEF related areas. These include the items in the following tabulation, which are not necessarily in order of importance:

a. Investigate other material compositions, particularly as related to temperature effects.

b. Develop optimized electrode configurations in terms of mask geometry (line width, spacing, outside diameter, etc.)

c. Circuit development related to rapid switching requirements (e.g., capacitive energy storage system to conserve total power).

d. Assembly and test of an SSEF system mated with a CCD camera sensor.

e. Environmental qualification of an SSEF assembly

f. Perform operating life test.

g. Investigate improved polarizers.

APPENDIX "A"

BIBLIOGRAPHY

1. Albers, W. A. and Kaplit, M. Visible Light Scattering in Ferroelectric Ceramics, The Physics of Opto-Electronic Materials, Pg 151, W. A. Albers, Jr, Ed., Plenum Publishing Corporation, New York.

2. Ammann, E. O. Synthesis of Electro-Optic Shutters Having a Prescribed Transmission vs. Voltage Characteristic, J. Optical Soc. Am., Vol. 56, pp 1081-1088, Aug. 66.

3. Baerwald, H. G. "Two-Dimensional Analysis of Gap Fields in Electroded High-Dielectric Layers and Applications to the Design of Polarceroptic Devices", Sandia Laboratories, Albuquerque, N. M., Research Report, SC-RR-69-85, February 1969.

4. Berlincourt, D. A. "Properties of Lead Titanate Zirconate Ceramics", Tech. Rept. 3 Sandia Corp., Rept. 30135, 1957.

5. Berlincourt, D. A. "Variation of Electroelastic Constants of Polycrystalline Lead Titanate Zirconate with Thoroughness of Poling". J. Acoust. Soc. Am., Vol. 36, pp 515-520, March 1964.

6. Berlincourt, D. A. "Research on Piezoelectric Materials and Phenomena", Sandia Laboratories Summary Rept. 323160,1965.

7. O'Bryan, H. M. and Thomson, J. "Preparation of Transparent Ferroelectric Ceramics." Presented at the Joint 23rd Pacific Coast Regional Meeting and Electronics Division Fall Meeting of the Am. Ceram. Soc., October 29, 1970. San Francisco, California. Paper No. 19-E-70F, for Abstract see Bull. Am. Ceram. Soc., 49.833 (Sept. 1970).

8. Chang, I. C., et al, Optical Network Synthesis Using Birefringent Crystals. Pt I Journal of the Optical Society of America, Vol. 54, No. 10, October 1964, pp 1267-1279; Pt II Ibid, Vol. 55, No. 7, July 65, pp 835-841; Pt III Ibid, Vol. 56, No. 7, July 66, pp 943-951; Pt IV Ibid, Vol. 56, No. 7, July 66, pp 952-955; Pt V Ibid, Vol. 56, No. 12, Dec. 66, pp 1746-1754.

9. Cleveland, T. L., Technique for Attaining Fine Line Pattern Definition of Thin Film Transparent Electrodes. Report SC-TM-71-0217, Sandia Labs, Albuquerque, N.M. (AD-891, 893L).

10. Cummins, S. E. "A New Bistable Ferroelectric Light Gate or Display Element." Proc. IEEE (Letters), Vol. 55, pp 1537, August 1967.

11. Cummins, S. E. "A New Optically Read Ferroelectric Memory." Proc. IEEE (Letters), Vol. 55, pp 1536-1537, August 1967.

12. Cummins, S. E. and Cross, L. E. "Electrical and Optical Properties of Ferroelectric $Bi_4 Ti_3 O_{12}$ Single Crystals." J. Appl Phys., Vol. 39, pp 2258-2274, April 1968.

13. Cutchen, J. T., Harris, J. O., Jr. PLZT Electro-Optic Flashblindness Goggles. Internal Memo, Sandia Research Laboratories, Albuquerque, N. M.

14. Delly, J. G. "Microscopy's Color Key" Industrial Research, Vol. 15, No. 11, October 1973, pp 44-50.

15. Francombe, M. H., Wu, S. Y. Ferroelectric Displays, Westinghouse Research Labs. (AD-755, 746).

16. Fraser, D. B. and Maldonado, J. R. "Improved Aging and Switching of Lead Zirconate-Titanate Ceramics with Indium Electrodes," J. Appl. Phys., Vol. 41, pp 2172-2176, April 1970.

17. Fushimi, S. and Ikeda, T. "Optical Study of Lead Zirconate Titanate," J. Phys. Soc. Japan, Vol. 20, pp 2007-2012, Nov. 1965.

18. Gruver, R. M., Buessem, W. R. State-of-the-Art Review on Ferroelectric Ceramic Materials. Linden Labs, State College, Pa. (AD-801, 027).

19. Haertling, G. H. "Hot-Pressed Lead Zirconate-Lead Titanate Ceramics Containing Bismuth," Am. Ceram. Soc. Bull. 43 (December 1964) 875-879.

20. Haertling, G. H. "Improved Ceramics for Piezoelectric Devices," 1966 WESCON Conv. Rec., Vol. 10, pt. 3, Paper 3/1.

21. Haertling, G. H. and Zimmer, W. J. "An analysis of Hot-Pressing Parameters for Lead Zirconate-Lead Titanate Ceramics Containing Two Atom Percent Bismuth", Am. Ceram. Soc. Bull., 45 (December 1966) 1084-1089.

22. Haertling, G. H. "Improved Ceramics for Piezoelectric Devices," WESCON/66 Technical Papers, Vol. 10, pt. 3, Paper 3/1.

23. Haertling, G. H. "Grain Growth and Densification of Hot-Pressed Lead Zirconate-Lead Titanate Ceramics Containing Bismuth," J. Amer. Ceram. Soc., 49[3] 113-18 (1966).

24. Haertling, G. H. "Hot-Pressed Ceramics for Electrooptical Applications," Am. Ceram. Soc. Bull, Vol. 47, p. 389, April 1968.

25. Haertling, G. H. "Hot-Press Ferroelectric Lead Zirconate Titanate Ceramics for Electro-Optical Applications," Amer. Ceram. Soc. Bull, 49[6] 564-67 (1970).

26. Haertling, G. H. "Electrooptic Ceramic Materials," 1971 WESCON Convention Record, Paper 31.1.

27. Haertling, G. H. and Land, C. E. "Hot-Pressed (Pb,La) (Zr,Tl) Ferroelectric Ceramics for Electrooptic Applications J. Am. Ceram. Soc., Vol. 54, pp 1-11, Jan. 1971. (Sandia Reprint SC-R-70-4401)

28. Haertling, G. H. "Improved Hot-Pressed Electrooptic Ceramics in the (Pb,La) $(Zr,Ti)O_3$ System," J. Am. Ceram. Soc., Vol. 54, June 1971. (Sandia Reprint SC-R-71-3266).

29. Haertling, G. H. and Land, C. E. "Recent Improvements in the Optical and Electrooptic Properties of PLZT Ceramics," IEEE Transactions Sonics and Ultrasonics, 1972 SU-19, pp 269-280. Also Published in Ferroelectrics, 1972, Vol. 3, pp 269-280.

30. Haertling, G. H. and McCampbell, C. B. A New Longitudinal Display Mode for Ceramic Electrooptic Devices. Proc. IEEE 60 (April 1972), pp 450-451.

31. Harris, Jr., J. O. and Cutchen, J. T. "Electrooptic Variable Density Optical Filter," Internal Memo, Sandia Research Laboratory, Albuquerque, N. M.

32. Harris, J. O. "Switching Characteristics for Electrooptic Flashblindness Goggles," Sandia Laboratories Internal Memo, June 5, 1972.

33. Hippel, A. N. Helectric-Constant Materials and Ferroelectricity. MIT Cambridge Lab for Insulation Research, Report TR 178 (AD-404, 776)

34. Not Used

35. Jona, F., Shirane, G., and Pepinsky, R. "Optical Study of $PbZrO_3$ and $NaNbO_3$ Single Crystals," Phys. Rev., Vol. 19, 1584-1590, March 1955.

36. Jona, F. and Shirane, G. Ferroelectric Crystals, (MacMillan, New York, 1962).

37. Kaminow, I. P. "Electro-Optic Materials," Ferroelectricity, E. F. Weller, Ed., (Elsevier, New York, 1967), pp 183-96

38. Kaminow, I. P. and Turner, E. H. "Electrooptic Light Modulators," Proc. IEEE, Vol. 54, 1374-1390, Oct. 1966.

39. Kanzig, W. "Ferroelectrics and Ferroelectronics," Solid State Physics, Vol. 4, F. Seitz and D. Turnbull, eds. New York: Academic Press, 1947, pp 97-124.

40. Land, C. E., Smith, G. W. and McKinney, I. D. Polycrystalline Ferroelectric Multiremanence Memory Elements," 1964 IEEE International Conv. Rec.,Vol. 12, Pt 9 pp. 149-160, March 1964.

41. Land, C. E. Ferroelectric Ceramic Electrooptic Storage and Display Devices, 1967 International Electron Devices Meeting, October 1967, Washington, D. C., Sandia Laboratories, Albuquerque, N. M., Reprint SC-R-67-1219, October 1967.

42. Land, C. E. and Thacher, P. D. "Ferroelectric Ceramic Electrooptic Materials and Devices," Proc. IEEE, Vol. 57, pp 751-768, May 1969, Sandia Laboratories, Reprint SC-R-69-1218, Albuquerque, N.M.

43. Land, C. E. "Ferroelectric Ceramics See The Light," Industrial Research, 11 (May 1969) 62-64.

44. Land, C. E. and Haertling, G. H. "Optical Properties of Ferroelectric Ceramics," Proc. Second International Meeting of Ferroelectricity, Sept. 1969, Kyoto, Japan. Also Published in Supplement to J. Phys. Soc. Japan, 1970, Vol. 28, pp 96-99.

45. Land, C. E. "Electrooptic Ceramic Storage and Display Devices," Oyo Butsuri, 39[1] 18-29 (1970)

46. Land, C. E. and Thacher, P. D. "Electrooptic Ceramics — New Materials for Information Storage and Display," The Western Electric Engineer, Vol. 14, pp 13-24, Jan. 1970.

47. Land, C. E. and Holland, R. "Electrooptic Effects in Ferroelectric Ceramics," IEEE Spectrum, Vol. 7, 71-78, February 1970.

48. Land, C. E. "Recent Developments in Electrooptic Ceramics," Intl. J. of Nondestructive Testing, Vol. I, 315-335, 1970.

49. Land, C. E. "Ferroelectric Ceramics for Information Storage and Display," AIME, Metallurgical Transactions, Vol. 2, March 1971, pp 781-788, Also Reprint SC-R-71-3171.

50. Land, C. E. and Thacher, P. D. "Electrooptic Properties of Ba, Sn, and La Modified Lead Zirconate Titanate Ceramics," in Physics of Opto-Electronic Materials, W. A. Albers, Jr., Ed., Plenum Publishing Co., New York, 1971, p. 169.

51. Landry, M. J., McCarthy, A. E. "Changes in Transmission Switching of PLZT Cells Under Different Voltage Excitation Conditions. Report SC-RR-720384, Sandia Labs, Albuquerque, N. M. (AD-910, 863L).

52. Maldonado, J. R. "Electrooptic Devices Using Strain-Biased PLZT Ferroelectric Ceramics," 1971 WESCON Convention Record, Paper 31.3.

53. Maldonado, J. R. and Meitzler, A. H. "Ferroelectric Domain Switching in Rhombohedral-Phase PLZT Ceramics," Presented at the 1971 IEEE Symposium on Appl. of Ferroelectrics, Yorktown Heights, N. Y., June 7-8, 1971.

54. Maldonado, J. R. and Meitzler, A. H. "Strain-Biased Ferroelectric-Photoconductor Image Storage and Display Devices," Proc. IEEE. Vol. 59, pp. 368-382, March 1971.

55. Maldonado, J. R. and Meitzler, A. H. "Ferroelectric Ceramic Light Gates Operated in a Voltage-Controlled Mode," IEEE Trans. on Electron Devices, Vol. ED-17, pp 148-157, Feb. 1970.

56. Marino, A. J. Jr., Battle, J. H. "Development of Manufacturing Process High Purity Electronic Ceramics, ITT Federal Labs, Nutley, N. J. (AD-410, 251).

57. Meitzler, A. H. Maldonado, J. R. and Portnoff, M. R. "Large-Area, Bistable, Ferroelectric Ceramic Polarization Switches," Presented at the IEEE/OSA Conf. on Laser Engrg. and Appl., Washington, D. C., June 2-4, 1971.

58. Meitzler, A. H., Maldonado, J. R. and Fraser, D. B. "Image Storage and Display Devices Using Fine-Grain Ferroelectric Ceramics," Bell System Tech. Journal 49. 953-967 (July-Aug. 1970).

59. Meitzler, A. H. and Maldonado, J. R. "Ferroelectric Display's Big Bonus Selective Erase-Write Capability," Electronics, Vol. 44, pp 34-39, Feb. 1, 1971.

60. Nettleton, R. E. "Polarization-Dependent Rayleigh Scattering in a Coarse-Grained Ferroelectric Ceramic," J. Appl. Phys. Vol. 39, pp. 3646-3654, July 1968.

61. Nettleton, R. E. "Domain Structure and Scattering of Visible Light in a Perovskite Ceramic," IEEE Trans. Electron Devices, Vol. ED-16, 602, June 1969.

62. Nye, J. F. "Physical Properties of Crystals. London: Oxford University Press, 1957, ch 13 and 14.

63. Plumlee, R. H. "Switching Life Properties of Polycrystalline Ferroelectrics," 1966 WESCON Conv. Rec. Session 3, Paper 3/2. Also Sandia Labs Research Report SC-RR-67-730, October 1967.

64. Samara, G. A. "Pressure and Temperature Dependence of the Dielectric Properties and Phase Transitions of the Ferroelectric Perovskites $PbTiO_3$ and $BaTiO_3$," Ferroelectrics, 1971, Vol. 2, pp 277-289.

65. Sawaguchi, E. "Ferroelectricity Versus Anti-Ferro-Electricity in the Solid Solutions of $PbZrO_3$ and $PbTiO_3$," J. Phys. Soc. Japan, Vol. 8, pp 615-629, Sept.-Oct. 1953.

66. Shabana, M. M. "Characteristics of Localized Domains in Ferroelectric Crystals," Air Force Cambridge Research Laboratories, Scientific Report 4, AFCRI65-506, May 1965, Available From CESTI 5285 Port Royal Rd., Springfield, Va. 22151.

67. Shabana, M. M and Jones, R. V. "Electro-Optical Activity of Localized Perpendicularly Switched Domains in Ferroelectric Crystals," Proc. IEEE, 54 (January 1966) 85-86.

68. Sholokhovich, M. L. and Fesenko, E. G. "Preparation and Structure of Crystals of Some Lead-Containing Ferroelectric Substances and Their Solid Solutions," Bull. Acad. Sci. USSR. Phys. Ser. 24, 1244-1247, 1960.

69. Smith, W. D. and Varnado, S. G. "Use of Ferroelectric Ceramics for Electronic Frequency Selection in Dye Lasers," Presented at the IEEE Device Research Conference, June 28-July 1, 1971.

70. Smith, W.D. and Land, C. E. "Scattering Mode Ferroelectric-Photoconductor Image Storage and Display Devices," Applied Physics Letters, Vol. 20, No.4, February 15, 1972, pp 169-171.

71. Smith, W. D. and Land, C. E. "Ferroelectric Ceramic Light Scattering Devices for Image Storage and Display" Sandia Laboratories Internal Report, Albuquerque, N. M.

72. Taylor, B. "Some Properties of the Lead Zirconate Titanate Ceramic AM 476," Report AUWE-TN-365/69, Admiralty Underwater Weapons Establishment, Portland, England (AD-871,835).

73. Taylor, G. W. "A Method of Matrix Addressing Polarization Rotating or Retarding Light Valve Arrays," Proc. IEEE, Vol. 58, pp 1812-1818, Nov. 1970.

74. Thacher, P. D. "Electrocaloric Effects in Some Ferroelectric Anti-Ferroelectric $PbZrTiO_3$ Components, Journal Applied Physics, Vol. 39, pp. 1996-2002, March 1968.

75. Thacher, P. D. and Land, C. E. "Ferroelectric Electrooptic Ceramics with Reduced Scattering," IEEE Trans. on Electron Devices, Vol. ED-16, pp 515-521, June 1969. Also Reprint SC-R-69-1252.

76. Thacher, P. D. "Electrooptic Coefficients of Pb-Containing Oxygen-Octahedra Ferroelectrics, Ceramic $(Pb,Ba)(Zr,Ti)O_3$," J. Appl. Phys., Vol. 41, pp 4790-4797, Nov. 1970

77. Thacher, P.D. "Optical Voltage Sensors," Sandia Laboratories, Albuquerque, N. Mex., Research Report, SC-RR-70-593, Jan. 1971.

78. Thacher, P. D. "A Linear Electro-Optic Effect in Ferroelectric Ceramics," Ferroelectrics, 1972, Vol. 3, pp 147-150.

79. Thacher, P. D. and Land, C. E. "Ceramic Electrooptic Properties and Devices," WESCON Convention Record, 1971, Paper 31.2.

80. Uchida, N. and Ikeda, T. "Electrostriction in Perovskite-Type Ferroelectric Ceramics," Japan J. Appl. Phys., Vol. 6, pp 1079-1088, Sept. 1967.

81. Waynick, Arthur H. Physics of Display Devices Meeting, Imperial College, London, October 25, 1972. Report ONRL-C-22-72. (AD-757, 649).

82. Wilcox, P.D. and Hall, C. A. "Dielectric Properties of Relaxator-Like Ceramics in the $(Pb,Ba)(Zr,Ti)O_3$ System," Presented at the Fall Meeting of the Basic Science and Electronics Divisions, The American Ceramic Society, St. Paul, Minn., Sept. 18, 1968 (Paper No. 21-BE-68F); for Abstract see Amer. Ceram, Soc. Bull. 47 [8] 754 (1968).

83. Yarborough, J. M. and. Ammann, E. O. "Experiments on Single Pass and Double Pass Birefringent Networks." J. Optical Soc. Am. Vol. 58 pp 776-783, June 1968.

84. IRE Standards on Piezoelectric Crystals: "Measurements of Piezoelectric Ceramics," 1961, Proc. IRE 49 (July 1961) 1162-1163.

85. Bloss, F. D. "An Introduction to the Methods of Optical Crystallography,"New York, Holt, Rinehart and Winston, 1967.

86. Born, M. and Wolf, E. "Principles of Optics, 3rd ed. London: Pergamon, 1965, ch. 14.

87. Brown, E. B. "Modern Optics" New York: Reinholt 1965, ch 2 and 3.

88. Shurcliff, W. A. "Polarized Light" Cambridge, Mass. Harvard University Press, 1962, ch 7.

89. Stone, J. M. "Radiation and Optics" New York: McGraw-Hill, 1963, ch. 13 and 17.

90. The Sadtler Standard Spectra, Vol. 3, Inorganics, Philadelphia, Pa. Sadtler Research Labs., 1967, N887K and N889K.

91. "Polarized Light" Pamphlet T-265, Published by Polaroid Corporation, March, 1970.

92. Evans, J. W., Solc Birefringent Filter, Journal of the Optical Society of America, Vol. 48, No. 3, March 1958, pp 142-145.

93. Snow, G. S., Fabrication of Transparent Electrooptic PLZT Ceramics by Atmosphere Sintering, Sandia Reprint SC-DR-720600. Presented at American Ceramic Society, Washington, D. C., May 9, 1972 (Paper 15-E-72).

94. Feldstein, N., Law, H. B., Method of Repairing or Depositing a Pattern of Metal Plated Areas on an Insulating Substrate, U.S. Patent 3,753,816 Dated August 21, 1973.

95. Kumada, A., et al., Light Modulator Element, U.S. Patent 3,586,415, Dated June 22, 1971.

96. Evans, J.W., Lyot Filters, Journal of the Optical Society of America, Volume 39, 1949, pp 229-42.

97. Solc, I., - Czechoslavakian Journal of Physics, Volume 3, 1957, pg 366.

98. Lyot, B., - Ann. d'Astrophys, Volume 7, 1944, pg. 31.

99. Billings, B.H., - Journal of the Optical Society of America, Volume 37, 1947, pp 738-46.